2D CFD Simulation of a Circulation Control Inlet Guide Vane

Hugh Edward Hill IV

Thesis submitted to the faculty of the Virginia Polytechnic Institute and State University
in partial fulfillment of the requirements for the degree of

Master of Science
In
Mechanical Engineering

Wing Fai Ng Co-Chair
Pavlos Vlachos Co-Chair
Danish Tafti Committee Member

January 15, 2007
Blacksburg Virginia

Keywords: Circulation control, Inlet Guide Vane,
CFD, Turbulence models

2D CFD Simulation of a Circulation Control Inlet Guide Vane

Hugh Edward Hill IV

Mechanical Engineering

ABSTRACT

This thesis presents the results of two 2-D computational studies of a circulation control Inlet Guide Vane (IGV) that takes advantage of the Coanda effect for flow vectoring. The IGV in this thesis is an uncambered airfoil that alters circulation around itself by means of a Coanda jet that exhausts along the IGV's trailing edge surface. The IGV is designed for an axial inlet flow at a Mach number of 0.54 and an exit flow angle of 11 degrees. These conditions were selected to match the operating conditions of the 90% span section of the IGV of the TESCOM compressor rig at the Compressor Aero Research Laboratory (CARL) located at Wright-Patterson AFB. Furthermore, using the nominal chord (length from leading edge of the IGV to the jet exit) for the length scale, the Reynolds number for the circulation control IGV in this region was $5e^5$. The first study was a code and turbulence model comparison, while the second study was an optimization study which determined optimal results for parameters that affected circulation around the IGV. Individual abstracts for the two studies are provided below.

To determine the effect of different turbulence models on the prediction of turning angles from the circulation control IGV, the commercial code GASP was employed using three turbulence models. Furthermore, to show that the results from the optimization study were code independent a code comparison was completed between ADPAC and GASP using the Spalart-Allmaras turbulence model. Turbulence models employed by GASP included: two isotropic turbulence models, the one equation Spalart-Allmaras and the two-equation Wilcox 1998 k-ω. The isotropic models were then compared to the non-isotropic stress transport model Wilcox 1998 Stress-ω. The results show good comparison between turning angle trends and pressure loss trends for a range of blowing rates studied at a constant trailing edge radius size. When the three turbulence models are compared for a range of trailing edge radii, the models were in good agreement when the

trailing edge is sufficiently large. However, at the smallest radius, isotropic models predict the greatest amount of circulation around the IGV that may be caused by the prediction of transonic flow above the Coanda surface.

The optimization study employed the CFD code ADPAC in conjunction with the Spalart-Allmaras turbulence model to determine the optimal jet height, trailing edge radius, and supply pressure that would meet the design criteria of the TESCOM (TESt COMpressor) rig while minimizing the mass flow rate and pressure losses. The optimal geometry that was able to meet the design requirements had a jet height of $h/C_n = 0.0057$ and a trailing edge Radius $R/C_n = 0.16$. This geometry needed a jet to inflow total pressure ratio of 1.8 to meet the exit turning angle requirement. At this supply pressure ratio the mass flow rate required by the flow control system was 0.71 percent of the total mass flow rate through the engine. The optimal circulation control IGV had slightly lower pressure losses when compared to the cambered IGV in the TESCOM rig.

2D CFD Simulation of a Circulation Control Inlet Guide Vane

Hugh Edward Hill IV

Mechanical Engineering

Preface

The use of the Coanda effect on circulation control airfoils has been highly documented with research dating back more than sixty years. However, research into using the Coanda effect for internal flows is relatively recent. This thesis presents CFD results of an Inlet Guide Vane (IGV) that employs the Coanda effect on the trailing edge. The motivation behind the work completed in this thesis was to show that uncambered circulation control IGVs may be a viable replacement for current mechanical IGVs. Mechanical IGVs are currently used by many of today's fan compressors to change the flow angles upstream of the compressor's first stage. In order to meet those conditions, IGVs use variable geometries and flaps. However, variable geometries and flaps increase the engine's part count, maintenance cost, and overall weight. Circulation control IGVs that are capable of vectoring the flow without mechanical actuation may reduce the engine part count and weight, resulting in an engine that is lighter and less expensive to maintain.

This thesis is laid out into two chapters and four appendices. The first chapter is a paper that will be submitted to the 5th Joint ASME/JSME Fluids Engineering Conference. The first paper provides the results of a two-dimensional CFD turbulence model study of the same inlet guide vane presented in the first chapter. The second chapter is a paper that was submitted to the 2007 International Gas Turbine Institute (IGTI) Conference. The paper describes the results of a two-dimensional optimization study of a circulation control Inlet Guide Vane, using CFD. Following the first two chapters are the Appendices. The first appendix (A) presents further results from the turbulence model study, and a grid study of the mesh used in both the first and second chapters. The last three appendices are an overview of work, which was completed before the optimization study in chapter one.

Attribution

The following section provides the co-authors contributions to the two chapters of this thesis. The first and second co-authors of the two chapters of this thesis were, Dr. Wing Ng and Pavlos Vlachos, who were my advisors at Virginia Tech. They assisted me with my research as well as provided me with technical guidance. The third co-author was Stephen Guillot, the vice president of Techsburg Incorporated. He provided me with technical guidance for both chapters, as well as the training that I needed to generate meshes and run the CFD codes. Financial support for the circulation control Inlet Guide Vane project was provided by the Air Force Research Laboratory (AFRL), located at Wright-Paterson Air Force Base in Dayton Ohio. The original technical point of contact (TPOC) for the AFRL was David Carr. He provided the design requirements for the Air Force compressor test rig TESCOM (TESt COMpressor), as well as technical advice for Chapter 2, which was completed before Chapter 1. Todd Bailey took over the TPOC position from David Carr after the completion of Chapter 2, thus he was listed as the final co-author of Chapter 1.

Acknowledgments

I would like to thank my wife who has been behind me the whole way. Without her support I would not have had the desire to finish both my undergraduate and masters degrees. “I’ll be home soon honey.”

I would like to thank my daughter Victoria Hill for allowing me to slow down and enjoy a few smiles. Her presence alone was a great motivator. “da da”

Thank you to my parents who have been my cheering section throughout my life. With out their guidance and the lessons they taught me, I would have never finished a degree at all. Thanks for making me stay on the baseball team dad.

I would like to thank my old active duty supervisor SSgt Tammy Woodard, “get a hair cut Hugh”, wherever you are. She taught me that education was a privilege not a right. You never know how important something is until you are denied the ability to do it.

I would like to thank Stephen Guillot who has acted as my mentor throughout the entire program. He has taught me how to use the programs that I needed for my research, and has helped me immensely along the way. I still like him, even though he snowboards.

I would like to thank Rob English for, listening to my problems, showing me the best fishing spots, and providing my family and me “a place where everybody knows your name.” Long live the Rivermill.

I would like to thank my co-Advisor Dr. Pavlos Vlachos for his wisdom and Guidance. I would also like to thank him for the opportunity to work outside projects.

I would like to thank Jonathan McGlumphy who has been my friend, and colleague throughout my time at Virginia Tech. “Watch out for the trees Jonathan.”

I would also like to thank Shannon McGlumphy for being there to help both Kerri and I whenever we needed help.

I would like to thank Dr. Danish Tafti for teaching me the reasoning and methods behind computation fluid dynamics.

I would lastly like to thank Dr. Wing Fai Ng whose patience and understanding have allowed to me finish this degree.

Table of Contents

List of Tables

List of Figures

Chapter 1:

2D CFD Studies using Different Turbulence Models of a Circulation Control Inlet Guide Vane

H. E. Hill, W. F. Ng, and P. P. Vlachos
Virginia Polytechnic and State University
Blacksburg, VA 24061

S. A. Guillot
Techsburg Inc.
2901 Prosperity Rd.
Blacksburg, VA 24060

S.T. Baillie
Air Force Research Laboratory
WPAFB, Dayton OH

Paper for submission to the 2007 5th ASME/JSME Fluids Engineering Conference

Abstract

Circulation control inlet guide vanes (IGVs) may provide significant benefits over current IGVs that employ mechanical means for flow turning. This paper presents the results of a two-dimensional computational study, employing three turbulence models, on a circulation control IGV that takes advantage of the Coanda effect for flow vectoring. The IGV in this study is an uncambered airfoil that alters circulation around itself by means of a Coanda jet that exhausts along the IGV's trailing edge surface. Two isotropic turbulence models, the one equation Spalart-Allmaras and the two-equation Wilcox 1998 k-ω models are compared to the non-isotropic stress transport Wilcox 1998 Stress-ω model. The results show good comparison between turning angle trends and pressure loss trends for a range of blowing rates studied at a constant trailing edge radius size. However, when the three turbulence models are compared for a range of trailing edge radii, the results indicate that the accuracy of the isotropic models may breakdown due to the effects of streamline curvature at the smallest trailing edge radius. The isotropic models predict greater circulation than the stress transport model at the smallest trailing edge radius, due to jet separation locations further downstream on the Coanda surface. For the isotropic models, jet attachment on the smallest radius may be a direct result of the radial pressure gradients above the Coanda surface, which are created by shock waves when the entrained flow becomes transonic. The normal pressure gradients above the jet

balance the centripetal forces and allow the jet to overcome adverse pressure gradients tangent to the Coanda surface.

Nomenclature

C_n – Nominal chord length
C_t – Total Chord length
C_m – Mass flow rate ratio
h – Coanda jet height
$\dot{m}$ – Mass flow rate
M – Mach number
P – Pressure
P_{ref} – Reference Pressure
R – Trailing-edge radius
r – Normal distance from the center of the Trailing-edge radius
s – Blade Pitch
t – Blade thickness
T – Temperature
T_{ref} – Reference Temperature
U – Velocity
α – Turning angle
ρ – Density
σ – Cascade solidity (scaled by C_n)
ω_c – Mass averaged loss coefficient
θ – Trailing edge radius curvature

Subscripts

a – Axial
o – Stagnation conditions
c – Corrected
e – Exit conditions
i – Inlet conditions
n –Nominal
p – Plenum conditions
s – Static conditions
te – Trailing edge

Abbreviations

IGV – Inlet Guide vane
TESCOM – Three stage compressor test rig (TESt COMpressor)

Introduction

Motivation

In order to operate at peak performance, many of today's fan compressors require variable flow angles into their first rotating stage. To meet those conditions, Inlet Guide Vanes (IGVs) control the flow angle into a fan compressor first stage with the use of variable geometries and flaps. The problems that arise with variable IGVs relate to the mechanical devices that are utilized to turn the vane or flap. These devices add significantly to the engine part count, resulting in added weight and maintenance cost. The use of an un-cambered circulation control IGV, capable of vectoring the inlet flow without being mechanically actuated, may be able to reduce the number of blades and parts, resulting in an engine that is lighter and less expensive to maintain. Prior CFD results using a non-commercial code ADPAC (Advanced Ducted Propfan Analysis Code) showed that a circulation control inlet guide vane could match the design conditions in the three stage compressor test rig TESCOM (Air force acronym for TESt COMpressor), at Wright-Paterson Air Force Base. However, the results were specific to one code using only the Spalart-Allmaras turbulence model. To find out if the results from ADPAC were code independent the commercial code GASP (General Aerodynamic Simulation Program) was used with three turbulence models to examine the effects of different turbulence models on the prediction of turning angle from a circulation control IGV.

Literature Review

Variable inlet guide vanes are used to improve compressor performance through a range of operating conditions [1-4]. The use of a circulation control IGV was suggested by Lord et al. as a means to replace complex flapped inlet guide vanes with a simpler configuration to reduce weight and cost [5]. One such method of circulation control is by means of the Coanda effect on the trailing edge of an airfoil. The Coanda effect was first patented by Henri Coanda in 1934 after he noticed that hot gasses and flames remained attached to his 1910 air reactive airplane [6]. The Coanda effect occurs when the free stream flow above a curved surface is entrained by a parallel high momentum wall jet blown tangentially along the curved surface. The jet stays attached to the curved surface due to the balance between centrifugal forces around curved surface and the sub-ambient

pressure in the jet sheet [7]. The jet's momentum allows the oncoming boundary layer to overcome an adverse pressure gradient along the curved surface, and it entrains the flow above it due to its lower pressure. The entrained flow is accelerated around the curved surface by the jet, increasing the amount of circulation over the suction side of a body. This increased circulation translates to higher lift and flow turning for an airfoil that employs the Coanda effect. An example of the Coanda effect, applied to an inlet guide vane, can be seen in Figure 1.1, in which the flow is turned 11 degrees using a plenum pressure ratio of 1.8 (ratio of plenum pressure to inlet pressure).

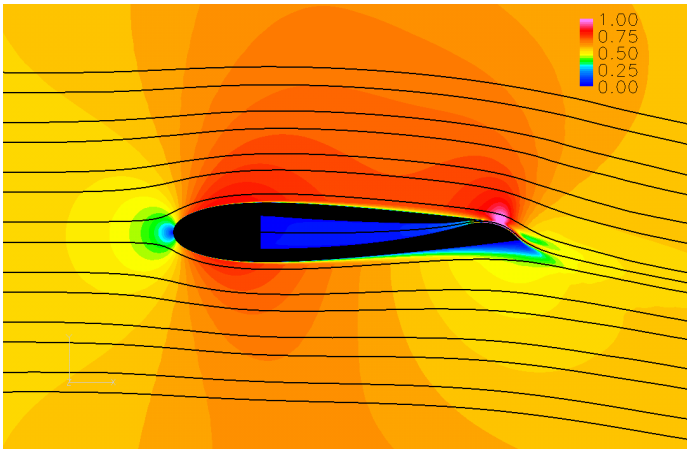

Figure 1.1: Coanda effect applied to an IGV, Mach number flow field

The use of the Coanda effect in external flows is very well documented with research dating back more than 60 years. It was applied to the wings of a Grumman A-6A and flight tested in 1979, resulting in reductions in the aircraft's take-off and landing speeds [8]. The use of leading and trailing edge Coanda blowing on a circulation control wing has been demonstrated by Englar et al. to have the potential to increase lift, increase liftoff gross weight, reduce runway take-off / landing speeds, and reduce system complexity in high lift airfoils for subsonic aircraft [9-11].

Parameters that affect circulation control airfoils that employ Coanda jets have been explored [12- 15]. Larger jet heights have been shown to produce more lift for a given supply pressure, while smaller jet heights produce more lift for a given momentum due to

their higher velocities along the Coanda surface. The shape and size of the Coanda trailing edge affect the ability of an airfoil to perform at a given Mach number. Round trailing edges have been shown to create more lift at lower Mach numbers than elliptical tailing edges, which have been shown to create more lift at higher Mach numbers. However, circulation control airfoils with round trailing edges suffer from increased drag at cruise conditions.

Literature pertaining to the Coanda effect in internal flows is very limited. Harff et al. [28] used counter flow blowing in combination with the Coanda effect to augment flow turning on a circulation control IGV, and found that the circulation control IGV yielded higher losses than a flapped IGV at both on and off design conditions. Furthermore, the circulation control IGV did not meet the desired turning angles for the off design case (achieved 22 degrees of the desired 39). Hill et al. (Chapter 1) showed that a two-dimensional circulation control IGV employing the Coanda effect on the trailing edge of an uncambered IGV could match on-design conditions of 11 degrees of flow turning upstream of the first stage of the compressor test rig TESCOM at 90 percent span.

For circulation control airfoils (external flows), comparisons between experimental data and RANS CFD codes using a variety of turbulence models have been done by many groups. The results of the different turbulence models are mixed when the comparison is made between CFD data and experimental data for pressure distributions, jet detachment, and lift prediction. Viswanathan et al[16], Baker et al[17], and Paterson et al[18], showed that use of isotropic model(s) have resulted in good prediction of pressure distribution when compared to experimental data. Swanson et al[19], and Slomski et al[20] have all shown that the isotropic models have given improper results for the prediction of pressure distribution when compared to experimental values. For the prediction of jet attachment Fasel et al.[21], and Chang et al.[22] showed than the stress transport models yielded good prediction of wall jet separation, while Swanson et al[19], and Slomski et al[20] showed that isotropic models improperly predicted jet detachment. For lift predictions Baker et al.[17], and Viswanathan et al.[16], showed that isotropic models predicted good results for lift coefficient, while Slomski et al.[20], Fasel et al.[21], Swanson et al[19],

showed that isotropic models improperly predicted lift coefficients since the models predicted jet separations further down stream than experimental data.

Objectives

The first object of this study was to determine if the results of a 2D optimization study (Chapter 1) were code independent. The second objective of this study was to determine the effect of using different turbulence models on the prediction of turning angles from the circulation control IGV. In order to accomplish these objectives the commercially available code GASP was employed in combination with three different turbulence models. The code and the turbulence model comparisons were both simulated at a 90% span section of the current IGV in the TESCOM rotating compressor rig, at on-design conditions. This particular radial section was selected because its low solidity (0.595), high inlet Mach number (0.54) and relatively high turning (11 degrees) represented a significant challenge. Furthermore, the TESCOM rig offers a fair representation of engine hardware and a future platform for experimental validation.

Geometry of Circulation Control IGV

The design of the circulation control IGV takes into account requirement to have an internal flow passage (Plenum) to provide air to the Coanda jet. As such, the circulation control airfoil geometry was developed using a relatively thick symmetric NACA series airfoil modified to incorporate a Coanda surface on the trailing edge (see Figure 1.2). In order to prevent excessive blockage due to the thicker profiles, the blade count was reduced by a factor of two resulting in a solidity of 0.595 (based on nominal chord). It has a nominal chord length (C_n) of 4.486 cm, which is the distance of the jet exit from the leading edge of the IGV. However, the true chord can vary between 1.1 nominal chord lengths for the smallest trailing edge radius and 1.15 nominal chord lengths for the largest trailing edge radius. It has a maximum thickness ratio t/C_n of 0.192, located at 30 percent nominal chord length behind the leading edge, and a modified trailing edge thickness, $t_{te}/C_{n,}$ of 0.080 in the region of the jet exit. Unlike traditional Coanda airfoils, the trailing edge is only tangent to the suction surface. This accommodates trailing edge radii that are significantly larger than the thickness at the trailing edge section as shown in Figure 1.3.

This enables the Coanda surface to successfully turn larger circulation control jets without separation. The drawback for radii that are significantly larger than the trailing thickness is that the included angle of the Coanda surface is reduced, limiting the amount of turning (see Figure 1.3).

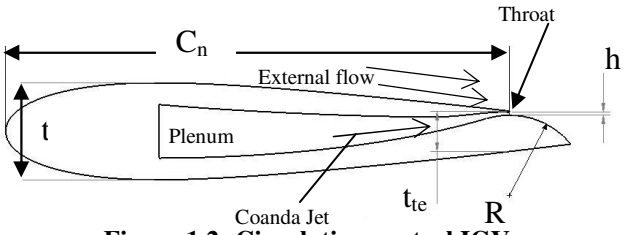

Figure 1.2: Circulation control IGV

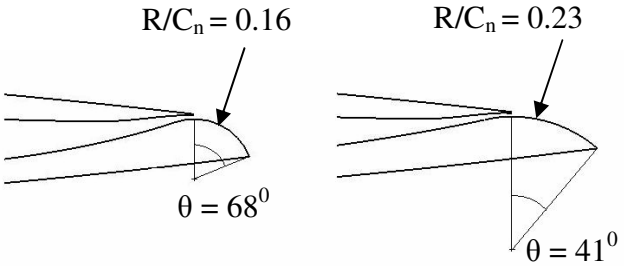

Figure 1.3: Trailing edge curvature comparison $h/C_n = 0.0057$

Methodology

A two dimensional circulation control IGV was simulated at design conditions that are seen at the TESCOM rig at a radial location that corresponded to 90% span of the current cambered IGV. The steady state conditions are simulated at an inlet Mach number of 0.54 and a solidity of 0.595 (based on nominal chord). Furthermore, using the nominal chord for the length scale, the Reynolds number for the circulation control IGV in this region was $5e^5$. To determine if the ADPAC solution using the Spalart-Allmaras model was independent of the code, GASP was employed using the same mesh, same turbulence model, and boundary conditions. The plenum pressure ratio was varied for three blowing rates on a constant radius of $R/C_n = 0.17$. Also the values for trailing edge radius were varied at the highest plenum pressure ratio, $P_{p,ratio}=2.0$, since the highest pressure

represented the most extreme case originally tested for the circulation control IGV. GASP was employed for the turbulence model study since it offered more choices for turbulence models. The turbulence models study was carried out in a similar fashion as the code dependency study, in that the plenum pressure ratio was varied on a constant radius and the trailing edge radius was varied at a constant plenum pressure ratio for both the k-ω and Stress-ω models.

Turbulence models

The first model is the one equation Spalart Allmaras turbulence model, which has been calibrated for flows over airfoils. The Spalart Allmaras (S-A) uses the Boussinesq approximation to relate the mean strain rate to the Reynolds stresses, however the turbulent kinetic energy term is dropped. The basic formulation of the Spalart Allmaras turbulence model is shown below. Full details on the S-A turbulence model formulation and closure coefficients are given in Spalart's and Allmaras's orginal work. [24].

Kinematic Eddy Viscosity

$$\nu_T = \tilde{\nu} f_{v1}$$

Eddy Viscosity Equation

$$\frac{\partial \tilde{\nu}}{\partial t} + U_j \frac{\partial \tilde{\nu}}{\partial x_j} = c_{b1} \tilde{S} \tilde{\nu} - c_{w1} f_w \left(\frac{\tilde{\nu}}{d} \right)^2 + \frac{1}{\sigma} \frac{\partial}{\partial x_k} \left[(\nu + \tilde{\nu}) \frac{\partial \tilde{\nu}}{\partial x_k} \right] + \frac{c_{b2}}{\sigma} \frac{\partial \tilde{\nu}}{\partial x_k} \frac{\partial \tilde{\nu}}{\partial x_k}$$

The second model used, the Wilcox 1998 k-ω model, is a two equation turbulence model that has been shown by Wilcox to predict better results for free shear flows than the 1988 version. Similar to the Spalart-Allmaras model the k-ω model uses the Boussinesq approximation to relate the mean strain rate to the Reynolds stress. However, the k-ω model does not drop the turbulent kinetic energy term. Unlike the k-ε model that calculates the turbulence dissipation ε, the k-ω model uses the specific dissipation rate, which is the ratio of turbulence dissipation to turbulent kinetic energy ω = ε/k. The basic formulation of the model is shown below. For full details on the model as well as closure coefficients the reader should consult Wilcox 1998 [25].

Kinematic Eddy Viscosity

$$\nu_T = \frac{k}{\omega}$$

Turbulence Kinetic Energy

$$\frac{\partial k}{\partial t} + U_j \frac{\partial k}{\partial x_j} = \tau_{ij} \frac{\partial U_j}{\partial x_j} - \beta^* k\omega + \frac{\partial}{\partial x_j}\left[(\nu + \sigma^* \nu_T) \frac{\partial k}{\partial x_j} \right]$$

Specific Dissipation Rate

$$\frac{\partial \omega}{\partial t} + U_j \frac{\partial \omega}{\partial x_j} = \alpha \frac{\omega}{k} \tau_{ij} \frac{\partial U_j}{\partial x_j} - \beta\omega^2 + \frac{\partial}{\partial x_j}\left[(\nu + \sigma \nu_T) \frac{\partial w}{\partial x_j} \right]$$

The last model used was the Reynolds transport model Wilcox 1998 Stress-ω. The Stress-ω model is a non-isentropic model that calculates Reynolds stresses directly, and specific dissipation rate is used in order to calculate turbulence dissipation. Non-isotropic models have been shown to be more accurate for, flows with sudden changes in mean shear rate, flows over curved surfaces, flows in rotating fluids, and flows with boundary layer separation [25], all of which apply to the study of a circulation control airfoil (i.e. circulation control IGV). The basic formulation of the Stress-ω model is given below. The reader should consult Wilcox 1998 [25] for full details on the models formulation and closure coefficients.

Reynolds-Stress Tensor

$$\rho \frac{\partial \tau_{ij}}{\partial t} + \rho U_k \frac{\partial \tau_{ij}}{\partial x_k} = -\rho P_{ij} + \frac{2}{3}\beta^* \rho\omega k \delta_{ij} - \rho I I_{ij} + \frac{\partial}{\partial x_k}\left[(\mu + \sigma^* \mu_T) \frac{\partial \tau_{ij}}{\partial x_j} \right]$$

Specific Dissipation Rate

$$\rho \frac{\partial \omega}{\partial t} + \rho U_j \frac{\partial \omega}{\partial x_j} = \alpha \frac{\rho\omega}{k} \tau_{ij} \frac{\partial U_j}{\partial x_j} - \beta\omega^2 + \frac{\partial}{\partial x_k}\left[(\mu + \sigma \mu_T) \frac{\partial w}{\partial x_k} \right]$$

Codes

Both APDAC and GASP are structured, multi-block codes that solve the integral form of the Reynolds Averaged Navier-Stokes (RANS) equations. ADPAC is a turbomachinery specific code that calculates the conservative variables for density, momentum, and total energy [26]. GASP solves the RANS equations for the primitive variables, density, velocity, and pressure, which requires a transformation between the conservative variables and the primitive variables [26]. The boundary layer across the entire IGV was simulated as turbulent in GASP using three turbulences models: the isotropic one-equation Spalart-Allmaras turbulence model, the two-equation isotropic model k-ω (Wilcox 1998), and the Reynolds stress transport model Stress-ω (Wilcox 1998). In ADPAC the boundary layer across the entire IGV was simulated as turbulent using only the Spalart-Allmaras turbulence model.

Mesh

The 2D circulation control mesh (Figure 1.4a) was built using GRIDGEN and had 28,992 cells that were broken up into 4 blocks: inlet block (832 cells), main block (25024 cells), exit block (1472 cells), and a plenum block (1664 cells). The main block was an O-mesh that wrapped around the IGV, and the other blocks where rectangular. To ensure that the O-mesh captured the boundary layer, 70 percent of the O-mesh cells were within a distance of 5 percent C_n from the walls of the IGV. The near wall spacing of the first cells around the IGV were set to 0.0034 percent C_n in order to capture the sublayer with average y+ values less than 1. Furthermore, the cell spacing before and after the jet exit were also held to 0.0034 percent C_n (Figure 1.4b) in order to capture the shock that occurs when the jet reaches sonic velocities at the jet's exit (throat). The mesh topology stayed constant for each geometric change of the trailing edge radius.

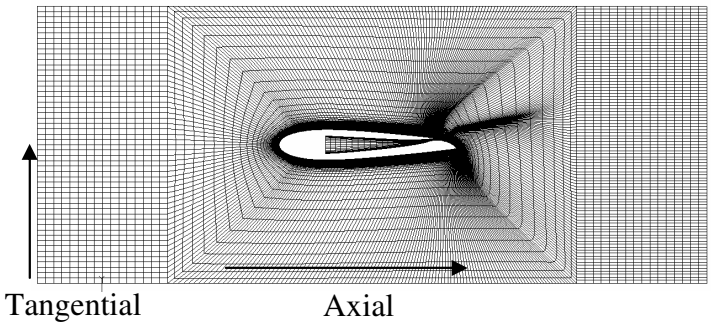

Figure 1.4a: Circulation control IGV mesh

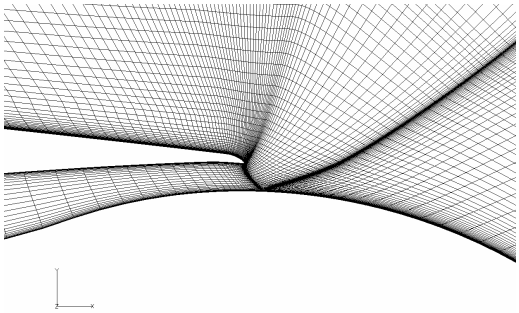

Figure 1.4b: Circulation control IGV Mesh details near the jet exit

Boundary conditions

The mesh had four boundaries: main inlet, plenum inlet, exit, and walls. The total temperature and pressure at the main inlet were set to reference values of standard day conditions (P_{ref} = 101 kPa, T_{ref} = 288 K). At the plenum inlet, the total temperature was set to the reference value, while the ratio of total pressure ($P_{o,p}/P_{ref}$) was varied between 1.4 and 2.0. To maintain an inlet Mach number of 0.54, the static pressure ratio at the exit of the circulation control IGV's mesh ($P_{e,s}/P_{ref}$) was set to 0.80. The wall conditions along the blade and inside the plenum were set to no-slip adiabatic. The upper most tangential cells and lower most tangential cells of the mesh were patched together to create a periodic boundary simulating a linear cascade.

Data reduction and measurement locations

Turning angle

The flow turning angle was defined as the inverse tangent of the mass averaged tangential velocity (U_t) divided by mass averaged axial velocity (U_a).

$$\alpha = \tan^{-1}\frac{U_t}{U_a} \qquad (1.1)$$

Normalized radial and tangential pressure gradients

Pressure gradients above the Coanda surface were determined from lines incremented every five degrees from the jet exit that extended two trailing-edge radius lengths above the Coanda surface. The normalized radial pressure gradients (pressure gradients normal to the Coanda surface) were found along each line using the equation below.

$$\frac{R}{P_{ref}}\frac{\partial P}{\partial r} \tag{1.2}$$

The normalized tangential pressure gradients (pressure gradient tangent to the Coanda surface) were found between each line at a constant radius (r) , using the equation below.

$$\frac{R}{P_{ref} r}\frac{\partial P}{\partial \theta} \tag{1.3}$$

Traditional momentum coefficient

The traditional momentum coefficient used in circulation control airfoil literature is given below in equation 1.4. The quantities, C_t, b, and h are respectively the airfoil's chord length, span, and the jet height. For this study the nominal chord length C_n was used instead of C_t.

$$C_\mu = \frac{\dot{m}_j V_j}{\frac{1}{2}\rho_\infty V_\infty^2 A} = \frac{\rho_j V_j^2 hb}{\frac{1}{2}\rho_\infty V_\infty^2 C_t b} \tag{1.4}$$

Turbomachinery momentum coefficient

The momentum coefficient can be slightly altered for turbomachinery applications since the mass flow rate at the inlet is known. Thus, the turbomachinery momentum coefficient is the ratio of jet momentum to inlet momentum.

$$C_{\mu,Turbomachinery} = \frac{\dot{m}_j V_j}{\dot{m}_i V_i} \tag{1.5}$$

Mass flow rate ratio

The mass flow rate ratio was defined as the ratio of mass flow from the plenum to the total mass flow rate at the exit.

$$C_m = \frac{\dot{m}_j}{\dot{m}_e} \qquad (1.6)$$

Measurement locations

In order to reduce the data, three measurements (Figure 1.5) were taken on the mesh using a FORTRAN code that could interpolate the solution and reduce data into mass-averaged values. The first measurement was located 1.12 nominal chord lengths upstream of the leading edge of the IGV and was used to determine inlet conditions across the entire pitch. The second measurement was located at an axial location equivalent to 1.43 nominal chord lengths downstream of the leading edge of the IGV, and was used to determine exit flow conditions also across the entire pitch. This location represents the hypothetical location of the leading edge of the downstream rotor if the IGV was in the TESCOM test rig. The last measurement was taken across the throat of the plenum (see Figure 1.2) to determine the jet conditions.

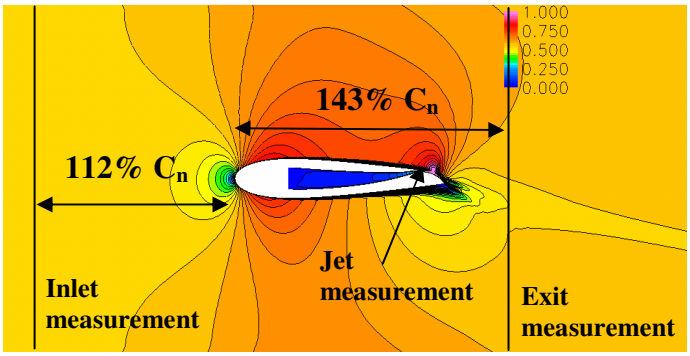

Figure 1.5: Measurement Locations

Results

In a parametric study completed by Hill et al. (Chapter 2) the Spalart-Allmaras turbulence model was used in conjunction with the turbomachinery specific code ADPAC in order

to determine optimal results for the parameters of: jet height, trailing edge radius size, and plenum pressure ratio. From this study, optimal results were found that were able to meet on-design specifications for the TESCOM test rig. Although ADPAC has three turbulence models available, only the S-A model was used for the parametric study. The zero-equation Baldwin-Lomax model was not used because of its poor prediction of separated flows. While use of the k-R model, a modified version of k-ε, was abandoned since attempts to use the k-R model resulted in diverging solutions. Thus, in order to determine the effects of other turbulence models on the prediction of circulation around a circulation control IGV the commercial code GASP was employed, since more turbulence models were available. The results section will first discuss the comparison between the codes, then the results from the turbulence model study. The final conclusion will reference both the code comparison and the turbulence model comparison.

Code comparison results

Results in Figure 1.6 show the comparison between ADPAC and GASP on a turning angle versus trailing edge radius plot. The results for the two codes were compared using the same inlet Mach number and boundary conditions. Furthermore, the comparison was done using the highest plenum pressure ratio used in the optimization study, since the highest pressure ratio was the most extreme case for flow control tested. Both codes were able to predict the same optimal result for trailing edge radius size (R/C_n=0.16) with less than four percent variation between the codes at the peak value (0.4 degree variation). Furthermore, the maximum variation of five percent (0.5 degree variation) between the two codes occurred at the smallest trailing edge radius. Results for the effects of plenum pressure ratio on both turning angle and pressure loss show that both codes also predicted similar trends (Appendix A). From this study, it was concluded that the CFD results were independent of the code. The results from GASP for different turbulence models will be discussed next.

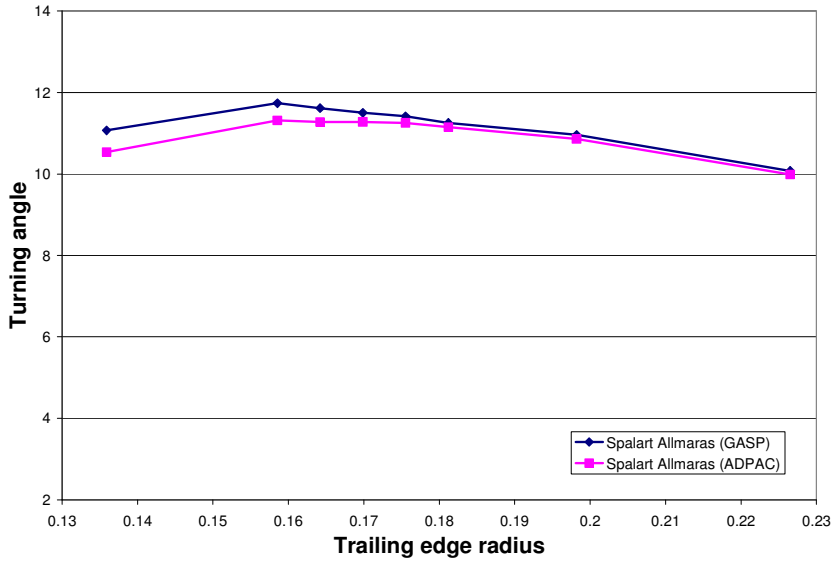

Figure 1.6: Turning angle versus Trailing edge radius, Plenum pressure ratio 2.0, Code comparison

Turbulence model results

Plenum pressure ratio study

The effects of plenum pressure ratio were studied using trailing edge radius size R/C_n = 0.17. This radius was chosen for the plenum pressure ratio study since it showed close agreement between all models for jet detachment locations (within last 2 percent trailing edge arc length) in the trailing edge study, which is discussed later. Figure 1.7, a plot of turning angle versus plenum pressure ratio, presents the results of the plenum pressure ratio study. The blue line indicates the results for the S-A model, while the purple and green lines represent the k-ω and Stress-ω, respectively. The good agreement between trends indicates that the all models predict the same effect of plenum pressure on turning angle. Furthermore, at the lowest plenum pressure ration (1.6) the maximum variation between the turning angle predictions from each model was one degree, which occurred between the Spalart-Allmaras and the Stress-ω models. Excellent trend agreement was also seen for the effect of plenum pressure on Corrected pressure loss, which is presented in Appendix A.

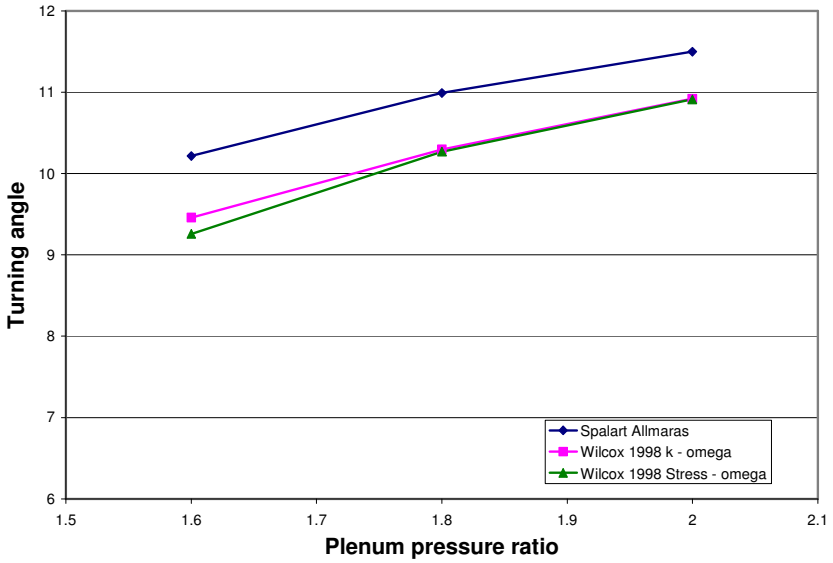

Figure 1.7: Turning angle versus Plenum pressure ratio, R/C_n=0.170

Swanson [19] showed that at higher free stream Mach numbers (0.6), isotropic models were better at capturing the flow physics of a circulation control airfoil at lower momentum coefficients than at higher momentum coefficients. The plenum pressure ratios used in this study resulted in small traditional momentum coefficients (table 1-1) which may explain the agreement of the trends for the variation of plenum pressure ratio.

Table 1-1: Momentum coefficients, R/C_n=0.16, h/C_n=0.0057

Plenum Pressure ratio	Traditional momentum Coefficient	Turbomachinery Momentum Coefficient	Mass flow rate ratio
1.6	0.037	0.011	0.64%
1.8	0.043	0.012	0.72%
2.0	0.048	0.014	0.81%

Trailing edge radius study

A study of the effects of trailing edge radius was conducted using a plenum pressure ratio of 2.0. This blowing ratio was chosen since it was the most extreme of all the plenum pressure ratios studied in the 2D parametric study (Chapter 2). Furthermore, plenum pressure ratio trends were in good agreement in the parametric study indicating that the trend created by the highest blowing ratio would be the same for the lower blowing ratios. Results from the trailing edge radius study are shown in Figure 1.8, a plot of

turning angle versus trailing edge radius for a plenum pressure ratio of 2.0. The blue line indicates the results for the S-A model, while the purple and green lines represent the k-ω and Stress-ω, respectively.

For trailing edge radii above R/C_n=0.160 the models show good trend agreement, with a maximum difference 0.7 degrees occurring between the S-A and Stress-w models at R/C_n=0.160. From this radius size on, jet separation (found by finding the first vector of reverse flow tangent to the Coanda surface) occurs near the final 5 percent of the Coanda surface, as seen in the Mach number flow fields in Figure 1.9. Turbulence models were in closer agreement since the geometry studied has a sharp corner at the pressure side of the trailing edge, which forces the jet from the Coanda surface before the models could predict different jet detachment locations.

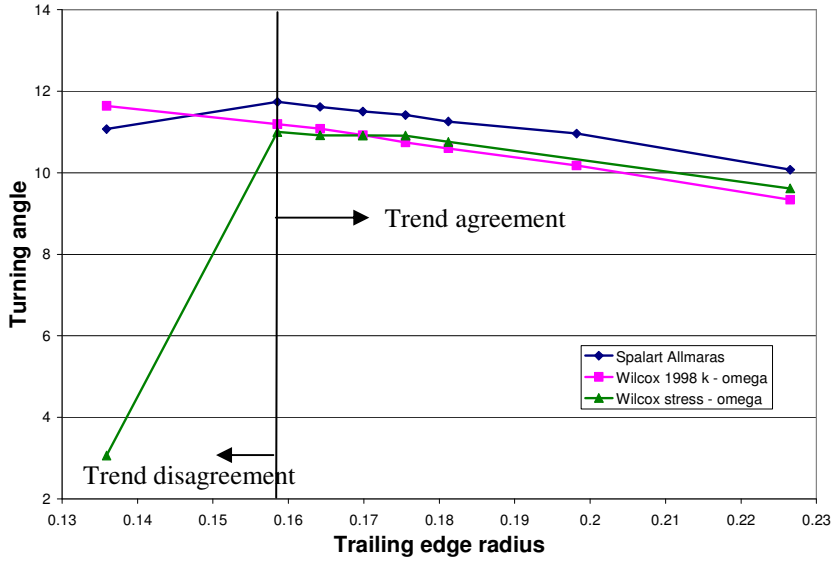

Figure 1.8: Turning angle versus Trailing edge radius, Plenum pressure ratio 2.0, R/C_n = 0.160

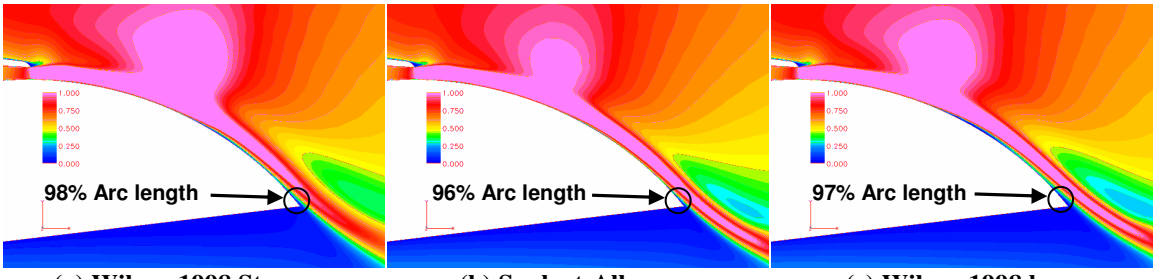

(a) Wilcox 1998 Stress-ω **(b) Spalart-Allmaras** **(c) Wilcox 1998 k- ω**

Figure 1.9: Jet separation locations, Mach number flow field, Plenum pressure ratio 2.0, R/C_n = 0.160

The disagreement between models for the smallest trailing edge radius (R/C_n=0.136) was a direct result of the prediction of jet separation; shown in Mach contour flow field visualizations in Figure 1.10. For the Stress-ω model (Figure 1.10a) the jet completely separates from the Coanda surface, reducing the amount of circulation, at a location that corresponded to 49 percent of the Coanda arc length. The S-A model (Figure 1.10b) predicts the jet separation at 54 percent of the Coanda surface; however, the jet remains close to the wall which resulted in greater circulation than the Stress-ω model. The k-ω model (Figure 1.10c), on the other hand, predicts that jet separation occurs on the final 6 percent of the Coanda surface. This result causes the k-ω model to predict the highest turning angle of all three models, since the fully attached jet is able to create the greatest circulation around the IGV. The results for the smallest trailing edge radius are not surprising since there are many cases in literature which show that isotropic models fail to properly predict jet separation locations for circulation control airfoils [19, 20, 21].

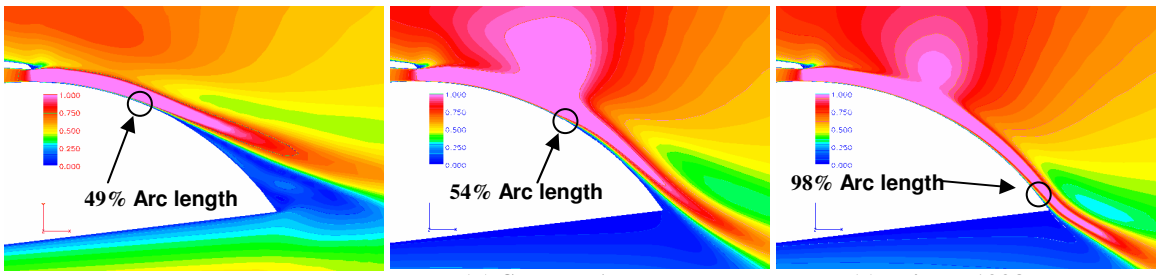

(a) Wilcox 1998 Stress-ω **(b) Spalart-Allmaras** **(c) Wilcox 1998 k- ω**

Figure 1.10: Jet separation locations, Mach number flow field, Plenum pressure ratio 2.0, R/C_n = 0.136

Jet attachment for the isotropic models may be due to the prediction of transonic flow above the IGV's Coanda surface. The transonic flow created a weak shock wave that created larger radial pressure gradients (pressure gradients normal to the Coanda surface) than the Stress-ω model. The larger radial pressure gradients of the isotropic models forced the jet to remain attached to the Coanda surface. Figure 1.11 shows both the tangential and radial pressure gradients just above the Coanda surface. The blue and purple lines represents the S-A and k-ω models respectively, while the green line represents the Stress-ω model. The maximum normalized radial pressure gradient (0.75)

shown in Figure 1.11a occurred at a distance of r/R =1.2 above the Coanda surface, at 30 degrees from the jet exit. While the maximum adverse tangential pressure gradient (1.66) in Figure 1.11b occurred at a distance of r/R=1.05 above the Coanda surface, also at 30 degrees from the jet exit. Both the radial pressure gradients and the tangential gradients were the same for the isotropic models; however the Stress-ω model predicts lower radial pressure gradients above the Coanda surface, implying that the jet separated due to the centripetal forces created by the jet overcoming the pressure forces. For the isotropic models the radial pressure gradient allowed the Coanda jet to overcome the adverse tangential pressure gradients on the Coanda surface. It is not known if the prediction of transonic flow above the Coanda surface is physical, due to the lack of experimental data. However, the effect of streamline curvature is a known mechanism for failure of isotropic models [25], since sharper curvature gives rise to unequal normal stress that the isotropic models cannot predict.

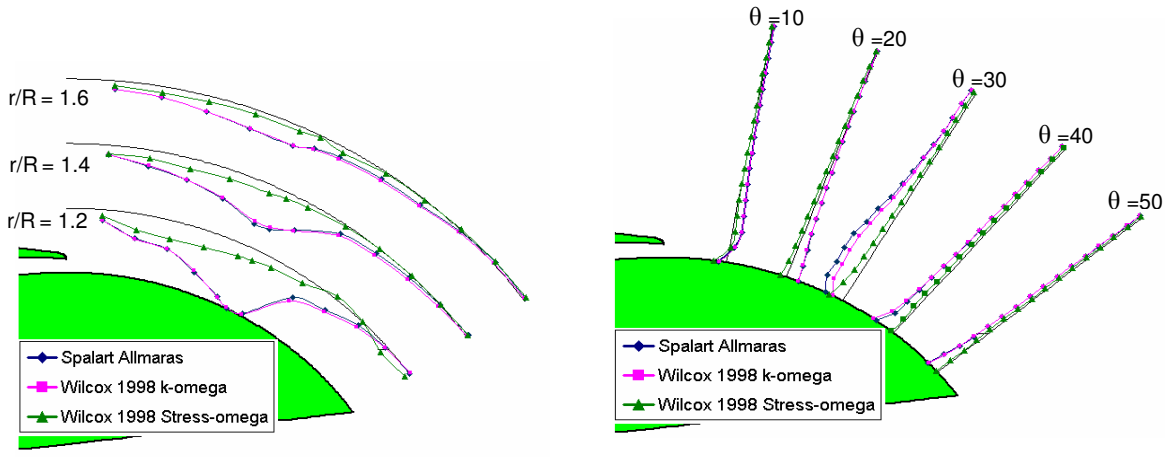

(a) Radial pressure gradient **(b) tangential pressure gradient**

Figure 1.11: Pressure gradient distribution on trailing edge radius R/C_n=0.136

Conclusion

The results of the code comparison showed that CFD results using the Spalart-Allmaras turbulence model were code independent, since both codes predicted the same optimal value for trailing edge radius size with only minor differences between solutions at the optimal trailing edge radius. In the turbulence model study, the range of plenum pressure ratios tested showed excellent agreement between trends, indicating that the results for

the plenum pressure ratio study for the optimization study may be correct. However, due to a lack of experimental data these results have not been validated. The results for the trailing edge radius study showed that the trends for all the models were in good agreement for the range of trailing edge radius beyond R/C_n=0.16. Beyond this radius the jet separation was within the final 5% of the trailing edge radius arc length for all the models studied. Furthermore, the geometry of the IGV did not allow for disagreement of jet separation between the models, since the Coanda surface came to a sharp edge at the pressure side of the IGV that forced the jet from the Coanda surface before the models could predict different jet separation locations. The models were in disagreement for the smallest trailing edge radius size. This may be a direct result of the isotropic models' prediction of transonic flow above the Coanda surface. Currently it is not known which model predicts solutions closer to actual physical results, since there is no experimental data available to validate this study. When the trailing edge radius was sufficiently large the trend agreement between the isotropic models and the non-isotropic model Stress-ω suggest that isotropic models are accurate for Coanda flow predictions as long as the trailing edge is sufficiently large. The decreased computational time of the Spalart-Allmaras model over both the k-ω (two times faster in GASP) and Stress-ω (six times faster in GASP) models makes the S-A model an attractive choice when there is a large number of cases to run. Furthermore, when the S-A model is employed in ADPAC the solutions converged nearly two times faster than when the S-A model is employed by GASP, thus for the parametric study in Chapter 2 ADPAC was employed using the S-A model.

References

1. Bensor, W.A., "Compressor Operation with One or More Blade Rows Stalled", pp. 341-364, NASA SP-36, 1965
2. Budinger, R. E., Kaufman, H. R., "Investigation of the Performance of a Turbojet Engine with Variable-Position Compressor Inlet Guide Vanes", NACA RM-E54L23a, 1955
3. Dobson, W. F., Wallner, L. E., "Acceleration Characteristics of a Turbojet Engine with Variable-Position Inlet Guide Vanes", NACA RM-E54I30, 1955.
4. Wallner, L. E., Lubick, R. J., "Steady State and Surge Characteristics of a Compressor Equipped with Variable Inlet Guide Vanes Operating in a Turbojet Engine", NACA RM-E54I28, 1955.

5. Lord, W. K., MacMartin, D. G., Tillman, T. G., "Flow Control Opportunities in Gas Turbine Engines", AIAA Paper 2000-2234, 2000.
6. *Romanian Inventions And Prioritites In Aviation*, Constantin C. Gheorghiu, Ed. Albatros, Bucharest, 1979.
7. Jones, G. S., Viken, A. E., Washburn, L, N., Jenkins, L, N., Cagle, C, M., "An Active Flow Circulation Controlled Flap Concept for General Aviation Aircraft Applications", AIAA Paper 2002-3157, 2002
8. Pugliese, A. J., Bethpage, N. Y., Englar, R. J., "Flight Testing the Circulation Control Wing", AIAA Paper 1979-1791, 1979.
9. Englar, R. J., Smith, M. J., Kelley, S. M., Rover, R. C., "Development of Circulation Control Technology for Application to Advanced Subsonic Transport Aircraft", AIAA Paper 1993-0644, 1993.
10. Englar, R. J., Smith, M. J., Kelley, S. M., Rover, R. C., "Application of Circulation Control to Advanced Subsonic Aircraft, Part I: Airfoil Development", *Journal of Aircraft,* Vol. 31, No. 5, 1994, pp. 1160-1168.
11. Englar, R. J., Smith, M. J., Kelley, S. M., Rover, R. C., "Application of Circulation Control to Advanced Subsonic Aircraft, Part II: Transport Application", *Journal of Aircraft,* Vol. 31, No. 5, 1994, pp. 1169-1168.
12. Abramson, J., Rogers, E. O., "High-Speed Characteristics of Circulation Control Airfoils", AIAA Paper 1983-0265, 1983.
13. Englar, R. J., Huson, G. G., "Development of Advanced Circulation Control Wing High Lift Airfoils", AIAA Paper 1983-1847, 1983
14. Jones, G. S., Viken, A. E., Washburn, L, N., Jenkins, L, N., Cagle, C, M., "An Active Flow Circulation Controlled Flap Concept for General Aviation Aircraft Applications", AIAA Paper 2002-3157, 2002
15. Wood, N., Nielsen, J., "Circulation Control Airfoils Past, Present, Future", AIAA Paper 1985-0204, 1985.
16. Viswanathan, A. K., Tafti, D. K., "Numerical Analysis of Circulation Control on a NCCR 1510-7607N Airfoil using RANS Models", 2004 Circulation Control Conference, March 16-17, Hampton, Virginia, USA. NASA/CP-2005-213509
17. Baker, W. J., Paterson, E. G., "RANS CFD Simulation of a Circulation-Control Foil: Validation of Performance, Flow Field, and Wall Jet", AIAA Paper 2006-3010, 2006
18. Paterson, E, G., Baker, W, J., "Simulation of Steady Circulation Control For Marine-Vehicle Control Surfaces", AIAA Paper 2004-748, 2004
19. Swanson, R, C., Rumsey, C, L., Anders, S, G., "Aspects of Numerical Simulation of Circulation Control Airfoils", *Applications of Circulation Control Technology (pp. 469-498)*, American Institute of Aeronautics and Astronautics
20. Slomski, J, F., Gorski, J, J., Miller, R, W., "Numerical Simulation of Circulation Control Airfoils as Affected by Different Turbulence Models", AIAA Paper 2002-0851, 2002
21. Fasel, H, F., Gross, A., Wernz, S., "Investigation of Turbulent Coanda Wall Jets Using DNS and RANS", *Applications of Circulation Control Technology (pp. 401-420)***,** American Institute of Aeronautics and Astronautics

22. Chang, P, A., Slomski, J, A., Marino, T., Michael, E, P., "Numerical Simulation of Two- and Three-Dimensional Circulation Control Problems", AIAA Paper 2005-80, 2005
23. Hill, H, E., "2D CFD Simulation of a Circulation Control Inlet Guide Vane," Masters Thesis, Virginia Polytechnic Institute and State University, 2007
24. Spalart, P, R., Allmaras, S, R., "A One-Equation Turbulence Model for Aerodynamic Flows", AIAA Paper 1992-0439, 1993
25. Wilcox, D, C. (1998), **Turbulence Modeling for CFD**, La Canada CA: DCW Industries.
26. Hall, E. J., Heidegger, N. J., Delaney, R. A., 1999. "ADPAC v1.0 User's Manual," NASA Contract Report 1990-20660, February.
27. *GASP 4.0 User Manual*, AeroSoft
28. Harff, M, R., Wolff, M, J., Copenhaver, W, W., "A CFD Investigation of IGV Flow Vectoring by Counter Flow Blowing" IGTI Paper GT2004-53941

Chapter 2:

2D PARAMETRIC STUDY USING CFD OF A CIRCULATION CONTROL INLET GUIDE VANE

H. E. Hill, W. F. Ng, and P. P. Vlachos
Virginia Polytechnic and State University
Blacksburg, VA 24061

S. A. Guillot
Techsburg Inc.
2901 Prosperity Rd.
Blacksburg, VA 24060

D. Car
Air Force Research Laboratory
WPAFB, Dayton OH

Submitted to the 2007 IGTI Conference

Abstract

Circulation control inlet guide vanes (IGVs) may provide significant benefits over current IGVs that employ mechanical means for flow turning. This paper presents the results of a two-dimensional computational study on a circulation control IGV that takes advantage of the Coanda effect for flow vectoring. The IGV in this study is an uncambered airfoil that alters circulation around itself by means of a Coanda jet that exhausts along the IGV's trailing edge surface. The IGV is designed for an axial inlet flow at a Mach number of 0.54 and an exit flow angle of 11 degrees. These conditions were selected to match the operating conditions of the 90% span section of the IGV of the TESCOM compressor rig at the Compressor Aero Research Laboratory (CARL) located at Wright-Patterson AFB, the hardware that is being used as the baseline in this study. The goal of the optimization was to determine the optimal jet height, trailing edge radius, and supply pressure that would meet the design criteria while minimizing the mass flow rate and pressure losses. The optimal geometry that was able to meet the design requirements had a jet height of $h/C_n = 0.0057$ and a trailing edge Radius $R/C_n = 0.16$. This geometry needed a jet to inflow total pressure ratio of 1.8 to meet the exit turning angle requirement. At this supply pressure ratio the mass flow rate required by the flow control system was 0.71 percent of the total mass flow rate through the engine. The optimal circulation control IGV had slightly lower pressure losses when compared with a reference cambered IGV.

Nomenclature

C_n – Nominal chord length
C_t – Total Chord length
C_m – Mass flow rate ratio
h – Coanda jet height
$\dot{m}$ – Mass flow rate
M – Mach number
P – Pressure
P_{ref} – Reference Pressure
q – Dynamic pressure
R – Trailing-edge radius
s – Blade Pitch
t – Blade thickness
T – Temperature
T_{ref} – Reference Temperature
U – Velocity
α – Turning angle
ρ – Density
σ – Cascade solidity (scaled by C_n)
ω_c – Mass averaged loss coefficient
θ – Trailing edge radius curvature

Subscripts

a – Axial
o – Stagnation conditions
c – Corrected
e – Exit conditions
i – Inlet conditions
j – Jet conditions
n – Nominal (length from the leading edge to jet exit)
p – Plenum conditions
s – Static conditions
te – Trailing edge

Abbreviations

IGV – Inlet Guide vane
TESCOM – Three stage compressor test rig (TESt COMpressor)

Introduction

Motivation

In order to operate at peak performance, many of today's fan compressors require variable flow angles into their first rotating stage. To meet those conditions, Inlet Guide

Vanes (IGVs) control the flow angle into a fan compressor first stage with the use of variable geometries and flaps. The problems that arise with variable IGVs relate to the mechanical devices that are utilized to turn the vane or flap. These devices add significantly to the engine part count, resulting in added weight and maintenance cost. The use of an un-cambered circulation control IGV capable of vectoring the inlet flow without being mechanically actuated may be able to reduce the number of blades and parts, resulting in an engine that is lighter and less expensive to maintain.

Literature Review

Variable inlet guide vanes are used to improve compressor performance through a range of operating conditions [1-4]. The use of a circulation control IGV was suggested by Lord et al. as a means to replace complex flapped inlet guide vanes with a simpler configuration to reduce weight and cost [5]. One such method of circulation control is by means of the Coanda effect on the trailing edge of an airfoil. The Coanda effect was first patented by Henri Coanda in 1934 after he noticed that hot gasses and flames remained attached to his 1910 air reactive airplane [16]. The Coanda effect occurs when the free stream flow above a curved surface is entrained by a parallel high momentum wall jet blown tangentially along the curved surface. The jet stays attached to the curved surface due to the balance between centrifugal force around curved surface and the sub-ambient pressure in the jet sheet [12]. The jet's momentum allows the oncoming boundary layer to overcome an adverse pressure gradient along the curved surface, and it entrains the flow above it due to its lower pressure. The entrained flow is accelerated around the curved surface by the jet, increasing the amount of circulation over the suction side of a body. This increased circulation translates to increased lift and flow turning for an airfoil that employs the Coanda effect. An example of the Coanda effect, applied to an inlet guide vane, can be seen in Figure 2.1, in which the flow is turned though 11 degrees using a plenum pressure ratio of 1.8; demonstrated by the streamlines.

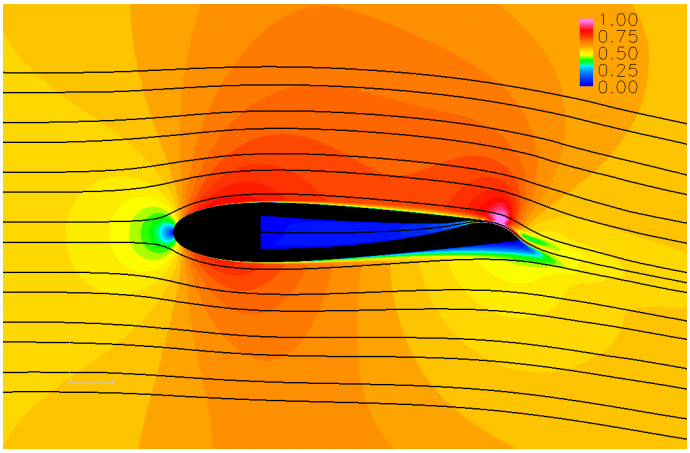

Figure 2.1: Coanda effect applied to an IGV, Mach number flow field

The use of the Coanda effect in external flows is very well documented with research dating back more than 60 years. It was applied to the wings of a Grumman A-6A and flight tested in 1979, resulting in reductions in the aircraft's take-off and landing speeds [6]. The use of leading and trailing edge Coanda blowing on a circulation control wing has been demonstrated by Englar et al. [7] to have the potential to increase lift, increase liftoff gross weight, reduce runway take-off / landing speeds, and reduce system complexity in high lift airfoils for subsonic aircraft [7-9].

Parameters that affect circulation control airfoils that employ Coanda jets have been explored [10- 13]. Larger jet heights have been shown to produce more lift for a given supply pressure, while smaller jet heights produce more lift for a given momentum due to their higher velocities along the Coanda surface. The shape and size of the Coanda trailing edge affect the ability of an airfoil to perform at a given Mach number. Round trailing edges have been shown to create more lift at lower Mach numbers than elliptical tailing edges, which have been shown to create more lift at higher Mach numbers. However, circulation control airfoils with round trailing edges suffer from increased drag at cruise conditions.

Literature pertaining to the Coanda effect in internal flows is very limited. Harff et al. [17] used counter flow blowing in combination with the Coanda effect to augment flow turning on a circulation control IGV, and found that the circulation control IGV yielded higher losses than a flapped IGV at both on and off design conditions. Furthermore, the

circulation control IGV did not meet the desired turning angles for the off design case (achieved 22 degrees of the desired 39).

Objectives

The first objective of this study was to prove that circulation control IGVs could physically replace cambered, variable IGV at design conditions. In order to accomplish this objective, a two-dimensional circulation control IGV was created to meet the design requirements of the 90% span section of the IGV in the TESCOM rotating compressor rig, hardware that offers a fair representation of engine hardware. This radial section was selected since its low solidity, high-inlet Mach number and relatively high turning represented a significant challenge. As such, a successful design of this section would represent a significant milestone toward designing a circulation-controlled replacement for the TESCOM IGV; henceforth called the baseline IGV. The second objective was to optimize the trailing edge of the circulation control IGV. This requires finding the optimal jet height and trailing edge radius that would use the least amount of supply pressure and create the least amount of pressure loss, making the circulation controlled IGV not only a capable replacement of the traditional IGV but a viable alternative. Once these objectives are met, future work will focus on designing and fabricating hardware to be tested in the Compressor Aero Research Laboratory (CARL) at Wright-Patterson Air Force Base (WPAFB).

Geometry of Circulation Control IGV

The design of the circulation control IGV takes into account requirement to have an internal flow passage (Plenum) to provide air to the Coanda jet. As such, the circulation control airfoil geometry was developed using a relatively thick symmetric NACA series airfoil modified to incorporate a Coanda surface near the trailing edge (see Figure 2.2). In order to prevent excessive blockage due to the thicker profiles, the blade count was reduced by a factor of two resulting in a solidity of 0.595 (based on nominal chord). It has a nominal chord length (C_n) of 4.486 cm, which is the distance of the jet exit from the leading edge of the IGV. However, the true chord can vary between 1.1 nominal chord lengths for the smallest trailing edge radius and 1.15 nominal chord lengths for the largest

trailing edge radius. It has a maximum thickness ratio t/C_n of 0.192 located at 30 percent nominal chord length behind the leading edge, and a modified trailing edge thickness, $t_{te}/C_{n,}$ of 0.080 in the region of the jet exit. The trailing edge is only tangent to the suction surface, which accommodates trailing edge radii that are significantly larger than the thickness at the trailing edge section as shown in Figure 2.3. This enables the Coanda surface to successfully turn larger flow control jets without separation. The drawback for radii that are significantly larger than the trailing thickness is that the included angle of the Coanda surface is reduced, limiting the amount of turning (see Figure 2.3).

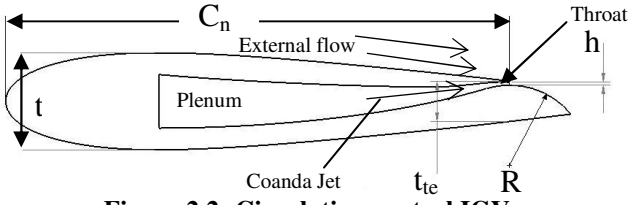

Figure 2.2: Circulation control IGV

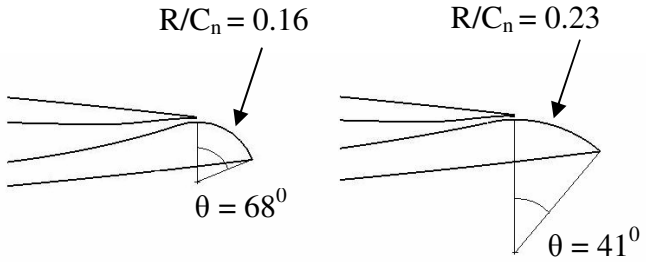

Figure 2.3: Trailing edge curvature comparison h/Cn = 0.0057

The 90% span section of the TESCOM IGV has an axial chord length of 5.1 cm with a maximum thickness ratio of 0.1 located 40 percent axial chord length behind the leading edge. Results from the circulation control IGV will be compared to this baseline.

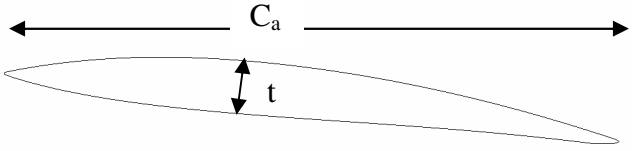

Figure 2.4: Baseline IGV

Methodology

A two dimensional circulation control IGV was simulated at design conditions that are seen at the TESCOM rig at a radial location that corresponded to 90% span of the current cambered IGV. The steady state conditions simulated are an inlet Mach number of 0.54 and an exit flow angle of 11 degrees into the first rotating fan stage of the compressor. Furthermore, using the nominal chord for the length scale, the Reynolds number for the circulation control IGV in this region was $5e^5$.

Code

The 2D circulation control IGV and cambered IGV were simulated using Advanced Ducted Propfan Analysis Code (ADPAC), which is a fully viscous Reynolds Averaged Navier Stokes (RANS) model [14]. The boundary layer across the entire IGV was simulated as turbulent using the one equation Spalart-Allmaras turbulence model. The Spalart-Allmaras (S-A) model was chosen because of its increased accuracy over the Baldwin-Lomax turbulence model in predicting separated flows and its decreased computational time over a two-equation turbulence model [Chapter 1]. Furthermore, ADPAC was chosen over the commercial code GASP due to the lower computational time when employing the S-A model [Chapter 1].

Mesh

The 2D circulation control mesh (Figure 2.5) was built using GRIDGEN and had 28,992 cells that were broken up into 4 blocks: inlet block (832 cells), main block (25024 cells), exit block (1472 cells), and a plenum block (1664 cells). The main block was an O-mesh that wrapped around the IGV, and the other blocks where rectangular. To ensure that the O-mesh captured the boundary layer, 70 percent of the O-mesh cells were within a distance of 5 percent C_n from the walls of the IGV. The near wall spacing of the first cells around the IGV were set to 0.0034 percent C_n in order to capture the sublayer with average y+ values less than 1. Furthermore, the cell spacing (Figure 2.5b) before and after the jet exit were also held to 0.0034 percent C_n in order to capture the shock that occurs when the jet reaches sonic at the jet's exit (throat). The mesh topology stayed constant for each geometric change of the Coanda jet, and trailing edge radius.

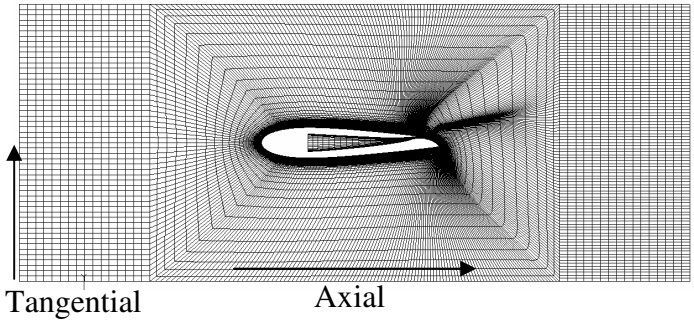

Figure 2.5a: Circulation control IGV mesh

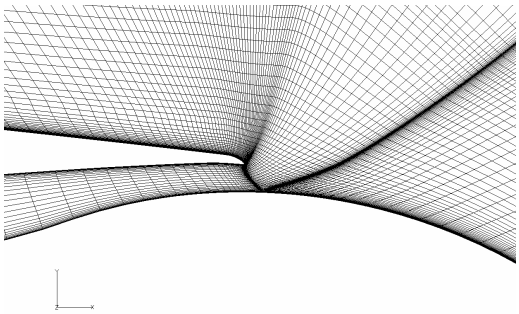

Figure 2.5b: Circulation control IGV Mesh details near the jet exit

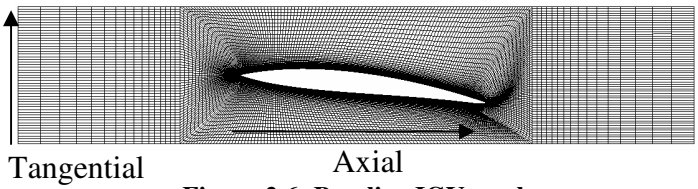

Figure 2.6: Baseline IGV mesh

The cambered IGV's mesh, which was used as the baseline, was set up in a similar fashion (Figure 2.6) with fewer cells in the main block (22,848) and exit block (960) due to the absence of a plenum, which was required for the circulation control IGV.

Boundary conditions

The mesh had four boundaries: main inlet, plenum inlet, exit, and walls. The total temperature and pressure at the main inlet were set to reference values of standard day conditions (P_{ref} = 101 kPa, T_{ref} = 288 K). At the plenum inlet, the total temperature was set to the reference value, while the ratio of total pressure ($P_{o,p}/P_{ref}$) was varied between 1.4 and 2.0. To maintain an inlet Mach number of 0.54, the static pressure ratio at the exit of the circulation control IGV's mesh ($P_{e,s}/P_{ref}$) was set to 0.80. The wall conditions along the blade and inside the plenum were set to no-slip adiabatic. The upper most tangential

cells and lower most tangential cells of the mesh were patched together to create a periodic boundary to simulate a linear cascade.

Studied parameters

The geometric parameters studied were along the trailing edge of the airfoil and included the jet height (h) and trailing edge radius (R) (see Figure 2.2). Along with the geometric study of the airfoils trailing edge there were four supply pressure ratios studied: 1.4, 1.6, 1.8, and 2.0.

Data reduction and measurement locations

Energy considerations

In order to compensate for the added total pressure from the Coanda jet, a corrected total pressure was calculated by mass averaging the inlet and supply total pressures.

$$P_{oc} = \frac{P_{oi}\dot{m}_i + P_{oj}\dot{m}_j}{\dot{m}_i + \dot{m}_j} \qquad (1.1)$$

The corrected pressure loss coefficient was calculated as the change in total corrected pressure loss normalized by the inlet dynamic pressure.

$$\omega_c = \frac{P_{oc} - P_{oe}}{P_{oi} - P_{si}} \qquad (1.2)$$

Turning angle

The flow turning angle was defined as the inverse tangent of the mass averaged tangential velocity (U_t) divided by mass averaged axial velocity (U_a).

$$\alpha = \tan^{-1}\frac{U_t}{U_a} \qquad (1.3)$$

Mass flow rate ratio

The mass flow rate ratio was defined as the ratio of mass flow from the plenum to the total mass flow rate at the exit.

$$C_m = \frac{\dot{m}_j}{\dot{m}_e} \qquad (1.4)$$

Traditional momentum coefficient

The traditional momentum coefficient used in circulation control airfoil literature is given below in equation 1.5. The quantities, C_t, b, and h are respectively the airfoil's chord length, span, and the jet height. For this study the nominal chord length C_n was used instead of C_t.

$$C_\mu = \frac{\dot{m}_j V_j}{\frac{1}{2}\rho_\infty V_\infty^2 A} = \frac{\rho_j V_j^2 hb}{\frac{1}{2}\rho_\infty V_\infty^2 C_t b} \qquad (1.5)$$

Turbomachinery momentum coefficient

The momentum coefficient can be slightly altered for turbomachinery applications since the mass flow rate at the inlet is known. Thus, the turbomachinery momentum coefficient is the ratio of jet momentum to inlet momentum.

$$C_{\mu,Turbomachinery} = \frac{\dot{m}_j V_j}{\dot{m}_i V_i} \qquad (1.6)$$

Measurement locations

In order to reduce the data, three measurements (Figure 2.7) were taken on the mesh using a FORTRAN code that could interpolate the solution and reduce data into mass averaged variables. The first measurement was located 1.12 nominal chord lengths upstream of the leading edge of the IGV and was used to determine inlet conditions across the entire pitch. The second measurement was located at an axial location equivalent to 1.43 nominal chord lengths downstream of the leading edge of the IGV, and was used to determine exit flow conditions also across the entire pitch. This location

represents the hypothetical location of the leading edge of the downstream rotor if the IGV was in the TESCOM test rig. The last measurement was taken across the throat of the plenum (see Figure 2.2) to determine the jet conditions.

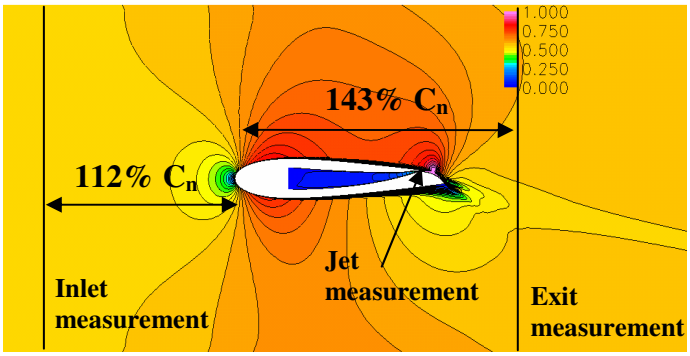

Figure 2.7: Measurement Locations, Mach number flow field

Results

The results section includes seven parts. The first three parts discuss the effects of jet height, trailing edge radius, and flow control supply pressure ratio on turning angle. The next three parts discuss the effect of the same parameters on pressure losses. Part seven, the final part is a comparison between the circulation control IGV and the reference cambered IGV.

Effects of Jet height on turning angle

Figure 2.8 shows the effect of jet height on turning angle when the trailing edge radius was varied between $0.10 \leq R/C_n \geq 0.23$ at a constant supply pressure ratio of 1.8. For the smallest jet height $h/C_n = 0.0045$, radii smaller than $R/C_n = 0.14$ resulted in diverging solutions. Furthermore, the largest radius was only tested on $h/C_n=0.0057$, due to the low turning angle generated. Each colored line in Figure 2.8 represents a constant jet height and the dashed line represents the IGV design goal of 11 degrees of turning. The jet height that met design conditions at the lowest supply pressure was $h/C_n = 0.0057$, as seen in Figures 2.8 and 2.9. However, depending on the compressor's tolerance to exit flow angle, the smaller jet height of $h/C_n = 0.0045$ would be better. For the same supply pressure ratio, the smallest jet height fell short of the desired turning angle by less than 0.5 degree but used only 0.56 percent of the total mass flow rate while the jet with the

height of $h/C_n = 0.0057$ used 0.71 percent of the total mass flow rate. Each increase in jet height, in Fig. 9, raised the total mass flow rate out of the plenum by 0.15 percent of the total mass flow rate. For $h/C_n = 0.0045$, a rise in supply pressure to 2.0 increased the mass flow rate out of the plenum by only 0.07 percent of the total mass flow rate, and allowed the smaller jet height to meet and exceed the required turning angle. The trade off for using the smaller jet to meet the exit turning angle was the higher supply pressure ratio that was required and thus greater pressure losses that will be discussed later.

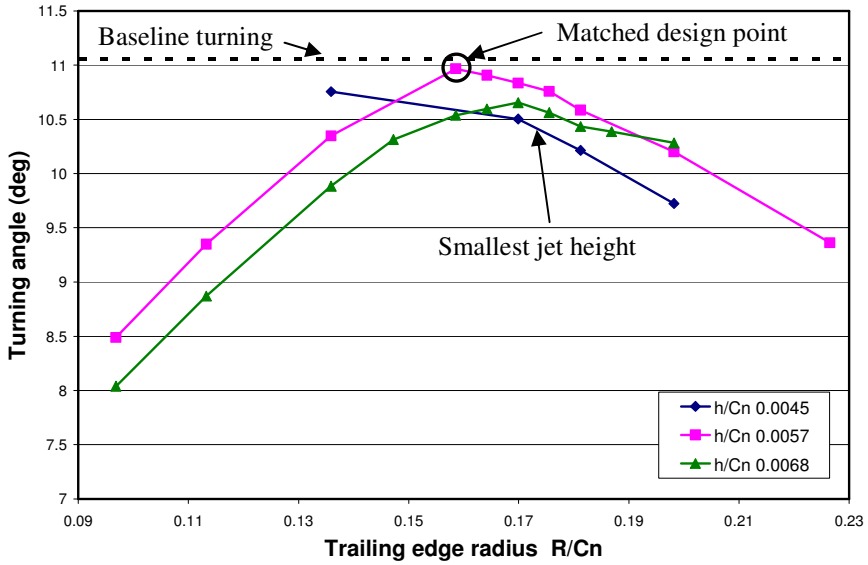

Figure 2.8: Effect of jet height - Turning angle vs. Trailing edge Radius for Supply pressure ratio 1.8

Intuition would lead one to believe that the higher momentum of the larger jets would have more control authority to create the desired turning. However, in order for the geometry to incorporate a larger jet height the amount of curvature of the trailing edge radii was slightly reduced when compared to a smaller jet height. Thus, the larger jet heights fell short of the design goal due to the reduced curvature of the trailing edge radius, especially near the range of the larger jet height's optimal trailing edge radius. Smaller trailing edge radii generated higher radial forces that could not be counteracted by the opposing pressure forces, resulting in early jet separation from the Coanda surface. Early jet separation from the Coanda surface reduced the effective area of the Coanda surface resulting in lower circulation and flow turning. For the larger radii there was too

little curvature to be effective due to the finite thickness of the trailing edge, as described with Figure 2.3.

Effects of trailing edge radius on turning angle

Figure 2.9 shows the variation of turning angle for the range of trailing edge radii studied. In this Figure the jet height is held constant at $h/C_n = 0.0057$ and each line represents a constant supply pressure ratio. The dashed line represents the turning angle of the reference cambered IGV in the TESCOM rig at CARL. The optimal radius for a jet height of $h/C_n = 0.0057$ was $R/C_n = 0.16$. Using the jet height of $h/C_n = 0.0057$ and a supply pressure ratio of 1.8, this radius was able to achieve the required 11 degrees of exit flow turning. For a constant jet height of $h/C_n = 0.0057$, radii less than $R/C_n = 0.16$ did not allow the jets to remain fully attached. Early jet detachment along the trailing edge limited the amount of circulation around the IGV, because the IGV was essentially stalled. Separation indicated that pressure forces acting to hold the jet to the Coanda surface were no longer adequate to overcome the radial forces acting to pull it away. The larger radii did not have the same problems with jet detachment. However, the larger radii were not sharp enough to sufficiently expand the jet to create the lower pressures and higher velocities needed for maximum flow entrainment; hence, the flow turning was not sufficient. Additionally, the jet exits the trailing edge at a shallower angle (jet flap effect). Identification of the jet separation location along the trailing edge in the CFD solutions revealed that the most effective radii resulted in jet separation near the final five percent of the trailing edge arc length. This indicated that the optimal trailing edge radius had nearly fully utilized the jet's energy. Radii that did not experience jet detachment by the trailing edge indicated that the attached jets still had potential to entrain flow. Flow entrainment in these cases would be greater for larger trailing edge radii due to a larger surface area if they were allowed to have the same curvature as the optimal radius; however, the arc length of the trailing edge was limited by the airfoil thickness. Thus, the larger radii were less effective because the attached jets were forced off the trailing edge before they had sufficiently turned through enough curvature.

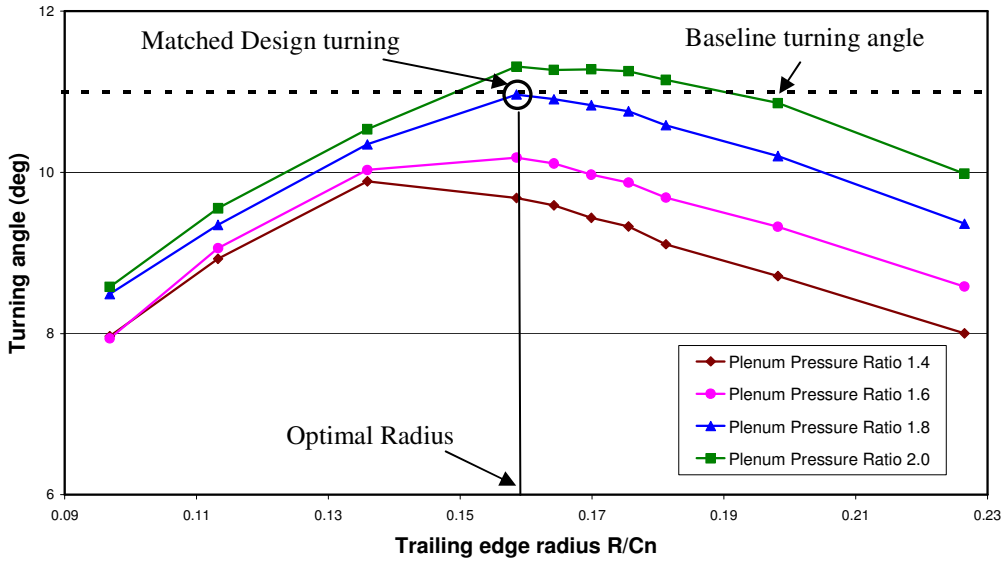

Figure 2.9: Turning angle versus Trailing edge radius for h/C_n 0.0057

Figures 2.10, 2.11, and 2.12 show flow field visualizations (Mach number contours) for the optimal radius, a radius smaller than optimum, and a radius larger than optimum respectively. From the flow field visualizations, it is important to note that the Mach contours ($0.7 < M < 1.0$) above the suction side of the of the IGV at the jet location in Figure 2.10 extended further away from the airfoil than in Figures 2.11 and 2.12, indicating a larger region of higher velocity flow above the suction side for trailing edge radius $R/C_n = 0.16$. Furthermore, Mach contours ($0 < M < 0.5$) are closer to the pressure side of the IGV (R/C_n 0.16), which indicated a larger area of lower velocity. The increased velocity above the suction side and decreased velocity below the pressure side indicate that the trailing edge radius R/C_n 0.16 generated a higher amount of circulation around the airfoil for the given jet height and supply pressure ratio (h/C_n=0.0057, $P_{p,o}$=1.8). The smaller Mach contours near the jet region for both the larger and smaller radii show reduced circulation for radii that are different from the optimal value. The trailing edge stagnation region below the pressure side of the airfoil in Fig. 2.10 was larger and extended farther away from the airfoil than in Figures 2.11 and 2.12, which also indicated higher circulation. The Mach contours for Figures 2.11 and 2.12 were similar, indicating that both the smallest trailing edge radii and the largest trailing edge radii studied had nearly the same amount of circulation; however, the larger radii had slightly increased turning, indicating that the larger radius had a higher amount of circulation.

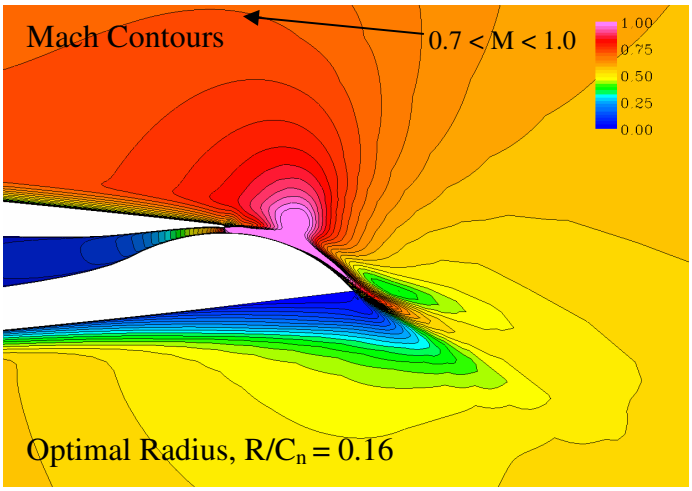

Figure 2.10: Optimal radius, $h/C_n = 0.0057$, $R/C_n = 0.16$, Plenum pressure ratio = 1.8

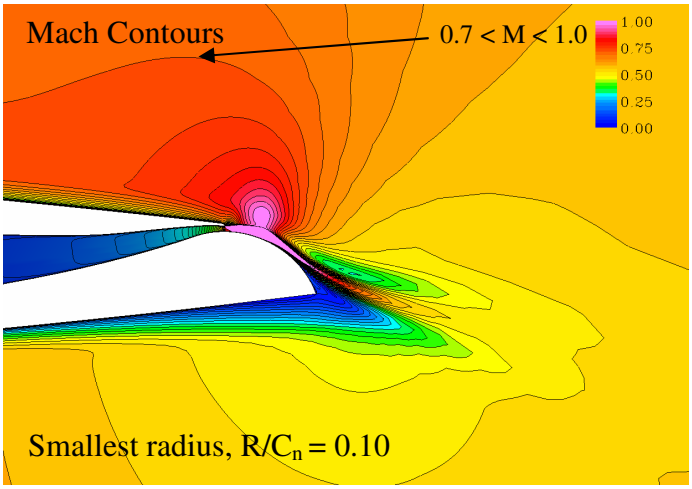

Figure 2.11: Smallest radius, $h/C_n = 0.0057$, $R/C_n = 0.10$, Plenum pressure ratio = 1.8

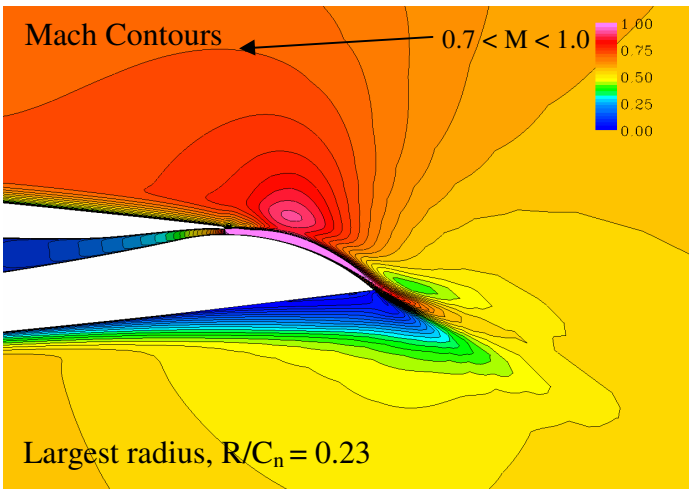

Figure 2.12: Largest radius, $h/C_n = 0.0057$, $R/C_n = 0.23$, Plenum pressure ratio = 1.8

Another important feature of the flow field was the sonic bubble above the Coanda jet. This bubble grew as the trailing edge radius increased from smallest radius to optimal radius. This phenomenon is linked to the separation location of the jet from the trailing edge of the Coanda surface. As trailing edge radius increases (from smallest to optimal) the separation location occurs closer to the end of the Coanda surface. The optimal radius was able to allow the jet to remain almost fully attached and reach a maximum expansion, which translated to higher circulation and increased turning. However, as the radius increased beyond the optimal value, the size of the bubble decreased because the jets were not expanding enough due to reduced curvature. The lower expansion of the jet coupled with reduced curvature limited the effectiveness of larger radii.

As the trailing edge radius of the IGV was further decreased (i.e. below $R/C_n = 0.10$, for $h/C_n=0.0057$), the curvature of trailing edge became too sharp, resulting in solutions that become periodic. The periodic nature of these solutions could be seen from the variation of the residuals, and measured turning angles. As the trailing edge radii became too small for a given jet height (i.e. below $R/C_n=0.14$ for $h/C_n=0.0045$), the solutions failed to converge. The nature of the solutions indicated that the jet may have been detaching from the Coanda surface close to the jet exit. Jet detachment, as detailed by Cornelius et al. [15], indicated that the jet may have been experiencing an oblique shock just after the jet exit that the CFD code may have had difficulty capturing. The nature of the jet detachment suggests that the flow around the IGV may have become unsteady. However, time dependent solutions were not considered due to the diminished performance of small radii in fully converged steady state solutions.

Effects of Pressure ratio

The optimal pressure ratio for this study was 1.8, which can be seen in Fig. 10. Supply pressure ratios below 1.8 did not meet the desired turning angle. Conversely, pressure ratios above 1.8 were able to meet and exceed the desired turning angles when the jet remained attached to the Coanda surface. However, higher supply pressures would require more bleed air, which would make a circulation control IGV less practical for compressor applications. Each rise in supply pressure ratio in Fig. 10 (constant jet height

of h/C_n = 0.0057) increased the ratio of mass flow rate by 0.08 percent, with the matched design case having a mass flow rate ratio of 0.71 percent.

Table 2-1: Momentum coefficients, R/C_n=0.16, h/C_n=0.0057

Plenum Pressure ratio	Traditional momentum Coefficient	Turbomachinery Momentum Coefficient	Mass flow rate ratio
1.4	0.032	0.009	0.55%
1.6	0.037	0.011	0.64%
1.8	0.043	0.012	0.72%
2.0	0.048	0.014	0.81%

Effects of Radii on pressure losses

Figure 2.13 is a plot of the corrected pressure losses over the range of trailing edge radii studied at a constant supply pressure of 1.8. The colored lines represent the corrected pressure losses from constant jet heights, and the dashed line represents the pressure losses from the reference IGV (design goal). The pressure losses were mostly constant when the jet height and supply pressure ratio were held constant. From Fig. 14 the pressure losses appear to decrease as the size of the trailing edge radius increases, however, the variation between pressure loss for the smallest radius and the largest radius is less than 1 percent, signifying that any conclusions based on their difference are subject to the numerical accuracy of the code.

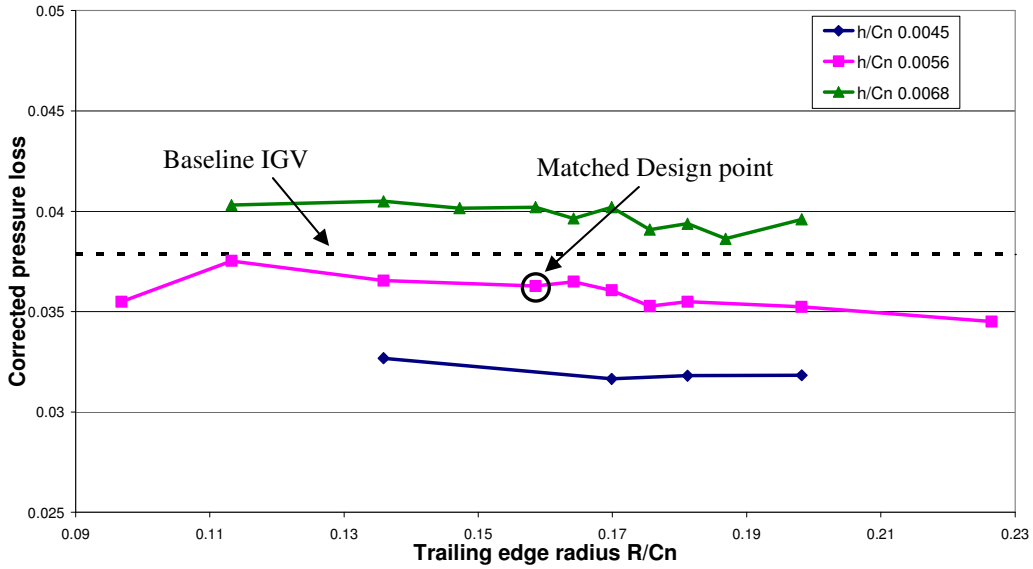

Figure 2.13: Radius vs. Corrected pressure loss, Supply pressure ratio 1.8

Effects of Jet height on pressure losses

For constant supply pressures, the change in pressure loss is proportional to the jet height. This effect was nearly linear, with losses increasing for each successive increase in jet height, as seen in Fig. 14. For the same supply pressure ratio, larger jet heights had higher momentums, which translated to higher pressure losses.

Effects of supply pressure ratio on pressure losses

Figure 2.14 is a plot of the corrected pressure losses over the range of trailing edge radii studied at a constant jet height of $h/C_n = 0.0057$. The colored lines represent the corrected pressure losses from constant supply pressure ratios and the dashed line represents the pressure losses from the reference IGV. The effect of supply pressure ratio on pressure losses was greater than the effect of jet height. This effect can be seen from the difference between pressure losses when the supply pressures are held constant in Fig. 15 and when the jet height is held constant as in Fig. 14. This is because as the supply pressure increases for a constant jet height, the amount of flow entrainment also increases due to the rise in the jets momentum. The jet's greater momentum allowed it to reach higher Mach numbers along the trailing edge and create more circulation for a given jet height and trailing edge radius. This resulted in greater viscous losses due to the higher shear rates that are associated with the higher velocity jet.

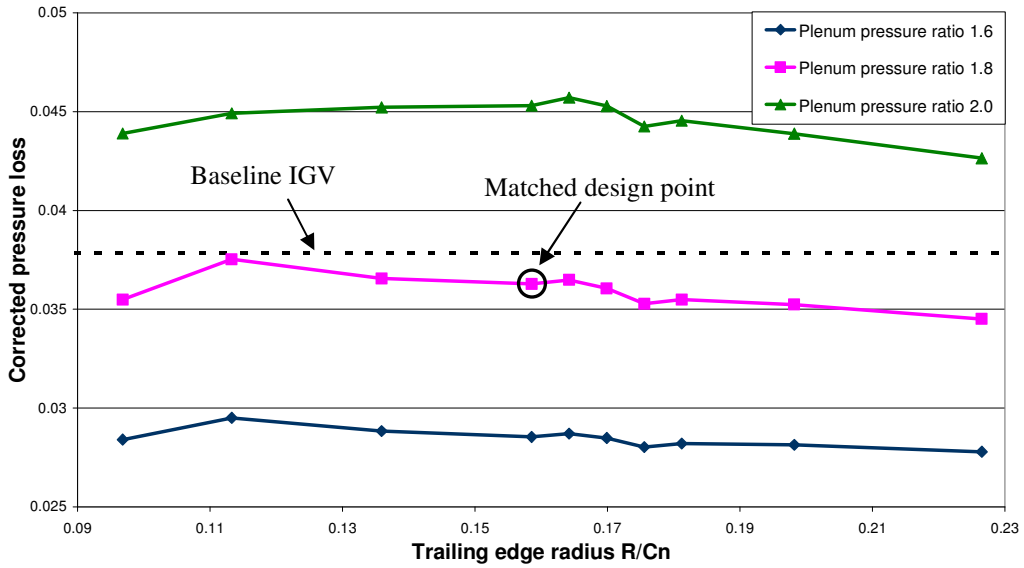

Figure 2.14: Radius vs. Corrected pressure loss, $h/C_n = 0.0057$

Comparison with Baseline IGV

Figure 2.15 shows flow field visualizations of stagnation pressure for both the circulation control IGV and the baseline IGV. The optimal case for the circulation control IGV (i.e. least amount of supply pressure and smallest jet height that could meet the desired turning angle) was compared with the current baseline IGV at CARL. For the comparison the corrected pressure loss coefficient was used, which reduced to normal pressure loss for cases without flow control. The magnitude of the losses from the circulation control IGV was slightly less than the baseline IGV, which can be seen from Figures 2.13 and 2.14. However, the sources of pressure loss were different. The baseline IGV's losses come from its wake mixing and boundary layer, which can be seen from the stagnation pressure flow field in Figure 2.15a. The major sources of losses incurred from the circulation control IGV come from the boundary layer, the stagnation point below the trailing edge, and viscous losses associated with jet mixing as seen in Figure 2.15b. For the circulation control IGV, the losses from jet mixing and the stagnation point below the trailing edge rise as the turning angle increase. Conversely the losses decrease as turning angle also is decreased. This effect would be similar to increasing and decreasing the angle of attack of the Baseline IGV.

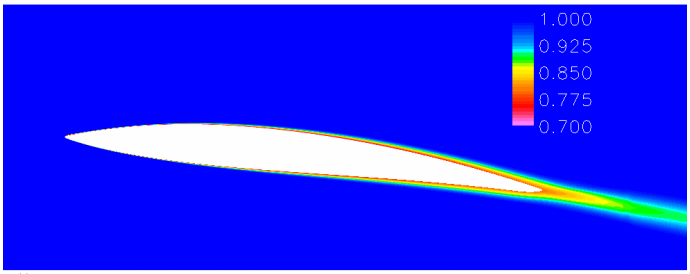

Figure 2.15 a: Stagnation pressure ratio (P_0/P_{ref}), Cambered IGV

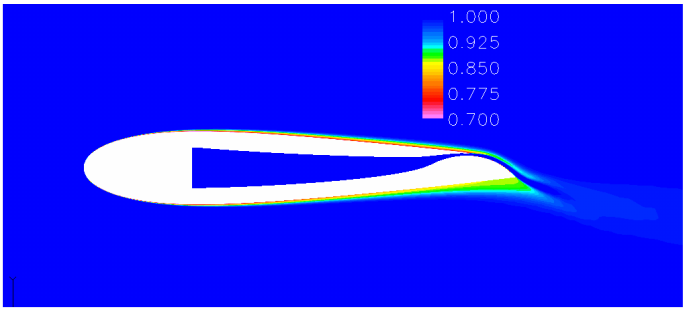

Figure 2.15 b: Stagnation pressure ratio (P_0/P_{ref}), Circulation Control IGV

Conclusion

It has been shown that a circulation control IGV can meet the same design conditions as the current cambered airfoil in the Air Force compressor rig with similar losses, but with half the number of blades. The optimal circulation control IGV was determined in this study based upon the optimal jet height, supply pressure ratio, and trailing edge radius. Losses from the circulation control IGV could be higher than the losses from the current cambered IGV if the jet height is too large or the supply pressure is too high. The pressure losses resulting from varying the geometry of the trailing edge radius were not dominant in this study. However, the effects of jet height and supply pressure did significantly affect pressure losses, with the high supply total pressure causing the most increase in losses.

In order to make the airfoil handle high speeds the trailing edge had to be as thin as possible, limiting the amount of curvature that could be utilized by the Coanda jet. This curvature limitation made the trailing edge radius the most dominant parameter in flow turning. The optimal case had a jet height of $h/C_n = 0.0057$ and a trailing edge Radius $R/C_n = 0.16$. This case needed a supply pressure ratio of 1.8 to meet the exit turning angle requirement. At this supply pressure ratio the jet used 0.71 percent of the total mass flow rate. The optimal circulation control IGV had slightly lower pressure losses when compared with a reference cambered IGV. Based on the ability of a circulation control IGV to meet the design exit turning angle with decreased/similar pressure losses indicates that a circulation control inlet guide vane may provide an alternative to current flapped IGV's.

Future work

In order to validate the results of this study, cascade testing will be performed in a wind tunnel facility at Techsburg Inc. Furthermore, three dimensional CFD studies will be performed to determine if the circulation control IGV could meet the desired exit turning angles along the radial direction as compared to the experimental rig TESCOM at CARL. Other future work for the circulation control IGV would be to maximize turning angles at off design conditions. In order for the current circulation control IGV to accomplish

maximum turning at lower Mach numbers other flow control methods such as leading edge blowing and counter flow blowing may be applied to the current airfoil.

References

1. Bensor, W.A., "Compressor Operation with One or More Blade Rows Stalled", pp. 341-364, NASA SP-36, 1965
2. Budinger, R. E., Kaufman, H. R., "Investigation of the Performance of a Turbojet Engine with Variable-Position Compressor Inlet Guide Vanes", NACA RM-E54L23a, 1955
3. Dobson, W. F., Wallner, L. E., "Acceleration Characteristics of a Turbojet Engine with Variable-Position Inlet Guide Vanes", NACA RM-E54I30, 1955.
4. Wallner, L. E., Lubick, R. J., "Steady State and Surge Characteristics of a Compressor Equipped with Variable Inlet Guide Vanes Operating in a Turbojet Engine", NACA RM-E54I28, 1955.
5. Lord, W. K., MacMartin, D. G., Tillman, T. G., "Flow Control Opportunities in Gas Turbine Engines", AIAA Paper 2000-2234, 2000.
6. Pugliese, A. J., Bethpage, N. Y., Englar, R. J., "Flight Testing the Circulation Control Wing", AIAA Paper 1979-1791, 1979.
7. Englar, R. J., Smith, M. J., Kelley, S. M., Rover, R. C., "Development of Circulation Control Technology for Application to Advanced Subsonic Transport Aircraft", AIAA Paper 1993-0644, 1993.
8. Englar, R. J., Smith, M. J., Kelley, S. M., Rover, R. C., "Application of Circulation Control to Advanced Subsonic Aircraft, Part I: Airfoil Development", *Journal of Aircraft,* Vol. 31, No. 5, 1994, pp. 1160-1168.
9. Englar, R. J., Smith, M. J., Kelley, S. M., Rover, R. C., "Application of Circulation Control to Advanced Subsonic Aircraft, Part II: Transport Application", *Journal of Aircraft,* Vol. 31, No. 5, 1994, pp. 1169-1168.
10. Abramson, J., Rogers, E. O., "High-Speed Characteristics of Circulation Control Airfoils", AIAA Paper 1983-0265, 1983.
11. Englar, R. J., Huson, G. G., "Development of Advanced Circulation Control Wing High Lift Airfoils", AIAA Paper 1983-1847, 1983
12. Jones, G. S., Viken, A. E., Washburn, L, N., Jenkins, L, N., Cagle, C, M., "An Active Flow Circulation Controlled Flap Concept for General Aviation Aircraft Applications", AIAA Paper 2002-3157, 2002
13. Wood, N., Nielsen, J., "Circulation Control Airfoils Past, Present, Future", AIAA Paper 1985-0204, 1985.
14. Hall, E. J., Heidegger, N. J., Delaney, R. A., 1999. "ADPAC v1.0 User's Manual," NASA Contract Report 1990-20660, February.
15. Cornelius, K. C., Lucius, G. A., "Physics of Coanda Jet Detachment at High-pressure Ratio", *Journal of Aircraft,* Vol. 31, No. 3, 1994, pp. 591-596.
16. *Romanian Inventions And Prioritites In Aviation*, Constantin C. Gheorghiu, Ed. Albatros, Bucharest, 1979.
17. Harff, M, R., Wolff, M, J., Copenhaver, W, W., "A CFD Investigation of IGV Flow Vectoring by Counter Flow Blowing" IGTI Paper GT2004-539

Appendix A: Chapter 1 Appendix

Introduction

The purpose for this section of the appendix is to present further results from the turbulence model study presented in Chapter 2. Furthermore, a grid study is presented to show grid independence. The first section of this appendix will cover further results from the comparison between ADPAC and GASP. Next, further results from the turbulence model are presented. The third section gives the momentum coefficients used in the turbulence model study, as well as the mass flow rate ratios. Furthermore, in the third section, the definition of both the traditional momentum coefficient found in literature and a proposed turbomachinery momentum coefficient are provided. The final section shows the results of a grid study of the grid used in both the first and second chapters.

Further code comparison results

Plenum pressure ratio study

Figure A1 presents the results for the comparison between ADPAC and GASP for the plenum pressure ratio study. The code comparison for plenum pressure ratio yielded excellent trend agreement when the plenum pressure ratio was varied on a constant radius size of R/C_n=0.17. The results show that GASP predicts slightly higher values for turning angle; however the variation between them is small with the highest variation occurring at the lowest plenum pressure ratio (2.4 percent variation between the two codes).

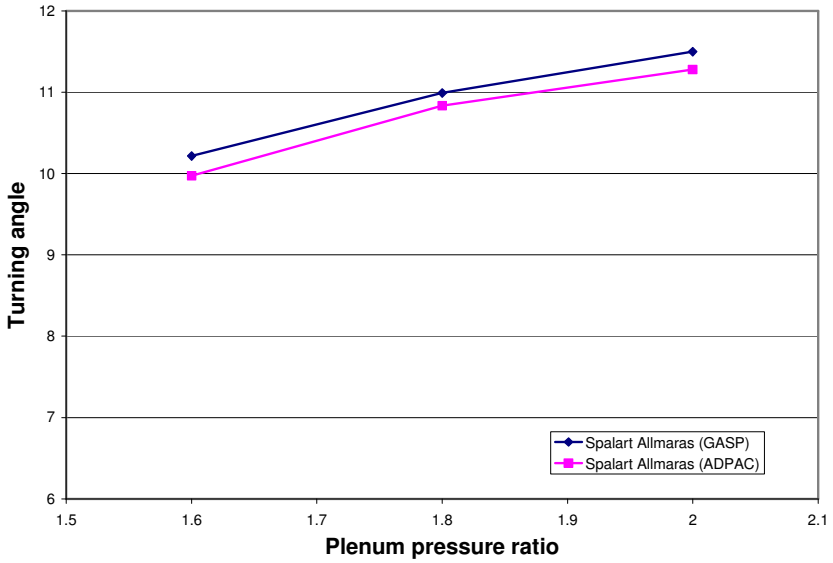

Figure A1: Code comparison Turning angle versus Plenum pressure ratio, R/C_n=0.170

Corrected pressure loss study

Figure A2 presents the pressure loss comparison between ADPAC and GASP. The graph shows that both codes had the same trends when the plenum pressure ratio was varied. The differences between the two codes were slight, with less than 6 percent difference between the codes occurring at the lowest plenum pressure ratio.

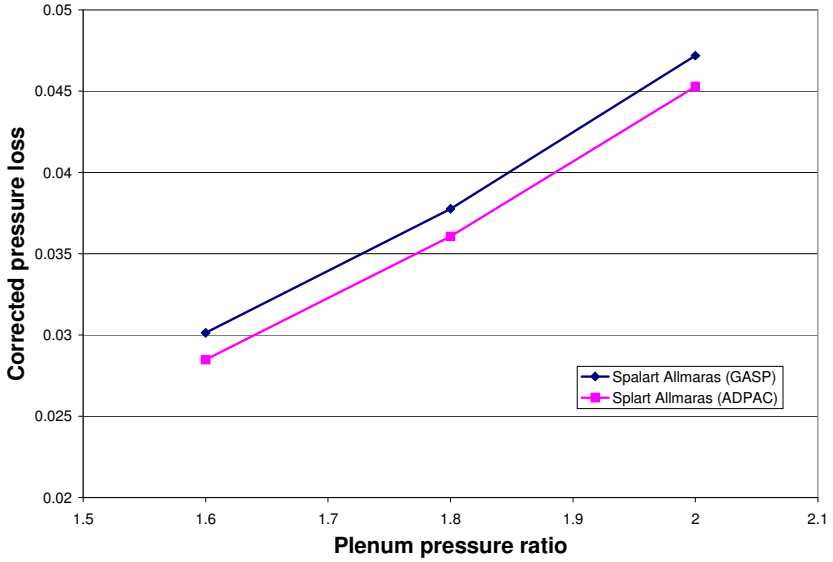

Figure A2: Code comparison Corrected pressure loss versus Plenum pressure ratio, R/Cn=0.170

Further turbulence model results

Turbulence model pressure loss study

Figure A3 presents the results of the pressure losses from the plenum pressure loss study. The blue line represents the S-A model and the pink and green lines represent the k-ω and the Stress-ω respectively. The pressure loss trends from the three turbulence models were in excellent agreement. However, the k-ω model predicted the highest pressure losses of all the models studied. A flow field visualization of corrected pressure loss can be seen in Figure A4. The S-A and Stress-ω flow fields are in near perfect agreement, with S-A predicting slightly higher levels of pressure loss around the IGV. The k-ω model predicts the greatest levels of pressure loss around the IGV, which resulted in the highest prediction of pressure loss for all three models. The agreement between trends indicates that all models may be accurately predicting the effects of varying the plenum pressure ratio on pressure loss. However, the prediction of the pressure loss magnitude is still in question since there is no experiential data to validate the CFD results.

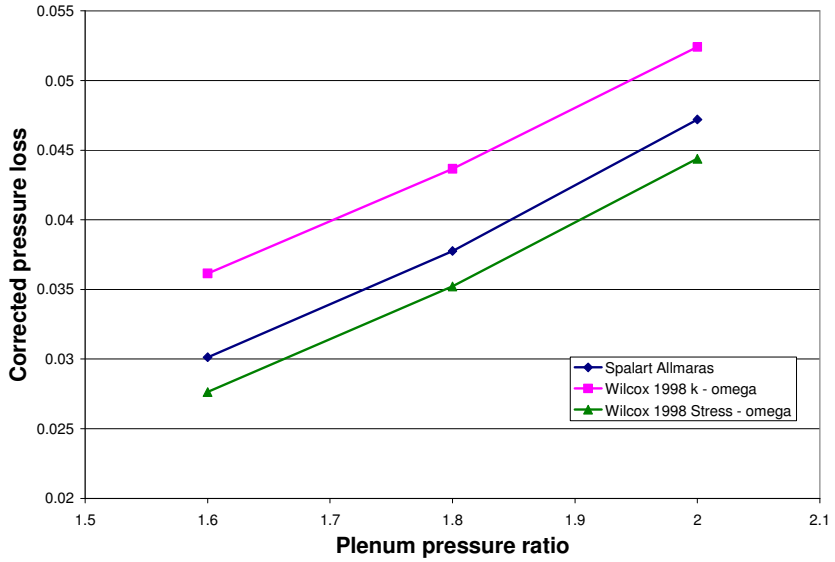

Figure A3: Corrected pressure loss versus Plenum pressure ratio, R/C_n=0.170

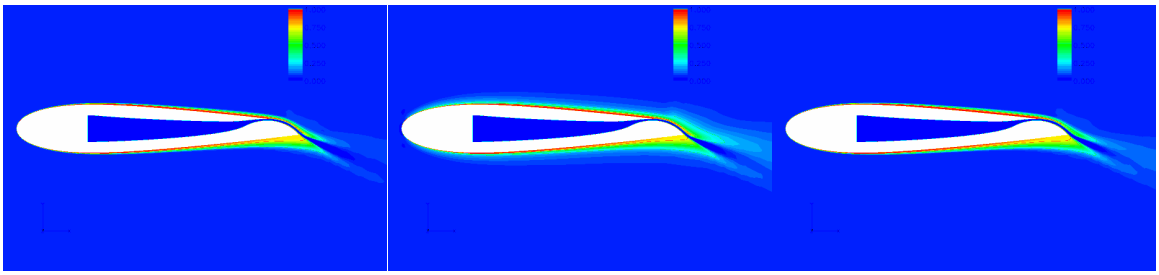

(a) Stress-ω **(b) Spalart-Allmaras** **(c) k-ω**

Figure A4: Corrected pressure loss flow field R/C_n=0.17, $P_{p,ratio}$=2.0

Cause of turning angle magnitude variation between models

There is only a minor difference between the models for the prediction of turning angles. However, the S-A model consistently predicts higher turning for radii greater than R/C_n = 0.16, and the highest turning values for all plenum pressure ratios studied. Figure 2.13, which is a plot of the static pressure distribution along the trailing edge radius for R/C_n=0.17, offers some insight as to why the Spalart-Allmaras turbulence model predicts higher levels of turning angle (i.e. greater circulation). The plot of static pressure distributions shows that the Coanda jet goes through two cycles of jet expansion and compression. For the first cycle (between three and twenty percent trailing edge radius arc length) all three models are in good agreement. However, in the second cycle the Spalart-Allmaras model shows lower static pressure drop between 35 and 50 percent of the trailing edge radius indicating that the jet continued to expand further along the trailing edge radius. Furthermore, between 50 and 65 percent of the arc length the jet experienced less compression than the other models. The lower jet static pressures predicted by S-A model translated to lower pressures above the Coanda surface. The lower pressure allowed for more flow entrainment which created slightly higher turning angle predictions than both the k-ω and Stress-ω. However, there are no experimental results to validate the CFD results from this study; thus, it is not known which model best predicts the pressure distribution on the Coanda surface.

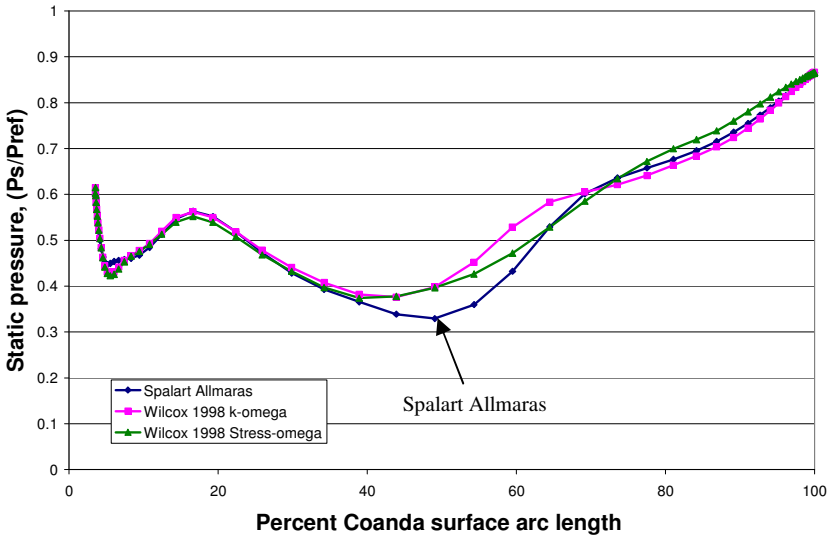

Figure A5: Static pressure distribution on Coanda surface, R/C_n=0.170, Plenum pressure ratio 2.0

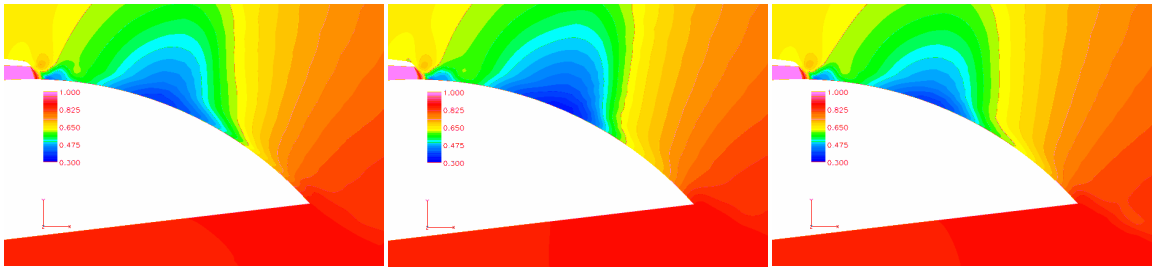

(a) Stress-ω **(b) Spalart-Allmaras** **(c) k-ω**

Figure A6: Static pressure distributions (P/P_{ref}), R/C_n=0.17, $P_{p,ratio}$=2.0

Momentum Coefficient

Traditional momentum coefficient

The traditional momentum coefficient used in circulation control airfoil literature is given below in equation A-1. The quantities, C_t, b, and h are respectively the airfoil's chord length, span, and the jet height.

$$C_\mu = \frac{\dot{m}_j V_j}{\frac{1}{2}\rho_\infty V_\infty^2 A} = \frac{\rho_j V_j^2 hb}{\frac{1}{2}\rho_\infty V_\infty^2 C_t b} \qquad \text{(A-1)}$$

Turbo machinery momentum coefficient

The momentum coefficient can be slightly altered for turbomachinery applications since the mass flow rate at the inlet is known. Thus, the turbomachinery momentum coefficient is the ratio of jet momentum to inlet momentum.

$$C_{\mu,Turbomachinery} = \frac{\dot{m}_j V_j}{\dot{m}_i V_i} \qquad \text{(A-2)}$$

Mass flow rate ratio

The mass flow rate ratio was defined as the ratio of mass flow from the plenum to the total mass flow rate at the exit (also known as the percent core flow).

$$C_m = \frac{\dot{m}_j}{\dot{m}_e} \qquad \text{(A-3)}$$

Table A1, which is shown for comparison between the IGV and other circulation control airfoils, shows the variation of traditional momentum coefficient, turbomachinery definition for momentum coefficient, and the percent mass flow rate from the plenum (i.e. percent core flow). The tradition momentum coefficient was calculated by using the nominal chord C_n in place of the total chord length C_t, and the span variable from the equation was dropped, since the ratio of the jet span to IGV span is unity.

Table A1: Momentum coefficients

Plenum Pressure ratio	**Traditional momentum Coefficient**	**Turbomachinery Momentum Coefficient**	**Mass flow rate ratio**
1.6	0.037	0.011	0.64%
1.8	0.043	0.012	0.72%
2.0	0.048	0.014	0.81%

Grid study

In order to establish grid independence, three grid sizes beyond the grid used in both the optimization study and the turbulence model ("studied grid") were examined. The geometry used for the grid study had a jet height of h/C_n=0.0056 and the trailing edge radius was R/C_n=0.17. The number of cells for each grid size is tabulate below in table

A2. Each grid was set up in a similar fashion as the "Studied Grid", with the same near wall distance and the same clustering near the IGV (see Chapter 1 for further details on mesh topology and cell clustering). The conditions used in the grid study included an inlet Mach number of 0.54, and a plenum pressure ratio of 2.0. Furthermore, the grid study was completed using the Spalart-Allmaras turbulence model in ADPAC.

Table A2: Grid sizes

Grid	Number of cells
Coarsest	7164
Medium	15976
"Studied Grid"	28992
Finest	44800

Figure A5 presents the results of the grid study in a percent variation of turning angle between each grid and the finest grid versus the number of cells of each grid. The variation of turning angle between the "Studied Grid" and the finest grid was only 0.6 percent. The maximum variation (3 percent) occurred between the coarsest grid and the finest grid.

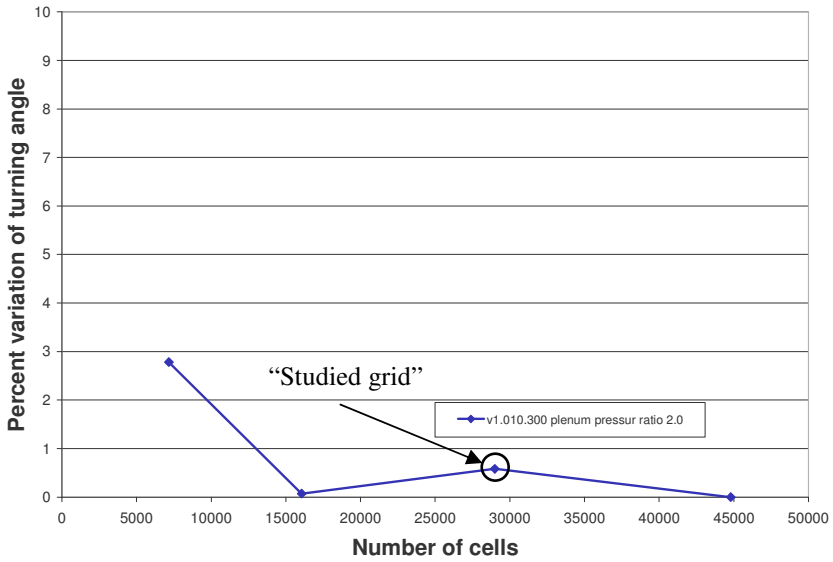

Figure A7: Percent variation of turning angle versus number of cells

Figure A6 shows the results of the grid study in a percent variation of corrected pressure loss between each grid and the finest grid versus the number of cells of each grid. The variation between the "Studied Grid" and the finest grid was 4 percent, while the maximum variation (11 percent) occurred between the coarsest grid and the finest grid.

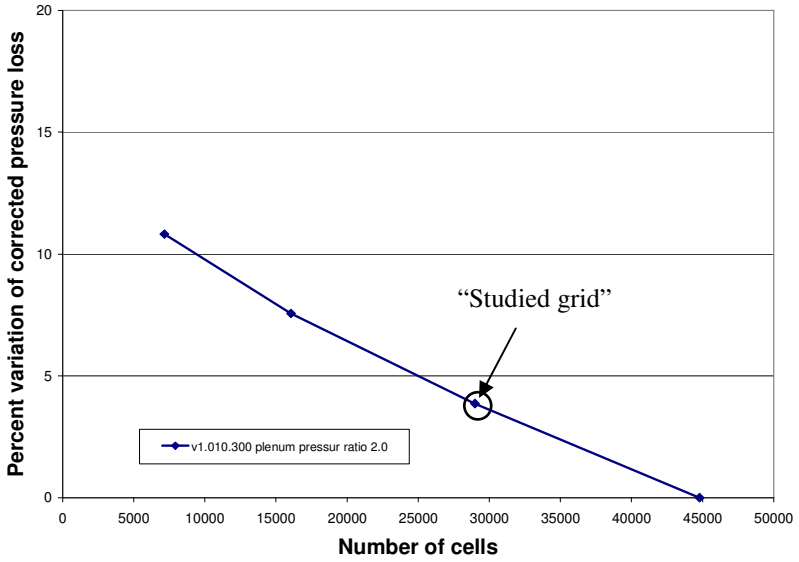

Figure A8: Percent variation of corrected pressure loss versus number of cells

The small variation between the "Studied Grid" and the finest grid for both turning angle and corrected pressure loss indicated that the grid size of the "Studied Grid" was sufficient enough too provide solutions that were grid independent.

Appendix B: Wedge Geometry

Introduction

To determine the effectiveness of a circulation control Inlet Guide Vane an off-design study was completed. For this study a-wedge shaped geometry was chosen due to a low inlet Mach number and the high amount of turning that was desired.

Objectives

The objective of this study was to show that circulation control Inlet Guide Vanes (IGVs) could physically replace variable IGVs at off-design conditions. In order to accomplish this objective, a two-dimensional circulation control IGV was created to meet the theoretical off-design requirements of an axial compressor. The theoretical off-design requirement included greater than 25 degrees of flow turning behind the IGV at an inlet Mach number of 0.3.

Geometry

A wedge-shaped geometry was chosen for this study due to the lack of loading on the front end of an airfoil-shaped geometry in an earlier portion of the project, in which the author did not contribute. The base geometry tested, seen in Figure B1 was symmetric from the leading edge up to 67 percent of the total chord length (C=0.44 cm). The design accounts for the need of an internal passage to supply air to Coanda jet. To account for the added plenum, the thickness at 67 percent of the IGV's total chord the ratio of thickness to chord was t/C = 0.37. There were four geometric parameters that were varied, the jet height (h), the trailing edge radius (R_{te}), the trailing edge fillet on the pressure side (R_{fillet}), and the jet exit angle (α_{jet}). The exit angle was measured from the horizontal such that a 90 degree exit angle would be tangent to the freestream flow. Table B1 shows the baseline values for the varied geometric parameters.

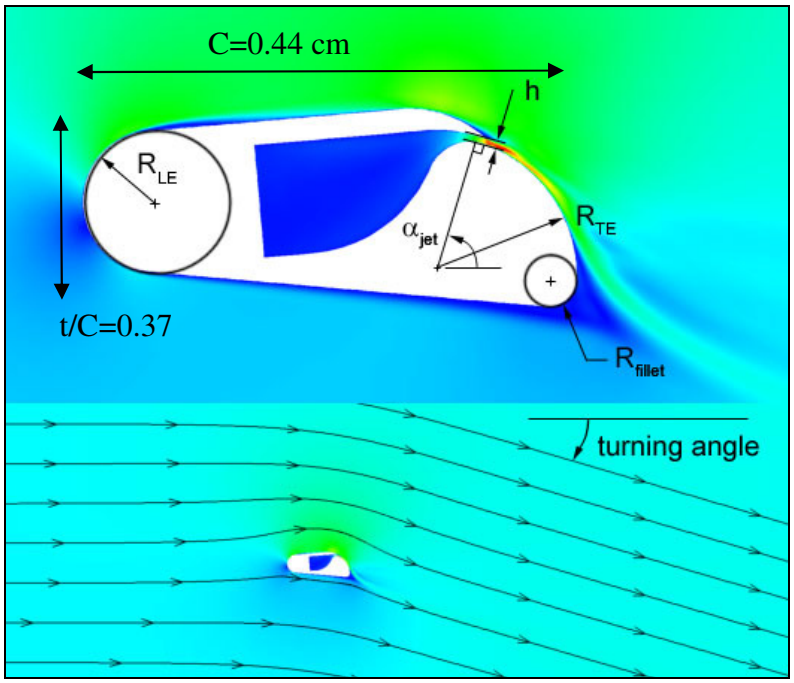

Figure B1: Wedge geometry parameters

Table B1: Baseline geometric parameters

Parameter	base value
chord length, C	0.44 cm
jet exit angle, α_{jet}	70°
jet height, h/C	0.011
trailing edge radius, R_{TE}/C	0.290
leading edge radius, R_{LE}/C	0.143
trailing edge fillet, R_{fillet}/C	0.057
angle of attack	0°

Common Methodology

Code

The two-dimensional circulation control IGV was simulated using Advanced Ducted Propfan Analysis Code (ADPAC), a fully viscous Reynolds Averaged Navier Stokes (RANS) model. The boundary layer across the entire IGV was simulated as turbulent using the one equation Spalart-Allmaras turbulence model. The Spalart-Allmaras model was chosen due to its increased accuracy over the Baldwin-Lomax turbulence model in predicting separated flows, and its decreased computational time over a two-equation turbulence model.

Mesh

The four block mesh for this study, pictured in Figure B2, was built using GRIDGEN. The first block, which was the inlet block, consisted of 416 cells. The second block was an O-mesh that wrapped around the IGV and consisted of 21488 cells. The exit block was built with 1664 cells. The plenum block had 1320 cells and was located inside the IGV. The near wall spacing for this mesh was held at 3e-4 percent of the total chord, which held the y+ values below 4 on the trailing edge of the IGV. The mesh topology remained constant for each geometric change.

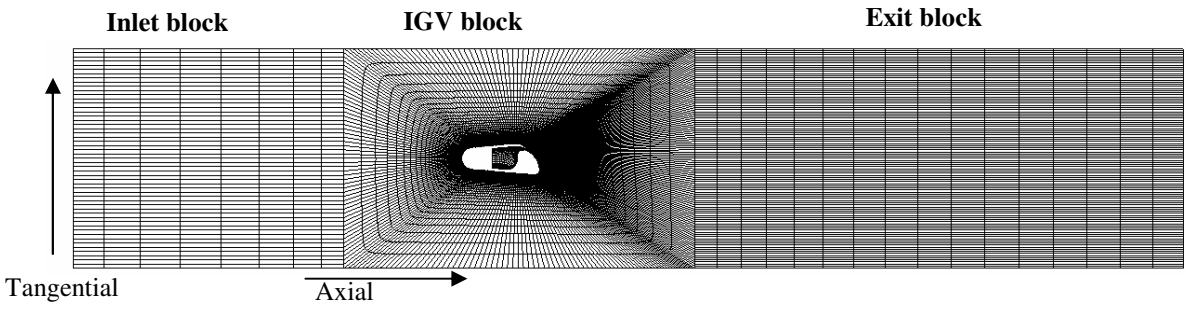

Figure B2: Mesh topology

Boundary conditions

The mesh had four boundaries: main inlet, plenum inlet, exit, and walls. The total temperature and pressure at the main inlet were set to reference values of standard day conditions (P_{ref} = 101 kPa , T_{ref} = 288 K). At the plenum inlet, the total temperature was set to the reference value, while the ratio of total pressure ($P_{o,p}/P_{ref}$) was varied between 1.3 and 2.0. The static pressure ratio ($P_{e,s}/P_{ref}$) at the exit block was varied to achieve the proper inlet Mach number. Boundary conditions at the walls were set to no-slip adiabatic. The upper most tangential cells and lower most tangential cells of the mesh were patched together to create a periodic boundary to simulate a linear cascade.

Measurements

Measurements, shown in Figure B3, were made at three locations in order to calculate important variables such as: turning angle, mass flow rate, Mach number, and pressure loss. These variables were then used to compare the results from each CFD case. Inlet measurements were taken at the first location, which corresponded to a distance of 1.5

chord lengths before the leading edge of the IGV. The second location was the exit measurement in which data was taken at a distance of 3.0 chords length behind the leading. Finally, the last location was the jet measurement where data was taken across the final x direction grid-line on the plenum block. The measurements were taken using probe files that were generated from ADPAC, which were set up to give mass averaged quantities across a constant *i* line on the mesh.

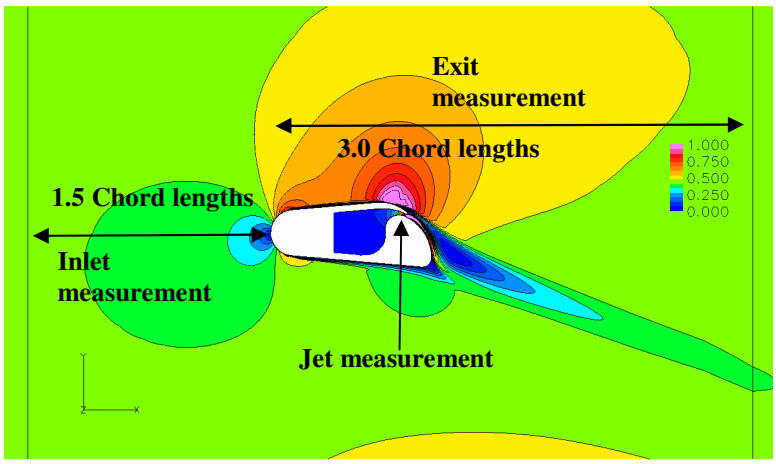

Figure B3: Measurement locations

Data reduction

The following section shows the equations for turning angle and momentum coefficient that were used in order to compare the results from each geometric and non-geometric variation.

The flow turning angle was defined as the inverse tangent of the mass averaged tangential velocity (U_t) divided by mass averaged axial velocity (U_a).

$$\alpha = \tan^{-1}\frac{U_t}{U_a} \qquad \text{(B-1)}$$

The blowing coefficient, also known as the momentum coefficient, was defined as the ratio of jet momentum to inlet momentum. The blowing coefficient was used to compare the results of plenum pressure ratio at different inlet Mach numbers.

$$C_\mu = \frac{\dot{m}_j V_j}{\dot{m}_i V_i} \qquad \text{(B-2)}$$

Wedge geometry phases

Testing of wedge-shaped geometry was performed in two phases. The first phase was an optimization phase in which only geometric parameters on the IGV were studied to determine which geometric parameter had the greatest impact on flow turning. The second phase employed the best case from the geometric parameters and varied non-geometric parameters. The remainder of appendix B presents the results from each phase. The discussion of each phase will give both the methodology and the results. At the end, the final remarks will reference both phases.

Methodology phase 1

In the first phase, four geometric parameters on the IGV were varied: jet exit angle α_{jet}, jet height h, trailing edge radius R_{te}, and the trailing edge fillet on the pressure side R_{fillet}. To test the individual parameters, a set of base variables were established, as seen in table 1. Each parameter was varied individually while holding the other base line variables constant. This resulted in four separate studies. The results from each study were compared to find which geometric parameters had the greatest impact on flow turning. Finally, a best case was determined by using the geometric parameter which showed the greatest impact on flow turning and varying the other parameters. The inlet Mach number for this study was held constant at 0.3 and the solidity was also held constant at 0.175. Furthermore, the supply pressure ratio (plenum pressure ratio) to the jet was held constant at 1.3.

Results Phase 1

Trailing edge Fillet study (R_{fillet})

The plot of turning angle versus trailing edge fillet radius (Figure B4) shows the variation of turning angle as the magnitude of the fillet radius on the pressure side of the trailing

edge is increased. The fillet radius was varied from $R_{fillet}/C=0.006$ to $R_{fillet}/C=0.016$. The data shows only a small change in turning angle as the magnitude of the trailing edge fillet increased. Furthermore, the results show that there is only two degrees of variation between the base line case and the best and worst cases. The main reason for this result is the location where the jet separates from the trailing edge of the airfoil. Figure B5a shows the Mach number flow field around the base case. Noted in Figure B5a is the jet detachment from the trailing edge radius (R_{te}/C) that occurs before the jet encounters the trailing edge fillet. This effect limits the effectiveness of the fillet thus, the fillet size was determined to have only a low order effect on the turning capability of the IGV.

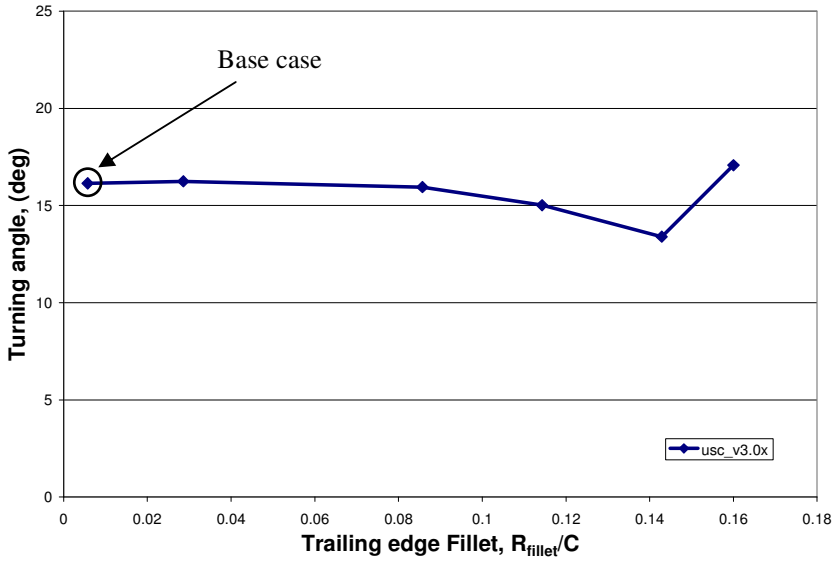

Figure B4: Turning angle versus Pressure side corner radius

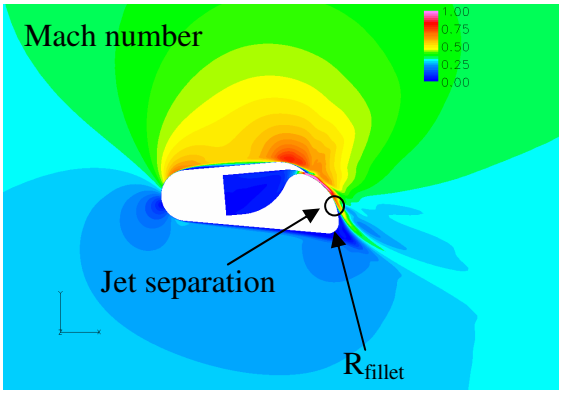

Figure B5: Fillet study Jet separation

Jet exit study (α_{jet})

The jet exit study varied the jet exit angle from $\alpha_{jet}=40^{o}$ to $\alpha_{jet}=85^{o}$ and held the rest of the base line variables constant. The plot in Figure B6 shows the variation in turning angle as the jet exit angle was varied. Figure B7 shows the velocity flow field at three exit angles. The greatest gain in turning was at an exit angle of 60 degrees; the limit to where the on coming boundary layer was able to remain attached to the lip just above the jet. At an exit angle of 60 degrees, the attached boundary layer along with the free stream flow above the suction side of the IGV was able to become entrained by the jet, as seen in Figure B7b. The smallest angle studied (40 degrees), shown in Figure B7a, had premature boundary layer separation at the top of the jet lip. The separated boundary layer in this case acted as a barrier to free stream flow above the jet resulting in the jet's diminished ability to entrain flow. The separation caused two counter-rotating vortices that behaved similarly to flow behind a cylinder, demonstrating that premature separation of the boundary layer from the surface of the airfoil was catastrophic to the ability of the circulation control IGV. Furthermore, the separation of the suction side boundary layer resulted in only five degrees of flow turning.

For jet exit angles beyond 60 degrees, the jet experienced earlier separation from the Coanda surface (R_{te}/C) as seen in Figure B7c. The most likely mechanism for this phenomenon is that the jet loses energy to the entrained flow, thus, its momentum is diminished earlier along the trailing edge of the IGV and it can no longer overcome the adverse pressure gradient along the Coanda surface. Once the jet separated from the Coanda surface, circulation along the IGV was diminished since the IGV was essentially stalled. The results from this study showed that jet exit angle had a large impact on the turning capability of the IGV since there was a larger amount of variation in turning angle between the worst and best cases (15 degrees).

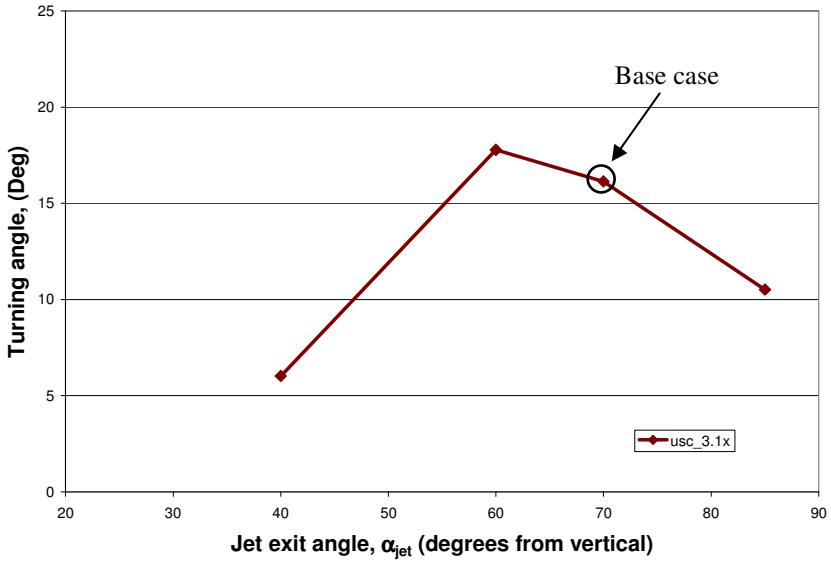

Figure B6: Turning angle versus Jet exit angle

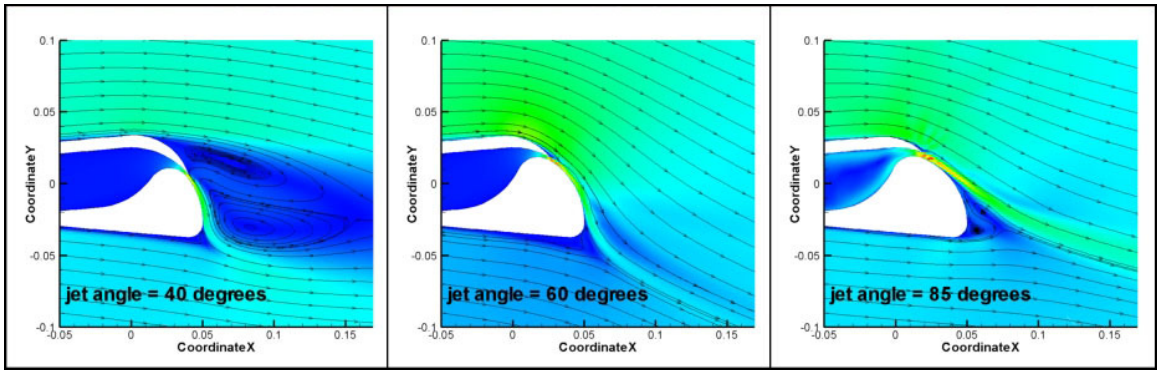

(a) exit angle 40 degrees **(b) exit angle 60 degrees** **(c) exit angle 65 degrees**

Figure B7: Jet exit velocity flow field

Jet height study (h)

In order to test the effect of jet height, the jet height was varied between h/C = 0.0057 and 0.0230 with all other variables in table 1 held constant. Figure B8 shows the plot of turning angle versus jet height. The results of the jet height study show that the most effective jet height (h/C = 0.017) was able to achieve 22 degrees of flow turning. The turning angle increases as the jet height is varied from the smallest jet height to the optimal jet height. Then as the jet height is further enlarged, the turning angle decreases. The physical phenomenon that governs this effect is the momentum of the jet. When the plenum pressure ratio is constant, the amount of mass flow rate out of the jet is proportional to the jet height. The larger the jet height the more mass is allowed through

the opening and the larger the jet momentum. As the momentum rises, the jet is better able to entrain flow above it; however, there is a point when the jet's momentum is too large. At this point, the jet separates from the Coanda surface of the IGV, which results in loss of circulation and flow turning. The variation between the best and worst cases was 15 degrees, which also showed that the jet height played an important role in flow turning.

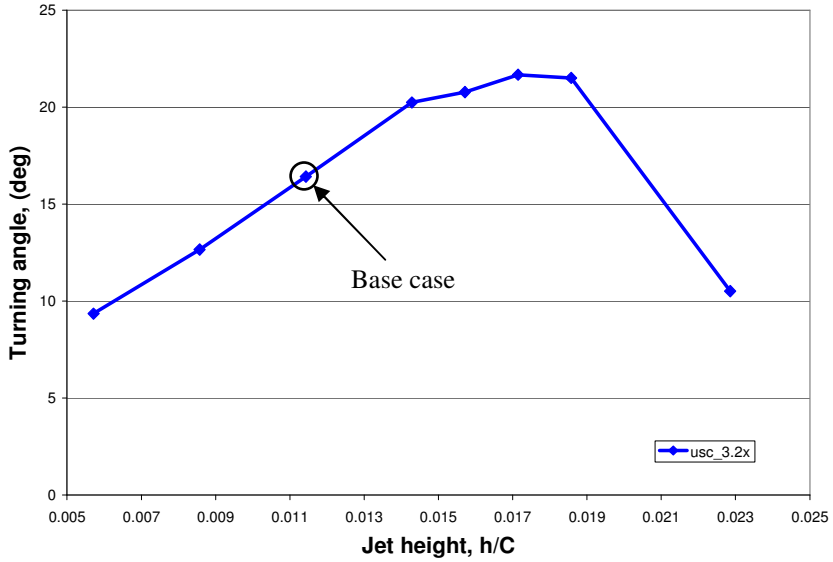

Figure B8: Turning angle versus Jet height

Trailing edge Radius study (R_{te})

The plot in Figure B9 shows the results from the trailing edge study. As seen in Figure B9, as the trailing edge radius was reduced, the turning angle increased. This is because as radius was reduced, the curvature of the trailing edge became sharper. The sharper surface allowed the jet a greater ability to expand and to create lower pressures along the Coanda surface. The lower pressures created along the Coanda surface allowed for more flow entrainment, thus greater turning. Although, the results prove that the trailing edge radius also plays an important role in flow turning, the peak radius was never found in this study because of the limitations of the SolidWorks model.

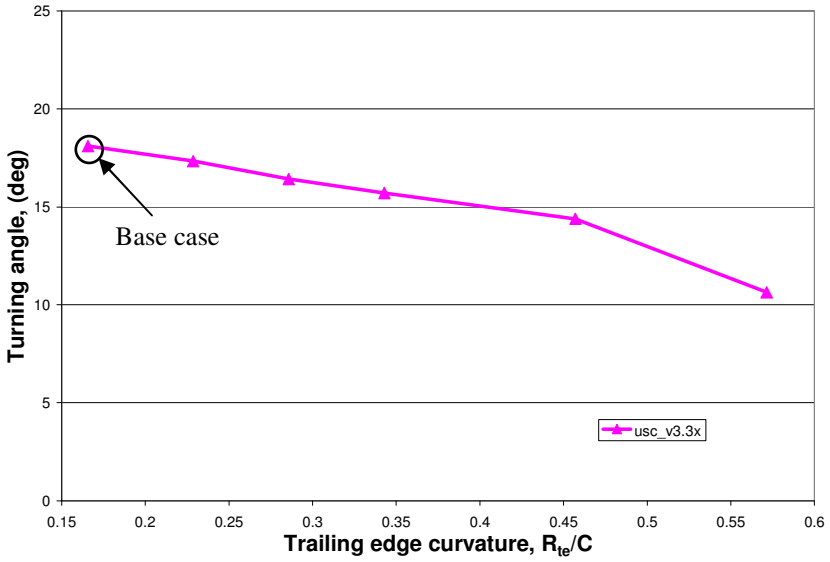

Figure B9: Turning angle versus Trailing edge radius

Best jet height optimization

The results from the geometric study showed that both the jet exit angle and the jet height had the greatest impact on flow turning. In order to reach an optimal design for the circulation control IGV, the number of geometric parameters had to be narrowed down. Thus, in order to optimize the design of the circulation control IGV, the jet height was held constant at the optimal result of the jet height study. Also, the size of the trailing edge fillet was held constant at the original baseline value as a result of the trailing edge fillet's low order effect on flow turning. Holding both the new jet height and trailing edge fillet constant, the remaining geometric parameters (R_{te}, α_{jet}) were varied. First, the optimal radius was found by holding the jet exit constant at the original baseline value. Then the new optimal radius was held constant and the exit angle was varied.

Figure B10, a plot of turning angle versus normalized trailing edge radius, provides the results of varying the trailing edge radius when the best jet height was used. As seen in Figure B10, the original base line trailing edge radius proved to be the most effective.

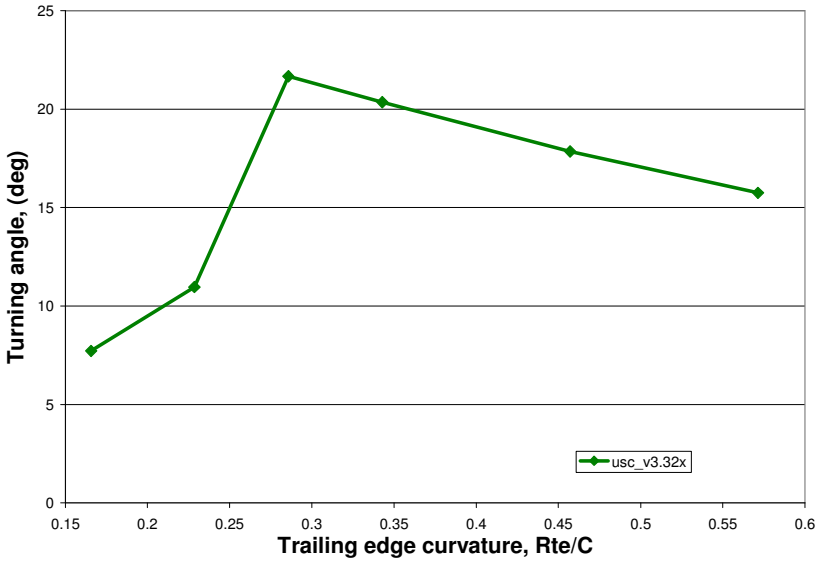

Figure B10: Turning angle versus Trailing edge radius

Once the optimal trailing edge radius (R_{te}/C=0.290) was determined, the jet exit angle was varied. The results from this study can be seen in Figure B11, which is a plot of trailing edge radius versus Jet exit angle. The optimal angle from this study turned out to be 65 degrees. From the constant best jet optimization, a best case was determined, which is pictured in Figure B12. The geometric parameters for the best case can be seen in table B2. This case was then used in the second phase, which varied non-geometric parameters.

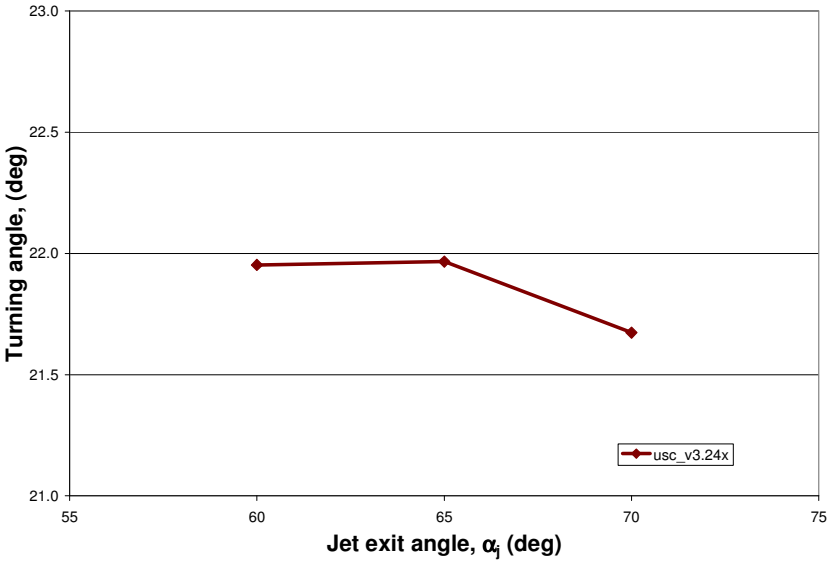

Figure B11: Turning angle versus Jet exit angle

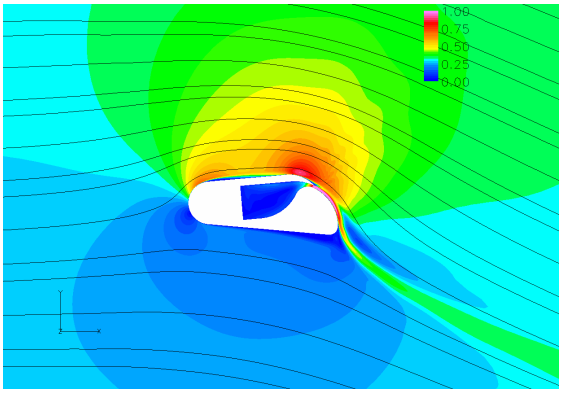

Figure B12: Best case Mach number flow field

Table B2: Best case geometric parameters

Parameter	value
chord length, C	0.175”
jet exit angle, α_{jet}	65°
jet height, h/C	0.017
trailing edge radius, R_{TE}/C	0.290
leading edge radius, R_{LE}/C	0.143
trailing edge fillet, R_{fillet}/C	0.057
angle of attack	0°

Methodology phase 2

Once a best case was established from the first phase, the second phase looked at non-geometric parameters that affected the ability of the wedge-shaped circulation control

IGV. This phase varied the solidity, the inlet Mach number, and the plenum pressure ratio.

Results phase 2

Solidity study

To maximize the effectiveness of the IGV, the effect of pitch was studied. In Figure B13, the effect of pitch can be seen on the plot of turning angle versus solidity. As seen Figure B12, as the pitch became smaller, the circulation control IGV became more effective. For the solidity study, the inlet Mach number was held constant at 0.3. However, one important thing to note is that the inlet Mach number would need to be increased, due to the amount of blockage that would be created by increasing the number of blades.

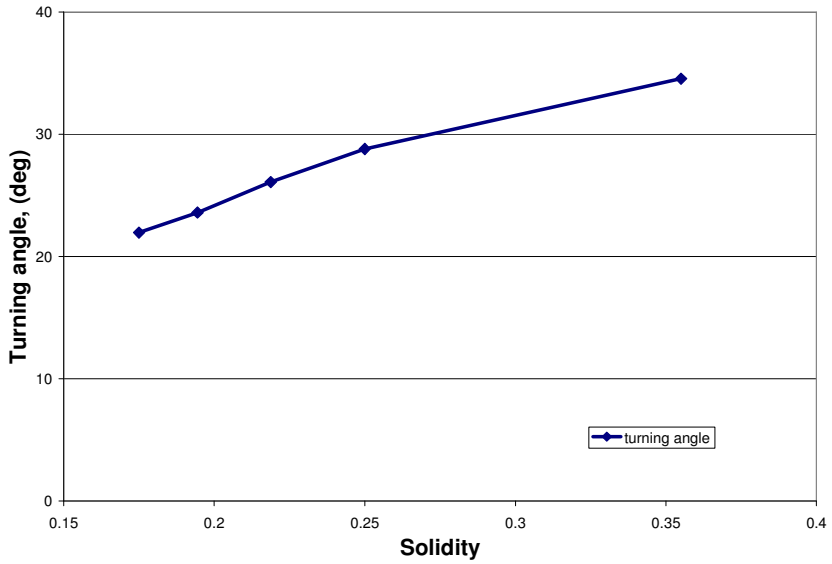

Figure B13: Turning angle versus Solidity

Plenum pressure ratio

The effect of plenum pressure ratio showed that increasing the supply pressure resulted in greater flow turning. Figure B14 is a plot of the turning angle versus the plenum pressure ratio. For this study, the solidity was held constant at 0.355 and the plenum pressure ratio was varied between 1.5 and 2.0. Each increase in plenum pressure ratio resulted in a gain in turning angle. Jet separation would most likely occur at higher plenum pressure ratios, however the point at which the pressure ratio would have become too high was never

studied. Furthermore, the curve in Figure B14 indicates that the optimal pressure ratio that would have created the greatest turning angle was also never studied.

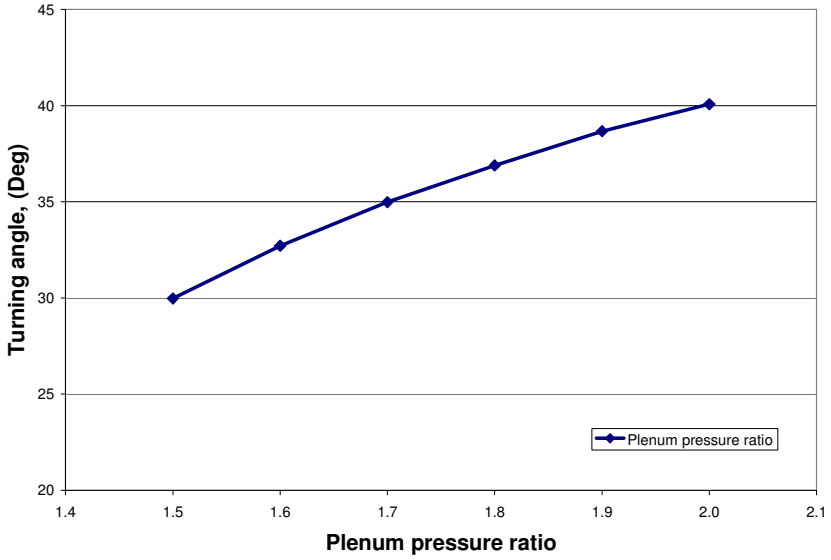

Figure B14: Turning angle versus Plenum pressure ratio

Inlet Mach number

In order to study full ability of the wedge-geometry, the inlet Mach number was varied. The results are shown in Figure B15, a plot of the turning angle versus inlet Mach number. At low inlet Mach numbers, the IGV demonstrated the ability to turn the flow almost 50 degrees; however, as the inlet Mach number was increased, the ability of the IGV quickly diminished. The diminished ability of the IGV at higher inlet Mach numbers was a direct result of the on-coming boundary layer separating before the jet. The separated boundary layer formed an obstacle between the jet and the free stream flow that kept the freestream flow from being entrained by the jet. Figure B16 shows the Mach contours at an inlet Mach number of 0.4 and a plenum pressure ratio of 2.0. This barrier, which can be seen in Figure B16, creates a large region of lower velocity flow behind the IGV that plays a large role in the diminished ability of the IGV to create turning at higher Mach numbers.

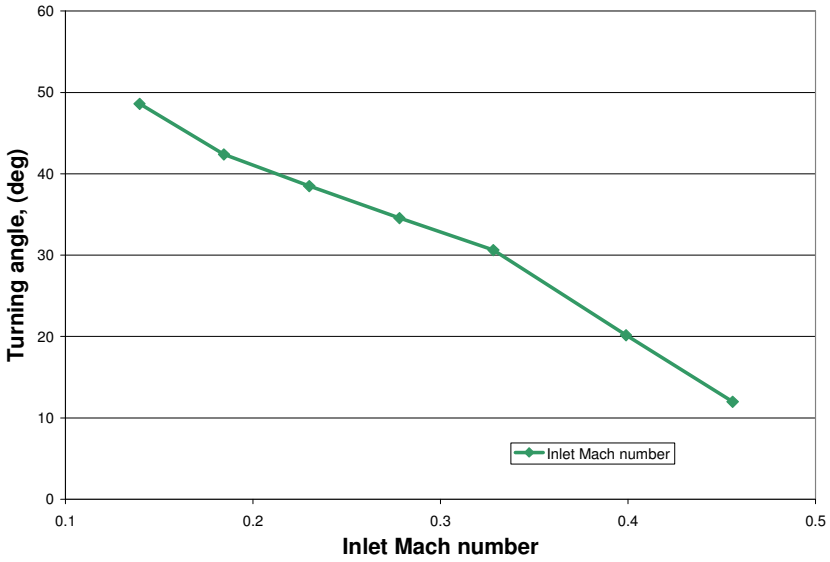

Figure B15: Turning angle versus Inlet Mach number

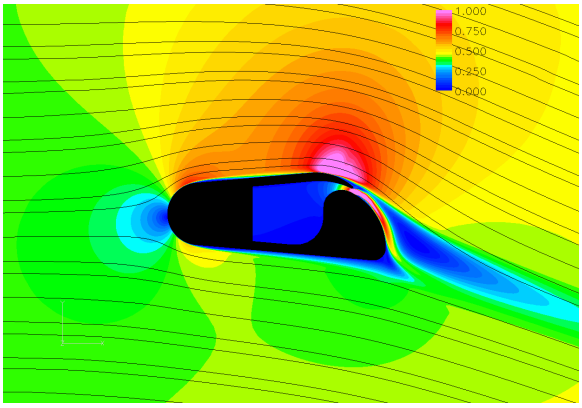

Figure B16: Best case Mach contours at an inlet Mach number of 0.4

Blowing Coefficient study

The final study in the wedge geometry portion of the circulation control inlet guide vane project was a blowing coefficient study (i.e. momentum coefficient). For this study, three inlet Mach numbers were studied: M.=0.2, M_i=0.3, and M_i=0.4 with varying momentum coefficients. Momentum coefficients were varied by changing the plenum pressure ratio. Figure B17, a plot of the blowing coefficient versus turning angle, shows the results of this study. One of the important things to note from this study is that the similar blowing coefficients for different Mach numbers produced slightly different turning angles. For up to blowing coefficient of 0.035, the greatest turning is seen from an inlet Mach number of 0.4. However, after 0.035, the greater turning angles are seen by an inlet Mach number of

0.3. Furthermore, the inlet Mach number 0.3 also performs better at similar blowing coefficients than Mi = 0.2. An important feature, which is not pictured on this graph, is the point at which a critical blowing coefficient was reached that resulted in jet separation and loss of turning (just after each inlet Mach number's final point). This feature would show that an inlet Mach number of 0.2 would also outperform Mi=0.3 beyond a certain blowing coefficient.

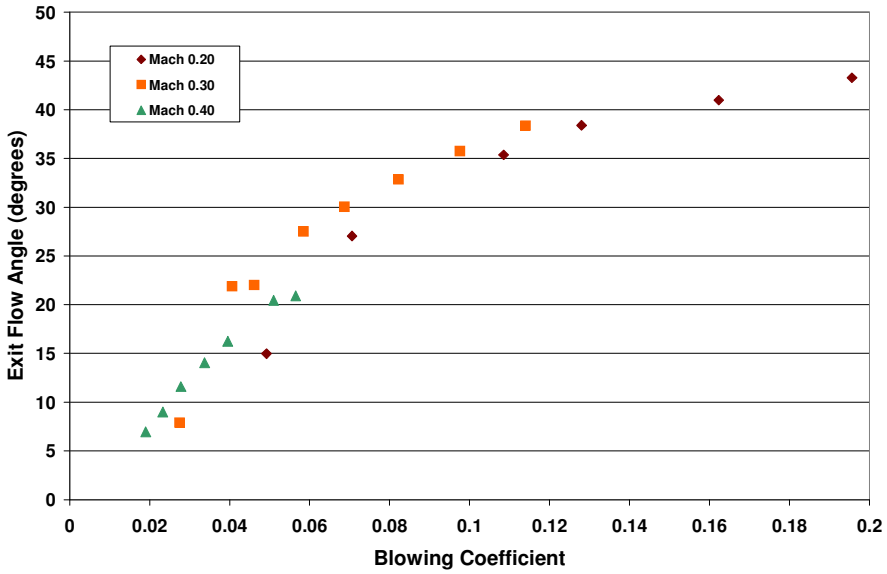

Figure B17: Turning angle versus Blowing Coefficient

Conclusion

In the first phase of the wedge geometry study, a best case geometry was reached. However, one of the drawbacks to this result was that all of the geometric parameters had a direct impact on the performance of the circulation control IGV. When one parameter was varied and all other parameters were held constant it was easy to find an optimal result, but when an optimal value was reached for any one parameter, there were new optimal results for the other parameters. In the second phase, the result of the inlet Mach number proved to be the most important. If the inlet Mach number is too high, the circulation control IGV could not reach the same turning when the inlet Mach number was low no matter how much the blowing rate increased.

Appendix C: TESCOM On-Design 2D

Introduction

A two-dimensional CFD on-design study of a circulation control Inlet Guide Vane (IGV) was completed in order to further demonstrate the IGV's flow turning ability. The previous off-design study (Appendix B) showed that the circulation control IGV's capability to create flow turning was diminished at higher inlet Mach numbers. As such, compressor on-design conditions represent the greatest challenge for a circulation control IGV since the IGV would experience higher Mach numbers at on-design conditions. The simulated conditions used for this study were the on-design conditions from the Air Force test rig TESCOM (TESt COMpressor), located at Wright-Patterson Air Force base in Dayton, Ohio. The TESCOM rig was chosen since it offers a fair representation of engine hardware and a future platform for experimental validation. Furthermore, in order to design a circulation control IGV that could actually be tested in the TESCOM rig, the blade count had to be reduced from 36 cambered IGVs to 18 circulation control IGVs. This is a direct result of the increased thickness of the IGV to accommodate a plenum and the limited number of positions that could house the circulation control IGV in the TESCOM rig (36).

Objectives

The on-design requirements of the TESCOM rig require a linear distribution of turning angle before TESCOM's first rotating blade stage, which is currently created by a variable cambered IGV at on-design conditions. The goal of the on-design study was to match the turning angles of the cambered IGV using a circulation control IGV at radial locations that corresponded to both the mid-span and the tip of the current IGV with the lowest bleed air requirements (plenum pressure ratio).

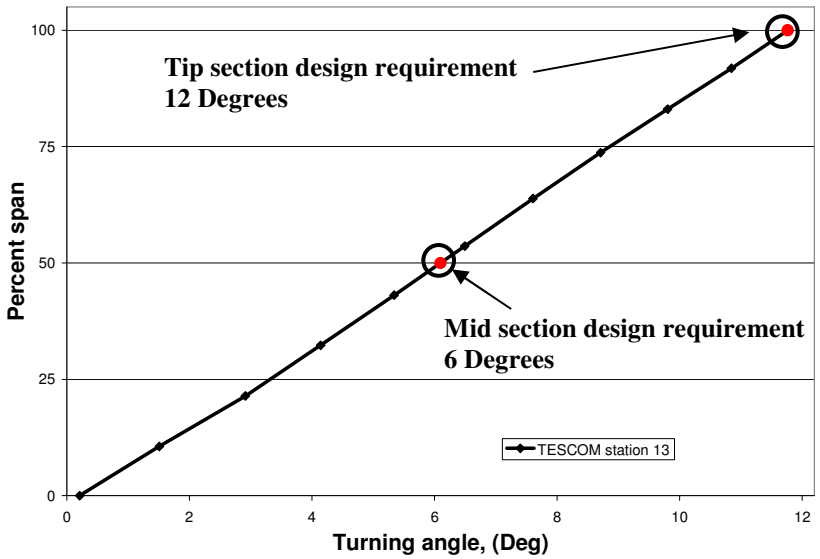

Figure C1: Percent span versus Turning angle, upstream of TESCOM's first stage

Common Methodology

On-design phases

Similar to the off-design study, the on-design study consisted of two phases. In the first phase (mid-span study) the use of a circulation control IGV at the conditions that corresponded to the mid-span location of the TESCOM rig was simulated. In the second phase (tip study) circulation control IGVs were tested at the radial location of the TESCOM rig which corresponded to the tip section of the cambered IGV (casing of the TESCOM rig). This logic proved to be flawed, which will be discussed in the methodology of the tip section study. The remainder of Appendix C presents the results from each phase. The discussion of each phase will give both the methodology and the results. At the end, the final remarks will reference both phases.

Code

The two-dimensional circulation control IGV was simulated using Advanced Ducted Propfan Analysis Code (ADPAC), a fully viscous Reynolds Averaged Navier Stokes (RANS) model. The boundary layer across the entire IGV was simulated as turbulent using the one equation Spalart-Allmaras turbulence model. The Spalart-Allmaras model was chosen due to its increased accuracy over the Baldwin-Lomax turbulence model in

predicting separated flows and its decreased computational time over a two-equation turbulence model.

Mesh

The four block mesh for this study, pictured in Figure C2, was built using GRIDGEN. The number of cells varied whenever the geometry was changed, but the topology remained the same. All meshes used in this study had an inlet block, an exit block, a main O-mesh block that wrapped around the IGV, and a plenum block that was located inside the IGV. The near wall spacing for the meshes was held at 2.54e-4 cm which kept the y+ values below 5.

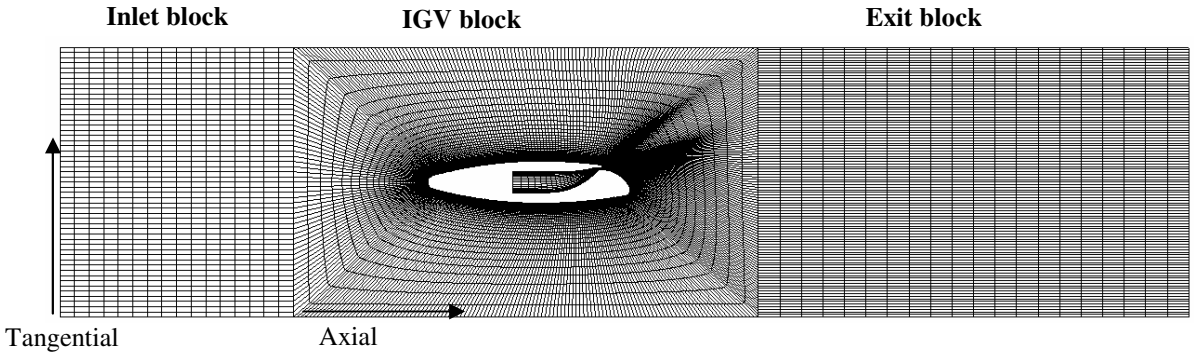

Figure C2: Mesh topology

Boundary conditions

The mesh had four boundaries: main inlet, plenum inlet, exit, and walls. The total temperature and pressure at the main inlet were set to reference values of standard day conditions (P_{ref} = 101 kPa T_{ref} = 288 K). At the plenum inlet, the total temperature was set to the reference value, while the ratio of total pressure ($P_{o,p}/P_{ref}$) was varied between 1.3 and 2.0. The static pressure ratio ($P_{e,s}/P_{ref}$) at the exit block was varied by setting the mass flow rate at the exit to achieve the proper inlet Mach number (0.5 for mid-span, 0.62 for tip). Boundary conditions at the walls were set to no-slip adiabatic. The upper most tangential cells and lower most tangential cells of the mesh were patched together to create a periodic boundary simulating a linear cascade.

Measurements

Measurements, shown in Figure C3, were made at three locations in order to calculate important variables such as, turning angle, mass flow rate, Mach number, and pressure loss. These variables were then used to compare the results from each CFD case. Inlet measurements were taken at the first location that corresponded to a distance of approximately 1 chord length before the leading edge of the IGV. The second location was the exit measurement in which data was taken at a distance of approximately 2.0 chords length behind the leading. Finally, the last location was the jet measurement where data was taken across the final x direction grid line on the plenum block. The measurements were taken using probe files that were generated from ADPAC. The probe files were set up to give mass averaged quantities across a constant *i* line on the mesh.

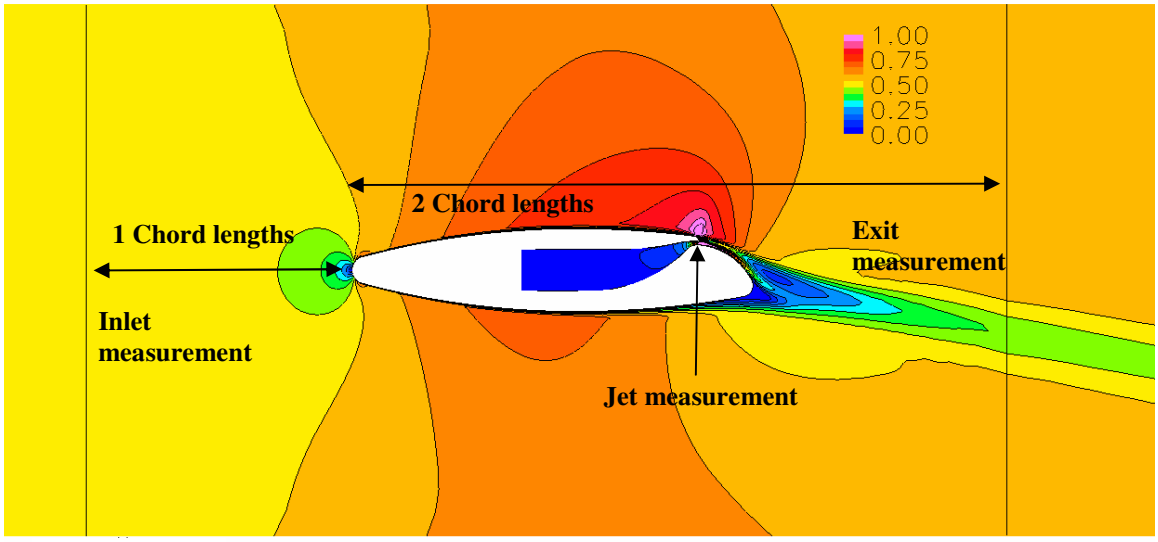

Figure C3: Measurement locations

Data reduction

Energy considerations

In order to compensate for the added total pressure from the Coanda jet, a corrected total pressure was calculated by mass averaging the inlet and supply total pressures.

$$P_{oc} = \frac{P_{oi}\dot{m}_1 + P_{oj}\dot{m}_j}{\dot{m}_i + \dot{m}_j} \qquad \text{(C-1)}$$

The corrected pressure loss coefficient was calculated as the change in total corrected pressure loss normalized by the inlet dynamic pressure.

$$\omega_c = \frac{P_{oc} - P_{o2}}{P_{o1} - P_{s1}} \qquad \text{(C-2)}$$

Turning angle

The flow turning angle was defined as the inverse tangent of the mass averaged tangential velocity (U_t) divided by mass averaged axial velocity (U_a).

$$\alpha = \tan^{-1} \frac{U_t}{U_a} \qquad \text{(C-3)}$$

Mid-span study

Geometry

In the mid-span study, a new circulation control IGV was developed (version 3) as the result of an emphasis on effectiveness at higher Mach numbers and the lower turning angles that were desired. This design, pictured in Figure C4, was a more streamlined version of the wedge design, used in the off-design study. It had a chord length of 3.63 cm and a maximum thickness of t/C=0.21 at 63 percent chord. The model was developed using SolidWorks so that the jet height, jet exit angle, and the trailing edge radius could be varied.

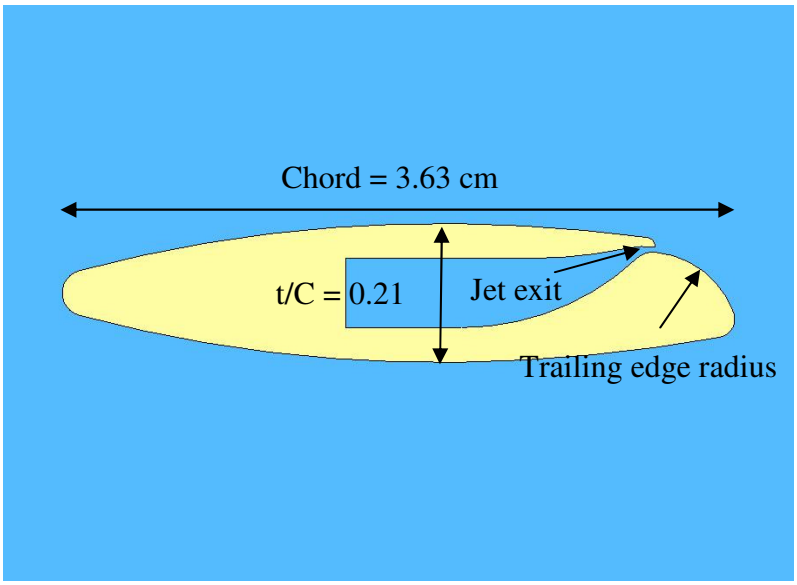

Figure C4: Mid-span Geometry, version 3

Mid-span study methodology

The first part of this study consisted of meeting the turning angle design requirement at the mid-span location of the TESCOM rig. At this particular location, the inlet Mach number was 0.5, the solidity was 0.76, and the turning angle requirement was six degrees. The geometric parameters varied in this study were the jet height, trailing edge radius, and the jet exit angle (measured from the vertical axis). Along with the geometric parameters, the plenum pressure ratio was also varied.

Trailing edge radius study

The first part of the mid-span study held the jet height constant at h/C = 0.008 and the ratio between jet height and trailing edge radius was varied between 0.05 and 0.12. Figure C5 shows the graph of turning angle versus h/R ratio for four different jet exit angles. The simulations in Figure C5 were run at the same plenum pressure ratio of 1.3. The results show that the greatest gain in turning angle was seen at an h/R ratio of 0.1 and a jet exit angle of 5 degrees from the vertical axis. The level of turning achieved by this case was nearly 11.5 degrees, nearly double the design requirement for the mid-span section.

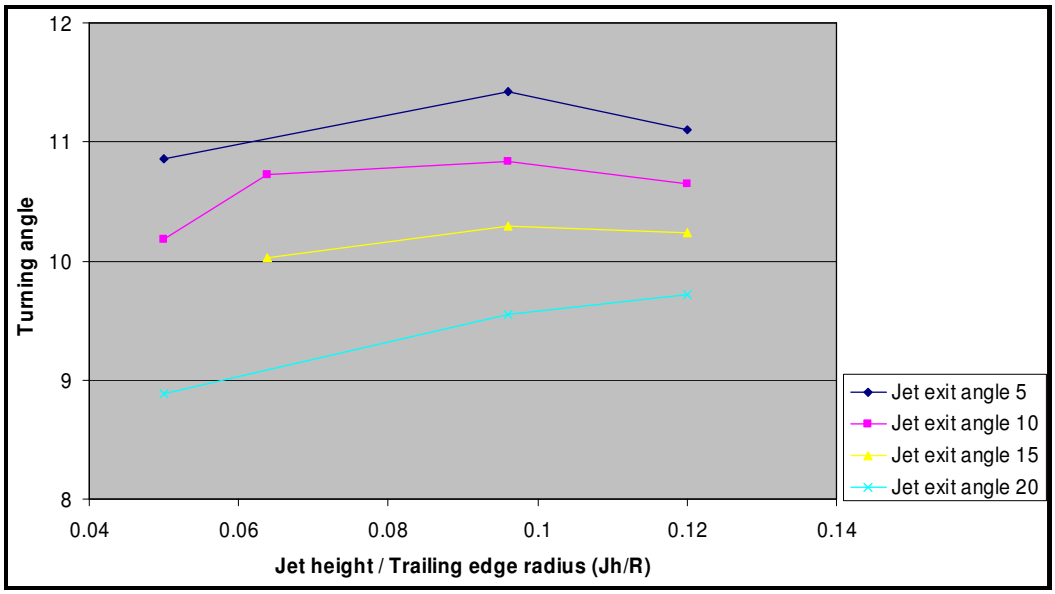

Figure C5: Turning angle versus h/R, plenum pressure ratio 1.3, h/C=0.008

One of the interesting things to note about this study was that as the jet exit angle became smaller (i.e. jet exit was more tangential to the flow), the turning actually increased, which is opposite of the results seen in the off-design study. This is a direct result of the higher Mach numbers of the free stream flow above. The higher inlet Mach number, coupled with the fact that the boundary layer would separate sooner for the stream-lined design of the new IGV than it did for the original wedge shaped geometry, limited the effectiveness of larger jet exit angles. Results from this study showed that the jet exit angle should be tangential to the free stream flow.

Another important factor in this study is the degree of pressure loss. In Figure C6, the corrected pressure loss is plotted against the h/R ratio for three exit angles at a plenum pressure ratio of 1.3.

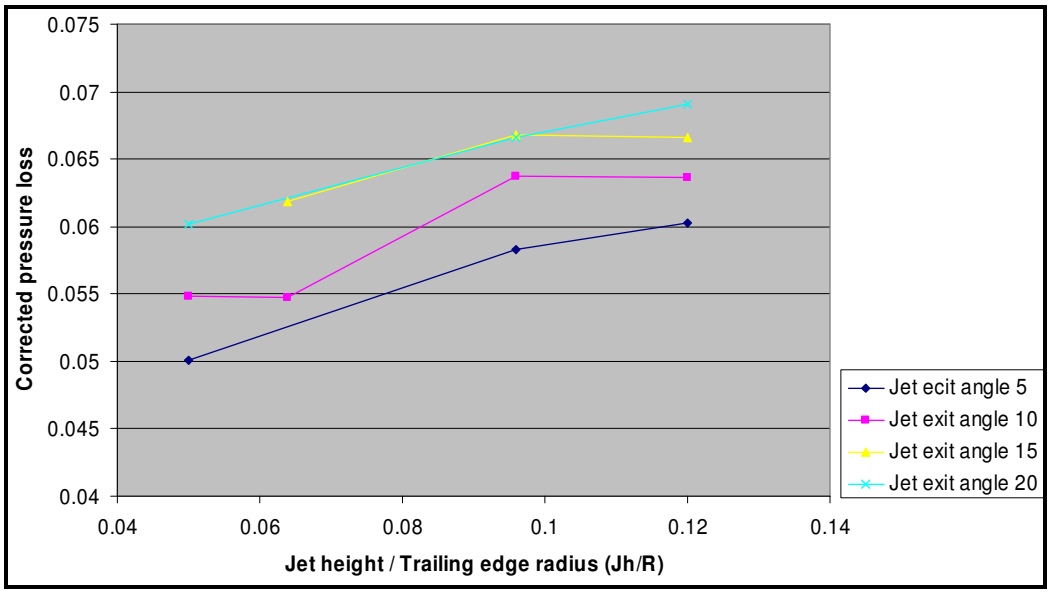

Figure C6: Corrected pressure loss versus h/R, plenum pressure ratio 1.3, h/C=0.008

The overall trend in Figure C6 is that the pressure loss is proportional to the h/R value. This is a direct result of the amount of entrainment the jet was able to generate. The less amount of entrainment that the jet created, the greater the amount of pressure loss due to the size of the vortex that was behind the IGV, as seen in the Mach number flow field in Figure C7. The larger exit angles (Figure C7b) generated larger vortices behind the IGV, resulting in higher pressure losses. The larger trailing edge radii generated more losses due to the increased turning.

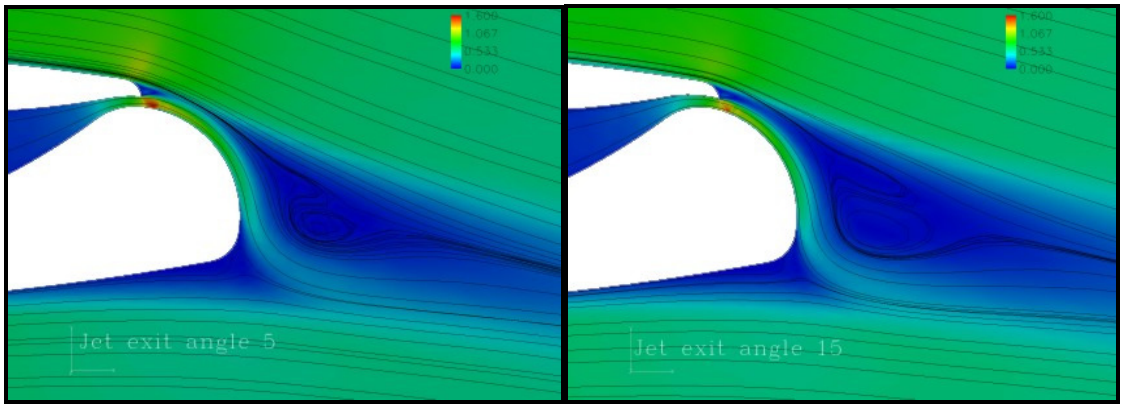

(a) 5 degree jet angle **(b) 15 degree jet angle**

Figure C7: Mach number flow field

Mid-span pressure ratio study

From the results of the trailing edge radius study, it was shown that an h/R ratio of 0.05 resulted in the lowest pressure losses. However, the turning angles at a plenum pressure ratio of 1.3 were higher than desired; thus the plenum pressure ratio study was done using a smaller jet height with the same h/R ratio. The jet height used in this study was reduced to h/C=0.006 and the trailing edge radius was R/C=0.11. The reasoning behind using a smaller jet height was to limit the amount of mass flow thought the jet, effectively reducing the jet's momentum to create lower turning angles and lower pressure losses. The results for the plenum pressure ratio are shown in Figure C8, a plot of turning angle versus plenum pressure ratio for a constant h/R value of 0.05.

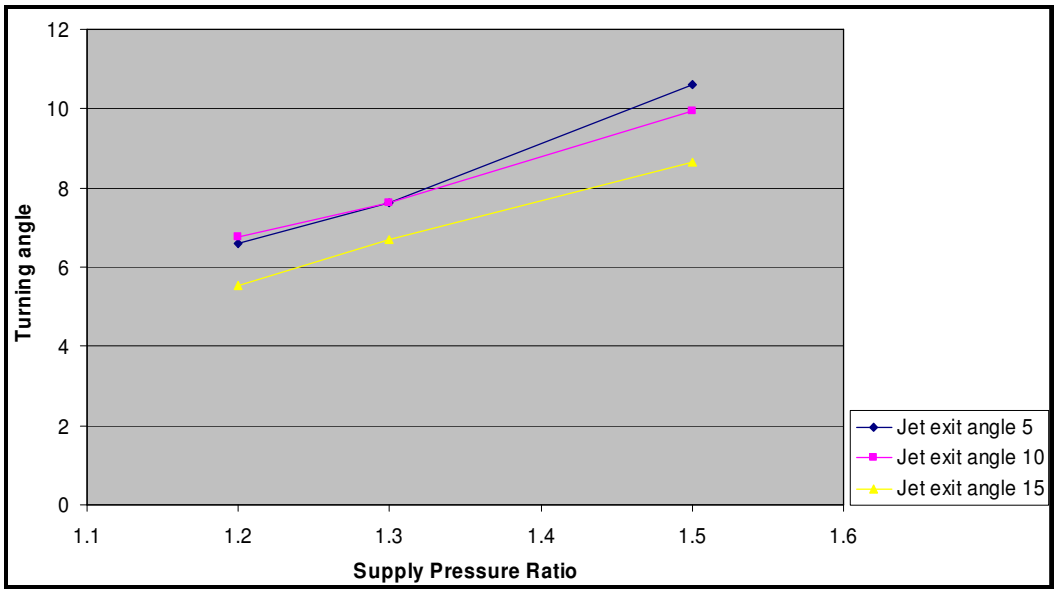

Figure C8: Turning angle versus Supply pressure ratio (plenum pressure ratio), h/R=0.05

The results show that the design goal (6 degrees of flow turning) could be achieved using a lower plenum pressure ratio (1.2). Furthermore from Figure C9, a plot of corrected total pressure versus supply pressure ratio (plenum pressure ratio), it can be seen that the lower pressure ratios create lower pressure losses.

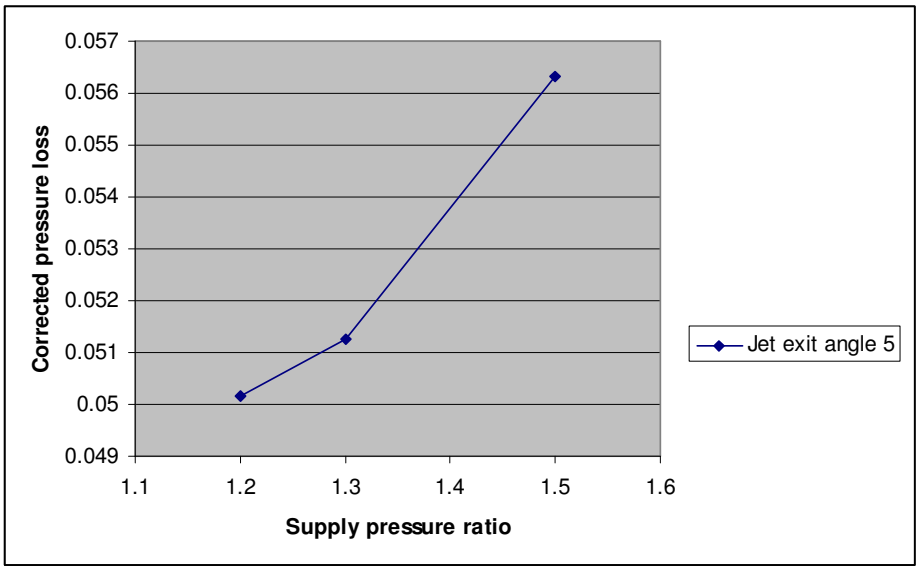

Figure C9: Corrected pressure loss versus supply pressure ratio, h/R=0.05

The results from the study of plenum pressure ratio (supply pressure ratio) showed that meeting the design requirement in the mid-span section would require a lower plenum pressure ratio. The problem with this result is that the supply ratio would be constant for the entire plenum in a three dimensional circulation control IGV, which means that the tip would have to use the same pressure to meet the design goal of 12 degrees with a 28 percent increase in pitch.

Tip Study

Methodology

The second part of this study consisted of meeting the design requirement at the tip section. The tip section required 12 degrees of flow turning at an inlet Mach number of 0.62. The pitch at the tip section was 6.3 cm and the solidity varied depending on the geometry. The initial result of using the same geometry from the mid-span section proved that the design on the IGV needed to be more streamlined. To meet the design requirements at the tip the design of the IGV was studied. When a more practical design was found the effect of jet height was studied at varying plenum pressure ratios.

Results

Mid-span geometry at the tip

The logic in beginning the on-design study at mid-span proved to be flawed since the higher inlet Mach number (0.62) at the tip section severely hindered the turning ability of the circulation control IGV geometry from the mid-span study. As seen in Figure C10, the Mach number flow field of the mid-span geometry at the tip location, there was a large region of sonic flow above the suction side of the IGV that extended all the way to the jet. The region of sonic flow above the jet destroyed the IGV's ability to entrain flow due to the fact that the flow directly above the jet is at nearly the same pressure as the jet itself. Similar pressures between the freestream flow and the jet created very little entrainment, which led to decreased circulation and flow turning.

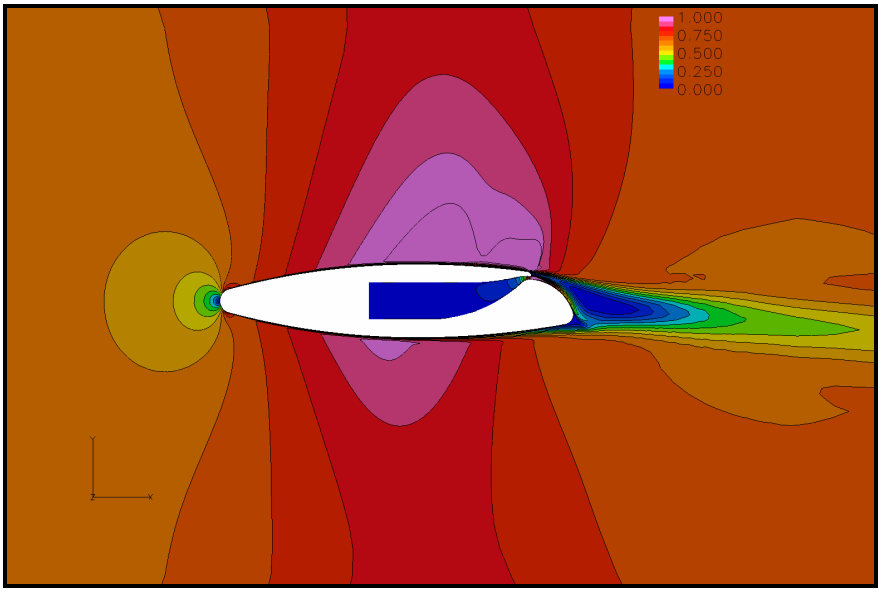

Figure C10: Mach contours, mid-span geometry at the tip

The same parameters that were studied at mid-span were also studied for this geometry at the tip section; however, all of the studies yielded poor results. The maximum turning seen by this model was on the order of 7 degrees – 5 degrees short of the design intent. To combat the poor ability of this model, new geometries were studied at the tip.

Geometric study at the tip

Various geometries with trailing edge circulation control were studied at the tip, five of which, beyond the first mid-span geometry, will be discussed. Models that are not discussed demonstrated poor performance for either turning angle or pressure loss. The next five geometries were variations of the mid-span geometry (version 3). For all of the versions tested, the jet height to pitch ratio remained the same at h/P = 0.0048.

Version 4

Version 4x, pictured in Figure C11, was the first geometry studied beyond the mid-span geometry. It had a chord length of 3.68 cm and it was 8 percent thinner than version 3 at the max thickness location (t/C=0.193).

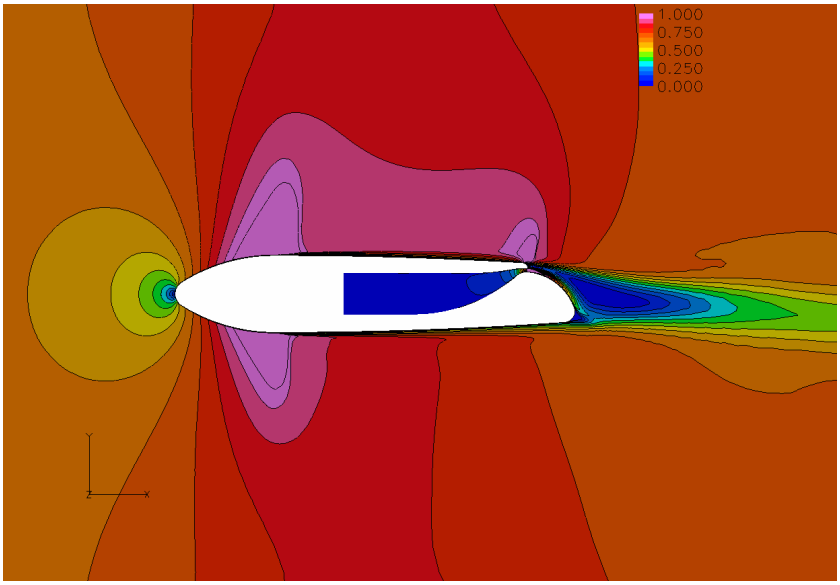

Figure C11: Version 4 Mach contours

The profile of the geometry was chosen to be more like a flat plate so that the reduction in thickness between the maximum thickness and thickness before the jet was only 17 percent. For this geometry, the location of maximum thickness was studied (measured as percent total chord from the leading edge). As seen in Figure C12, a plot of turning angle versus max thickness location at a constant plenum pressure ratio of 1.2, the closer the max thickness was to the leading edge, the greater the performance of the IGV. Plenum pressure ratio studies showed that this design could achieve a maximum turning of only

4.5 degrees at a plenum pressure ratio of 1.5. This design had the same problems that the mid-span geometry suffered: it had a region of high speed flow directly above the jet that mired the ability of the Coanda jet to entrain flow. Furthermore, it also suffered from boundary layer separation just above the jet. The combination of high speed flow and boundary layer separation caused major problems for this geometry.

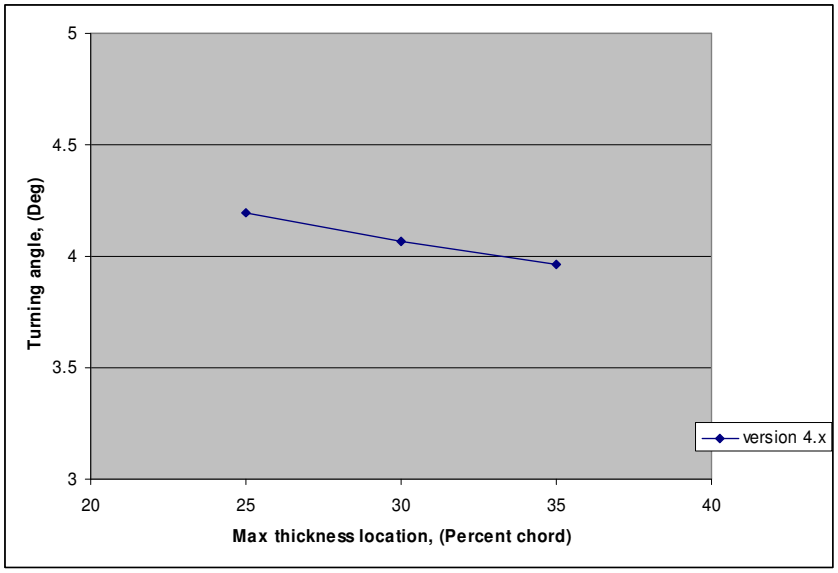

Figure C12: Turning angle versus Max thickness location, version 4

Version 5

The next geometry studied, version 5, was similar to version 4 (same chord and max thickness). However, the max thickness before the jet was reduced to $t_{jet}/C = 0.128$; 20 percent thinner than version 4. Furthermore, the location of the max thickness was 35 percent chord behind the leading edge. This geometry, pictured in Figure C13, performed slightly better than version 4 at a plenum pressure ratio of 1.2. However, it still suffered the same problems with high speed flow above the jet and boundary layer separation. The geometry was able to reduce the size of the high speed flow above the jet, which was very promising.

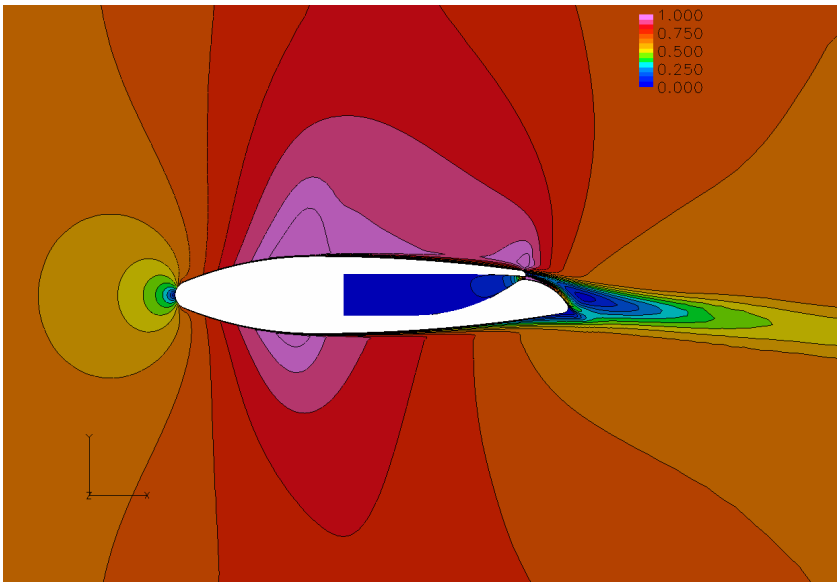

Figure C13: Version 5 Mach contours

Version 6

Version 6, pictured in Figure C14, was a departure from versions 4 and 5 because the location of max thickness was moved closer to the jet instead of further away (located at 70 percent behind leading edge). It had the same maximum thickness as versions 4 and 5, as well as the same chord length. This geometry was very inefficient and proved that the location of max thickness must be closer to the leading edge of the air-foil for high speed flows. The geometry only achieved 3 degrees of turning at a plenum pressure ratio of 1.2. It also suffered the same problems with high speed flow above the Coanda jet and boundary layer separation.

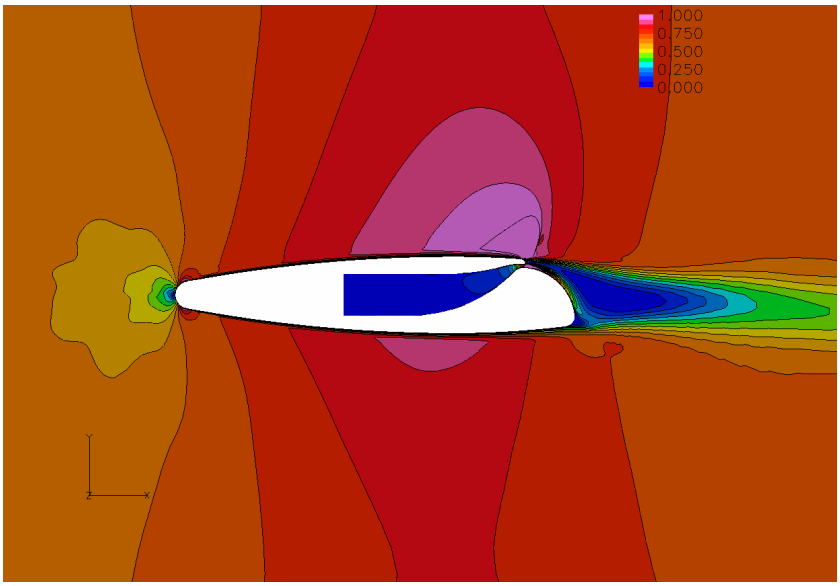

Figure C14: Version 6 Mach contours

Version 7

Version 7, pictured in Figure C15, had a larger reduction in thickness before the jet exit than versions 4 and 5. The max thickness was the same as versions 4, 5, and 6, as well as the same chord length. The thickness before the jet was reduced to $t_{jet}/C = 0.084$; a 34 percent reduction in thickness compared to version 5. This reduction in thickness allowed the IGV to reduce the high speed flow above the jet. However, due to the thickness of the jet lip, the boundary layer separated before the jet exit, only allowing the model to turn the flow 6 degrees at a plenum pressure ratio of 1.5.

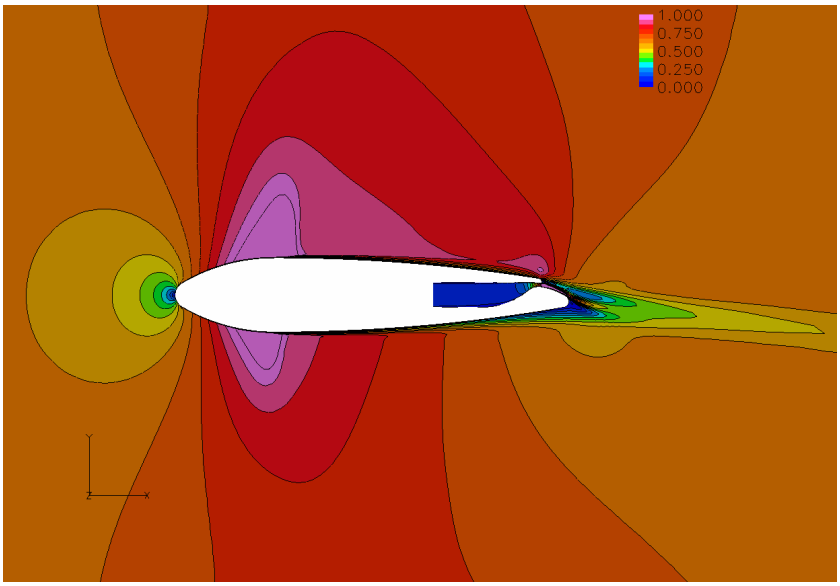

Figure C15: Version 7 Mach contours

Version 14, Best tip Geometry

One of the main problems with all the models studied up to this point was the thickness of the lip directly above the jet opening (jet lip). The ratio of the size of the jet lip to the size of the jet height was on the order of 2 times the jet height. If the jet lip were able to come to a knife edge (i.e. thinner), the boundary layer would not separate just above the jet, which would allow the circulation control IGV to be more effective. The next geometry reduced the thickness of the lip by a factor of ten and made the edge just above the jet round. This resulted in much more flow entrainment and better performance. The chord length was increased to 5.1 cm and the maximum thickness (located at 25 percent chord length behind the leading edge) was increased to t/C = 0.171; a 22 percent increase over version 7. The ratio of thickness to pitch in the region of the jet exit was t_{jet}/C = 0.056, which was a 14 percent increase over version 7. The ratio of trailing edge radius to chord length was held constant (R/C = 0.113) for this geometry and the jet exit angle was held constant so that the jet exited tangential to the freestream flow. The variable parameters for this model were the jet height and the plenum pressure ratio.

Figure C16 shows the performance of version 14 for the range of plenum pressure ratios studied and jet heights. The plot in Figure C14 is a plot of turning angle versus

normalized jet height h/C; the lines on the plot represent the various plenum pressure ratios studied. Figure C17, a plot of corrected plenum pressure ratio versus h/C for the range of plenum pressure ratios studied, shows the corrected pressure losses that are associated with increasing the plenum pressure and jet heights. This model was able to achieve two-thirds of the desired 12 degrees of turning. This was a significant gain in turning over any other geometry studied. Furthermore, this geometry achieved nearly two degrees higher turning and a lower amount of pressure loss than version 3.

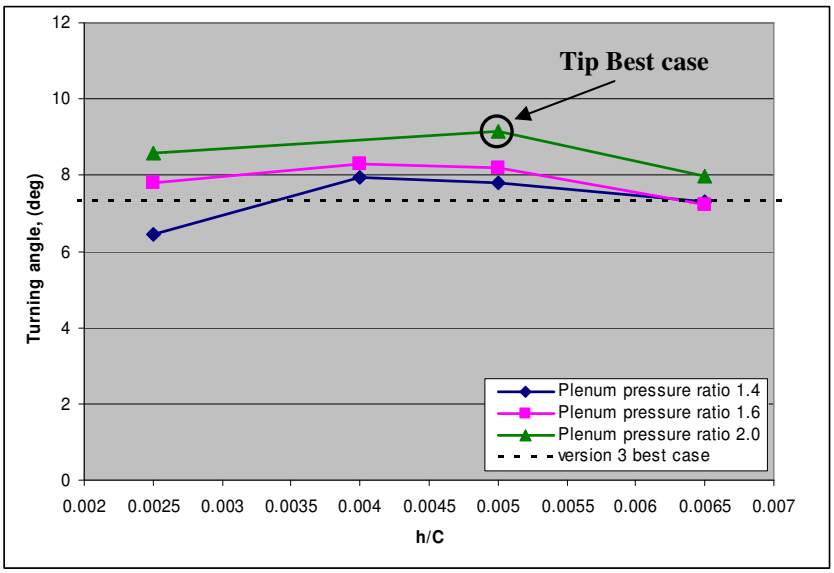

Figure C16: Turning angle vs. h/C, version 14

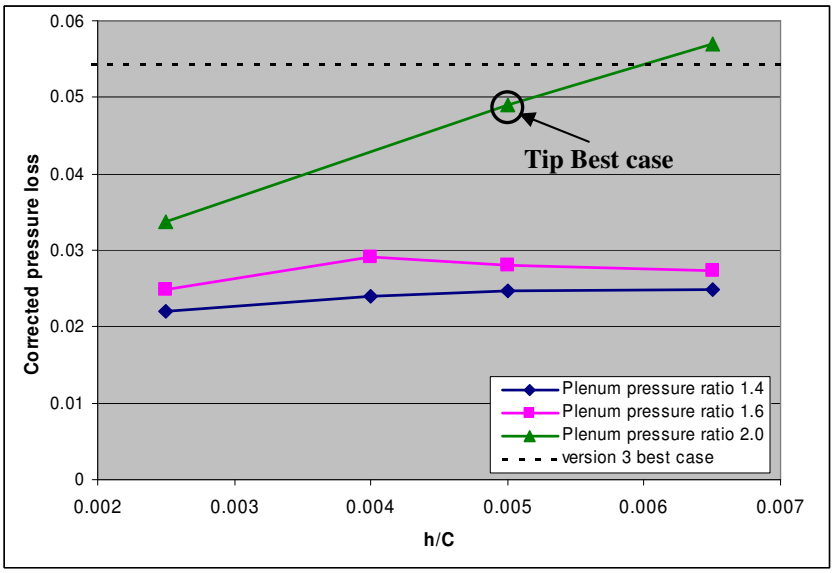

Figure C17: Corrected pressure loss vs. h/C, version 14

The amount of pressure loss increased as the plenum pressure ratio was raised. Also, the overall trend from Figure C17 shows that as the increasing the jet height resulted in larger pressure losses. This trend is not as strong for plenum pressure ratios 1.4, and 1.6. However, for a plenum pressure ratio of 2.0, the amount of pressure loss is directly proportional to jet height.

The flow field for version 14 best case is shown in Figure C18, which is a visualization of the Mach contours around the IGV. One of the most interesting things to note about this figure is that there is an area of high speed flow that extends from the attached jet on the Coanda surface into the freestream. This area of high speed flow indicates that boundary layer separation due to the jet lip is not as large of a problem as seen in prior geometries at the tip. Another important factor of interest is that there is a much smaller region of low speed flow behind the trailing edge of the IGV than was seen by other geometries at the tip. The fact that the region of sonic flow above the jet becomes sonic then immediately decelerates suggests that there is a shock. This shock is the most likely barrier to any further increase in turning.

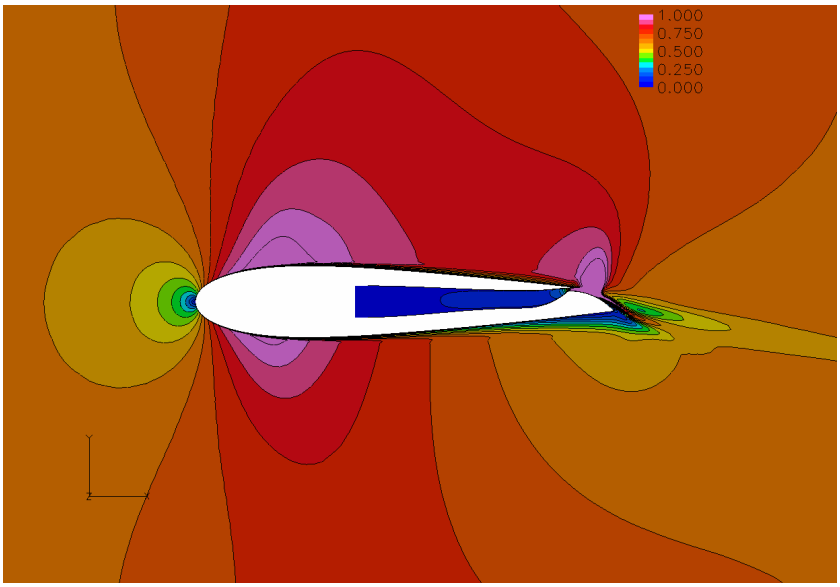

Figure C18: Version 14 Mach contours

Conclusion

One of the major conclusions of this study was that the problems experienced in the tip section would dominate the design of the IGV at all radial locations due to the fact that the plenum pressure ratio would be constant across the entire span of a 3D IGV. In order to meet the design goal of 6 degrees at mid-span, the geometry had to use a plenum pressure ratio of 1.2. However, the tip section needed a supply pressure ratio of 2.0. This meant that the design at mid-span would need to be changed in order to meet the design goal of 6 degrees with a much higher plenum pressure ratio. The results at the tip section showed that the turning ability of the IGV is affected by both the location of maximum thickness on the blade and the resulting thickness before the jet exit. It also showed that size of the lip above the jet exit was extremely important to the effectiveness of the IGV. Unfortunately, the design goal was not achieved at the tip section. Furthermore, it was realized at the beginning of the 3D circulation control IGV study that the inlet Mach numbers used for the 2D on-design study were too high (i.e. inlet Mach number at the tip was 0.62 when it should have been 0.54). The mistake proved to be detrimental for the on-design study.

Appendix D: TESCOM 3D

Introduction

The results from the 2D tip study showed that the circulation control Inlet Guide Vane (IGV) could only match two-thirds of the required turning angles. In order to find out how a circulation control Inlet Guide Vane would perform in an actual compressor, a 3D study was performed. Similar to the 2D study, the number of blades in this study was eighteen - half the number of mechanical cambered IGVs that are currently in the TESCOM rig.

Objectives

The 3D study had similar objects as the 2D study. The main objective of this study was to meet the turning angles that are created by the cambered IGV in the TESCOM rig with a circulation control IGV using the least amount of bleed air (i.e. plenum pressure ratio). Furthermore, this study set out to compare the effectiveness of the 3D circulation control IGV by comparing the amount of pressure loss from the circulation control IGV and the current cambered IGV in the TESCOM test rig.

Methodology

Geometries

Seven geometries were studied in the 3D simulations, of which three will be discussed in this appendix. Version 21, which represents a typical profile of a 3D circulation control IGV is show in Figure D1. Each geometry had slightly different variations; however the common traits between them are the leading edge location, the span at the leading edge (7.9 cm), and the nominal chord length up to the jet exit (C_n = 3.6 cm). The parameters that were varied on the models were: the trailing edge radius, the jet height, and the span of the jet along the radial direction. The geometric variations for each model will be discussed in the following results section.

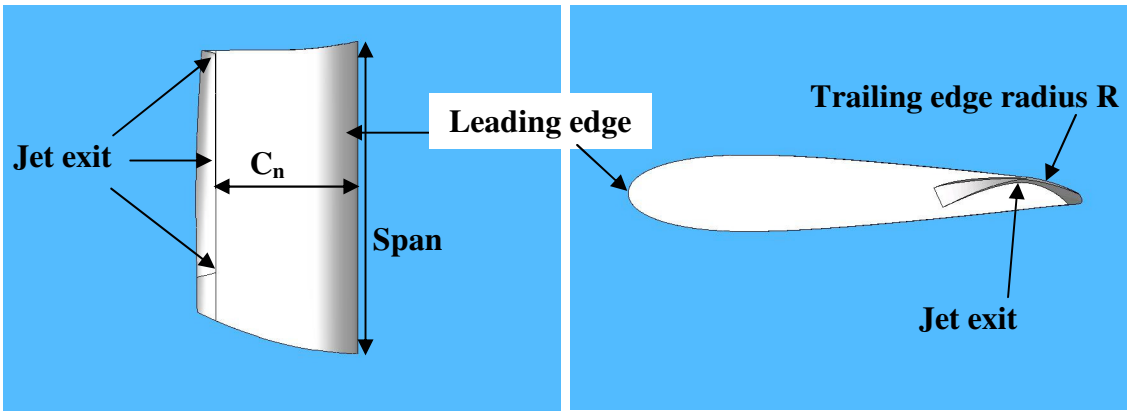

(a) suction side view **(b) top side view (case)**

Figure D1: 3D circulation control IGV, Version 21

Code

The three-dimensional circulation control IGV was simulated using Advanced Ducted Propfan Analysis Code (ADPAC), a fully viscous Reynolds Averaged Navier Stokes (RANS) model. The boundary layer across the entire IGV was simulated as turbulent using the one equation Spalart-Allmaras turbulence model. The Spalart-Allmaras model was chosen due to its better accuracy over the Baldwin-Lomax turbulence model in predicting separated flows and its decreased computational time over a two-equation turbulence model.

Mesh

The mesh topology remained similar for all designs tested, however, the number of cells varied between 1.1 million and 1.25 million due to changes in 3D geometric parameters along the radial direction. Each circulation control IGV mesh consisted of 7 blocks: inlet block, exit block, plenum block, and four blocks that wrapped around the IGV. Pictured in Figure D2 is a typical mesh for the three dimensional study. The blue area in Figure D2 shows the location and shape of the IGV. The green area is the hub side of the inlet and directly above the hub side is the casing (not colored). The ratio of near wall spacing to nominal chord was held at 4.6e-5 in order to keep the average y+ values on the Coanda surface below 3.

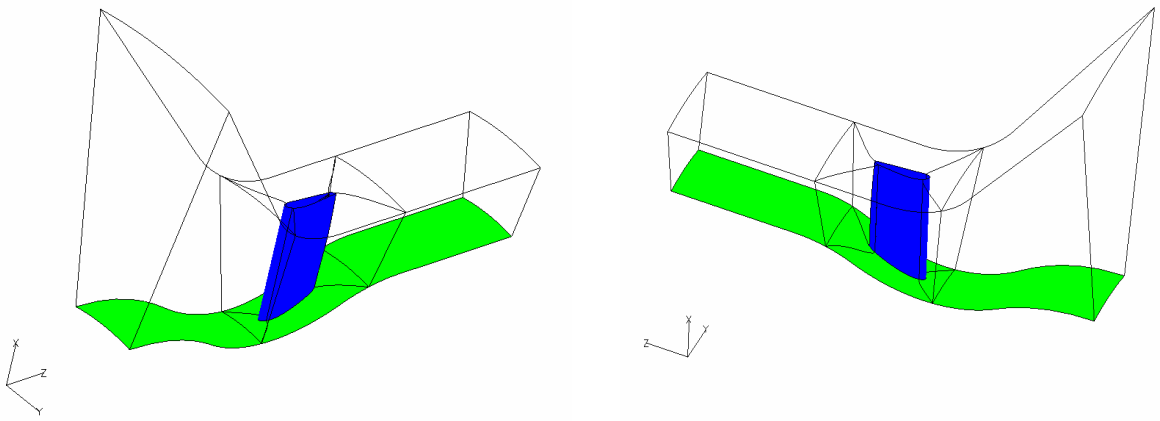

(a): pressure side **(b) suction side**

Figure D2: Typical 3D circulation control IGV mesh

The baseline cambered IGV pictured in Figure D3 was set up in a similar fashion to the circulation control IGV mesh. It had six blocks, 14960 cells, and its near wall spacing was set to 2.54e-4 cm, which held the average y+ values below 1.5.

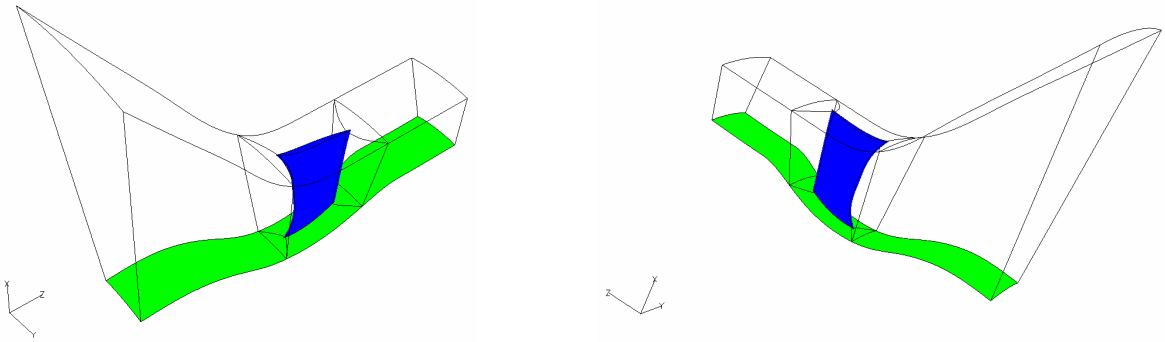

(a): pressure side **(b) suction side**

Figure D3: Cambered IGV

Boundary conditions

The circulation control mesh had four boundaries: main inlet, plenum inlet, exit, and walls, while the TESCOM mesh had three boundaries: main inlet, exit, and walls. The total temperature and pressure at the main inlets were set to reference values of standard day conditions (P_{ref} = 101 kPa , T_{ref} = 288 K), which were constant across the radial direction. At the plenum inlet, the total temperature was set to the reference value, while the ratio of total pressure ($P_{o,p}/P_{ref}$) was varied between 1.3 and 2.0. At the exits a mass flow rate boundary condition was set that varied the exit pressure ratio along the radial

direction to achieve both the proper mass flow rate and radial equilibrium. In order to simulate the design conditions of the TESCOM rig the mass flow rate (11.3 kg/s) into the first stage of the compressor was matched by dividing the total mass flow rate by the number of blades. The total number of circulation control IGVs was eighteen, thus to simulate the total mass flow rate of an entire annulus, the mass flow rate at the circulation control mesh's exit was set to 0.63 kg/s (i.e. 11.3/18 kg/s), while the mass flow rate for the baseline mesh was set to 0.31 kg/s since the blade count was thirty-six. Boundary conditions at the walls were set to no-slip adiabatic. The outer most tangential cells and inner most tangential cells of the mesh were patched together to create a periodic boundary simulating a full annulus.

Measurements

Measurements, shown in Figure D4, were made at three locations in order to calculate important variables such as turning angle, mass flow rate, Mach number, and pressure loss. These variables were then used to compare the results from each CFD case. All measurements were taken using a FORTRAN code that calculated mass-averaged quantities along fifty points in the radial direction. These points were mass averaged across the tangential direction so that their values were at the center of the tangential direction on a radial plane. The planes were extracted from the mesh and solution files at locations which corresponded to the inlet (station 4 of the TESCOM rig) and the exit (first rotating blade of the TESCOM rig). The axial location of the inlet plane varied along the radial direction with an axial distance of 1.1 C_n before the leading edge of the circulation control IGV at the hub and an axial distance of 1.2 C_n upstream of the leading edge of the circulation control IGV at the tip. The exit plane's axial location also varied along the radial direction with the hub side location being 1.31 C_n downstream of the leading edge of the IGV and the casing side location was 1.46 C_n downstream of the leading edge of the IGV. 1-D values such as total pressure, inlet velocity, and static pressure were calculated by mass averaging the Q-variables across the entire inlet and exit planes into single values, then the mass averaged 1D variables from an ADPAC probe file at the jet exit location were used to calculate the corrected pressure loss, and the momentum coefficient.

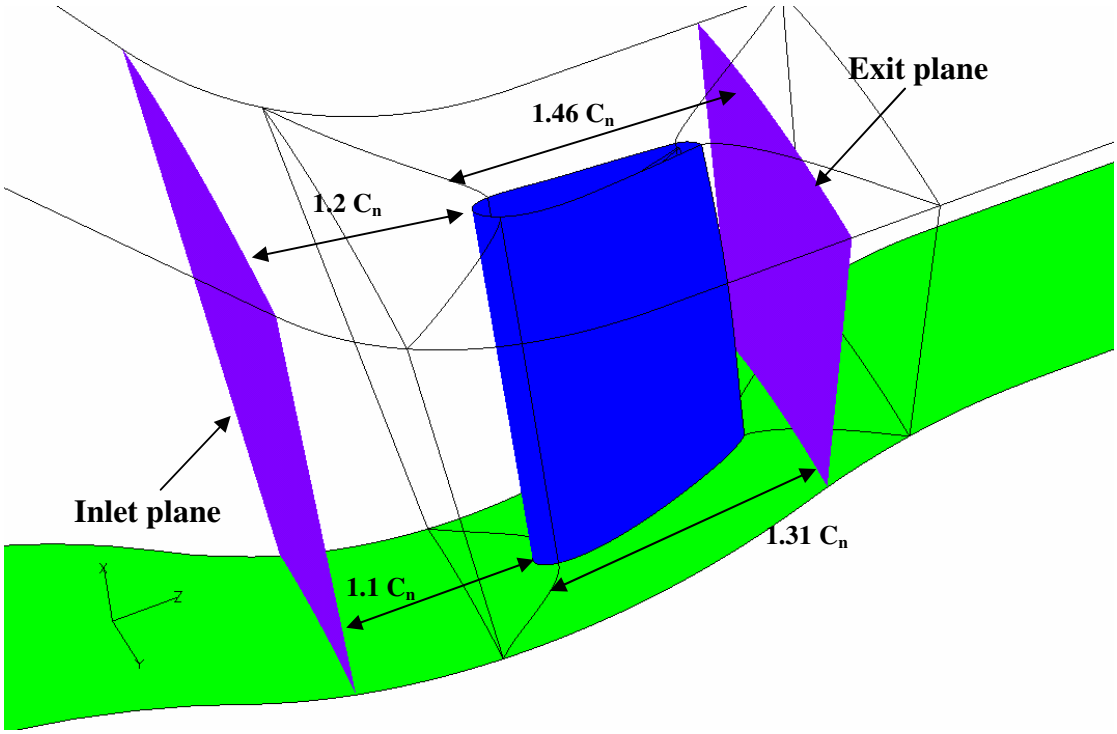

Figure D4: Measurement locations

Data reduction

Energy considerations

In order to compensate for the added total pressure from the Coanda jet, a corrected total pressure was calculated by mass averaging the inlet and supply total pressures.

$$P_{oc} = \frac{P_{oi}\dot{m}_1 + P_{oj}\dot{m}_j}{\dot{m}_i + \dot{m}_j} \qquad \text{(D-1)}$$

The corrected pressure loss coefficient was calculated as the change in total corrected pressure loss normalized by the inlet dynamic pressure. The corrected pressure coefficient was calculated as a one dimensional parameter using the inlet, exit, and jet exit planes.

$$\omega_c = \frac{P_{oc} - P_{o2}}{P_{o1} - P_{s1}} \qquad \text{(D-2)}$$

Turning angle

The flow turning angle was defined as the inverse tangent of the mass averaged tangential velocity (U_t) divided by mass averaged axial velocity (U_a). The turning angles were computed along the radial direction before the first rotating blade stage.

$$\alpha = \tan^{-1} \frac{U_t}{U_a} \qquad \text{(D-3)}$$

Results

In the results section the geometric variations of three 3D models will be discussed. Following the geometric variation of each model, the results of the model will be discussed; however the results for the final model (version 21) will be discussed in the version comparison section.

Version 15

V15, seen in Figure D5, was the first 3D circulation control IGV that was tested. At the hub location, the profile of the IGV was asymmetrical, meaning that the pressure side of the IGV and the suction side of the IGV were not the same. The radial distribution of the jet height started at 26 percent of the span and ended at 93 percent of the span at the trailing edge. The jet height was a linearly distributed along the span wise direction with the bottom portion of the jet having a height of h/C_n= 0.0014 and the top portion of the jet having a jet height of h/C_n=0.0036. The radius distribution between the hub and the bottom of the jet remained the same (R/C=0.25). However, between the bottom portion of the jet, and the top portion of the jet the radius decreased linearly to an h/R value of

0.125. From the top of the jet to radial location at the tip of the IGV, the radius size remained the same (R/C_n=0.125).

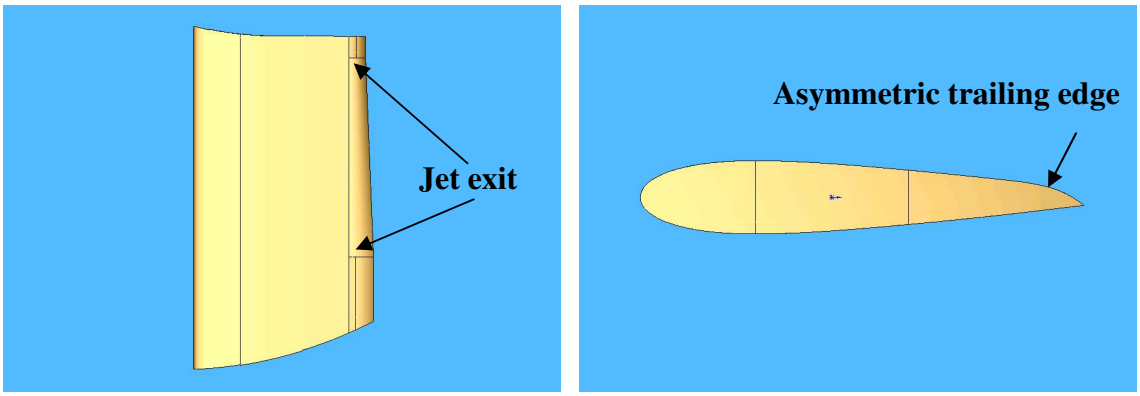

(a) suction side view **(b) hub side view**

Figure D5: 3D circulation control IGV, Version 15

Version 15 was tested at two plenum pressure ratios, 1.3 and 2.2. The results shown in Figure D6, a plot of percent span versus turning angle, shows that the model was able to achieve the nearly the same turning angle as the cambered IGV between 25 and 65 percent of the radial span before the first rotating stage of the TESCOM rig.

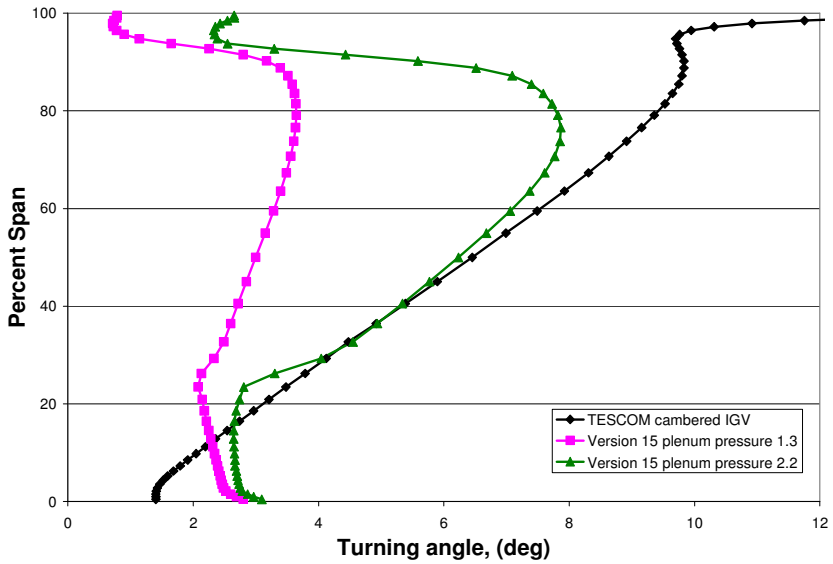

Figure D6: Turning angle results for version 15

Between 0 and 25 percent span, the IGV had a flat turning angle that was a result of the asymmetric profile at the hub (Figure D5b). The hub side profile allowed the on coming

boundary layer to remain attached to the curved surface, even though there was not a Coanda jet, which created unintended flow turning. Beyond 65 percent span, the tangential turning angle rapidly dropped off. This effect was due to a three dimensional vortex which formed just below the case section. This vortex, pictured in Figure D7, was due to an up-wash along the pressure side and trailing edge of the IGV and 3D dimensional effects due to the case boundary layer. Figure D8 shows the vectors along the radial plane before the first rotating stage.

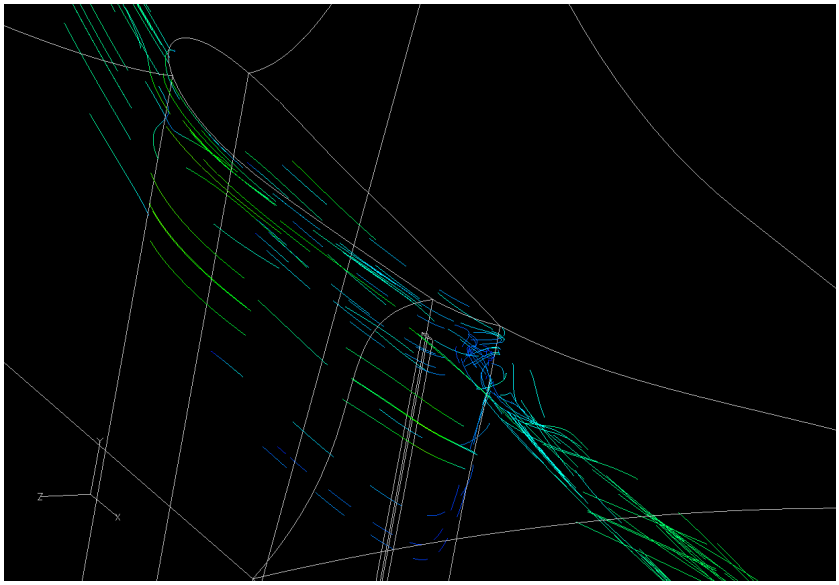

Figure D7: Flow visualization of the vortex behind the trailing edge near the tip of version 15

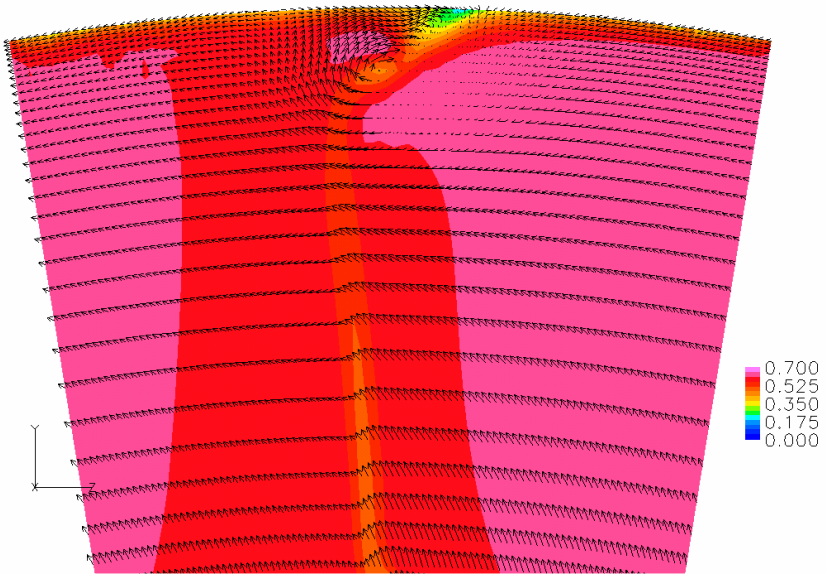

Figure D8: Plane view of the vortex before first rotating stage, Mach contours 0 to 0.7

Figures D7 and D8, show the overall shape of the vortex that diminished the ability of the 3D circulation control IGV. To combat the vortex the shape of the circulation control IGV was changed near the tip section.

Version 19

Version 19, pictured in Figure D9, was built to combat the effect of the vortex at the tip. In order to minimize the tip vortex the location of the jet closest to the case was moved up to 99 percent of the span. Furthermore, the distribution of the trailing edge radius was changed from a linear variation to an hour glass type variation. The jet was moved closer to the hub so that the jet was at a radial location of 15 percent of the span above the hub and the jet height at this location was held at h/C_n=0.0014. The trailing edge radius was lofted between a symmetrical profile at the hub (pressure side and suction side profiles were the same) and a radius of R/C_n = 0.214 at 15 percent span. At 89 percent of the span, the jet height was changed to h/C_n=0.005 and the radius was decreased to R/C_n=0.089. Both the trailing edge radius and jet height varied linearly between the span wise locations of 15 and 89 percent. From 89 percent to the 99 percent of the span, the radius varied linearly between R/C_n=0.089 and R/C_n=0.161. Furthermore, between the 89 and 99 percent span location, the jet varied linearly between h/C_n=0.005 and h/C_n=0.0079. From 99 percent span to the tip, the radius varied between R/C_n=0.161 and R/C_n=0.163. The reason that the trailing edge radius was decreased at 89 percent span was to provide a sharper trailing edge to increase turning. The jet size and trailing edge radius was increased after 89 percent to allow a higher momentum jet and to allow jet to remain attached near the tip section.

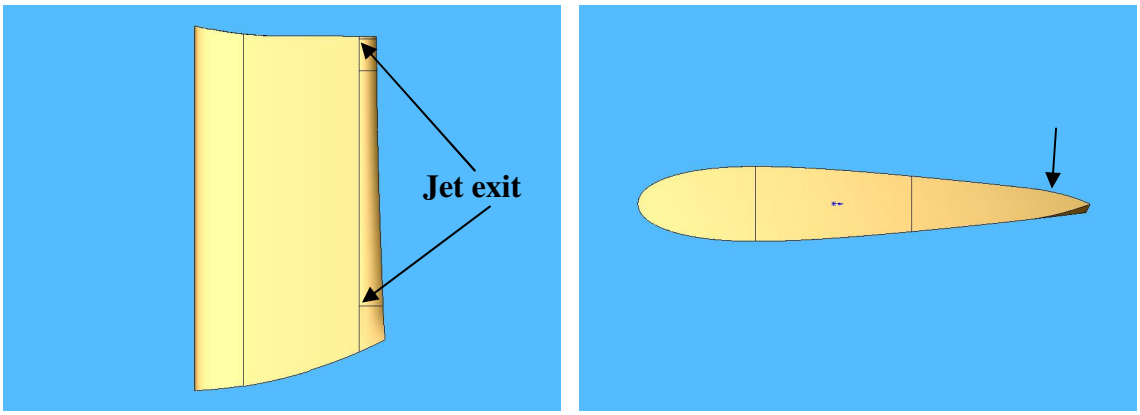

(a) suction side view **(b) hub side view**

Figure D9: 3D circulation control IGV, Version 19

The results shown in Figure D10, a plot of percent span versus turning angle for version 19 at a blowing ratio of 2.0, shows that the turning angles were actually increased beyond the IGV up to 70 percent of the span before the first rotating stage. The changes made to version 19 allowed the model to use a lower supply pressure to achieve better turning than version 15, however, the effect of moving the jet height closer did not diminish the effect of the tip vortex.

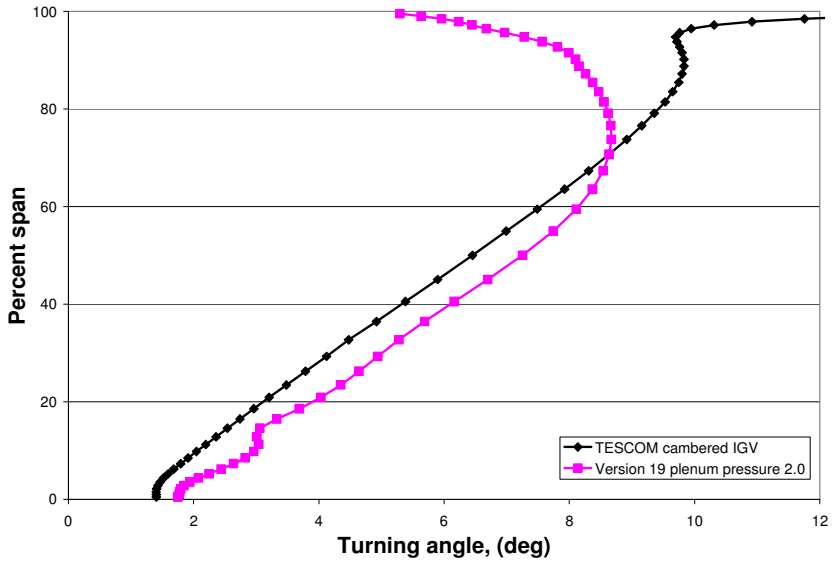

Figure D10: Turning angle version 19

Version 21

To further combat the vortex near the tip region, version 21 (pictured in Figure D1) incorporated a new feature inside the plenum which vectored the flow upward toward the tip. This new feature was simply a diverging wall on the top side of the jet that helped

combat the downwash on the suction side of the IGV. The lower side of the diverging wall started at a radial location of 95 percent span and the upper side ended at the jet exit at 99 percent of the span. The new design of the IGV included four planes along the radial direction that had varying trailing edge radii. The trailing edge of the IGV was created by a loft cut in SolidWorks between the four planes, as shown in table D1.

Table D1: Loft planes for trailing edge radius version 21

Plane number	Plain location (percent span)	R/C_n
1	13% below the hub	0.286 (symmetrical)
2	3.5% above the hub	0.286 (symmetrical)
3	54% above the hub	0.189 (suction side only)
4	104% above the hub	0.093 (suction side only)

The jet exit was also changed. It was no longer a linear variation between points instead the jet opening was governed by a straight line and a curve. The opening between the straight line and the curved line was governed by three points. At the first point, located at 18 percent of the span in the radial direction above the hub, the jet height was h/C_n=0.0036. At the second point located at 93 percent of the span above the hub, the maximum jet height was h/C_n=0.0114. At the last point, located at 99 percent span (top of the jet), the jet height was h/C_n=0.0043.

The effect of using the angle jet can be seen in differences in Figure D11, a vector flow field visualization of flow directly above the IGVs Coanda surface. Figure D8a shows the typical direction of the flow on the pressure side of the IGV when the top of the jet was not angled. In Figure D11a, the vectors on the trailing edge indicate that there is a down-wash along the Coanda surface, while the vectors in Figure D11b indicate that the down-wash has been reduced.

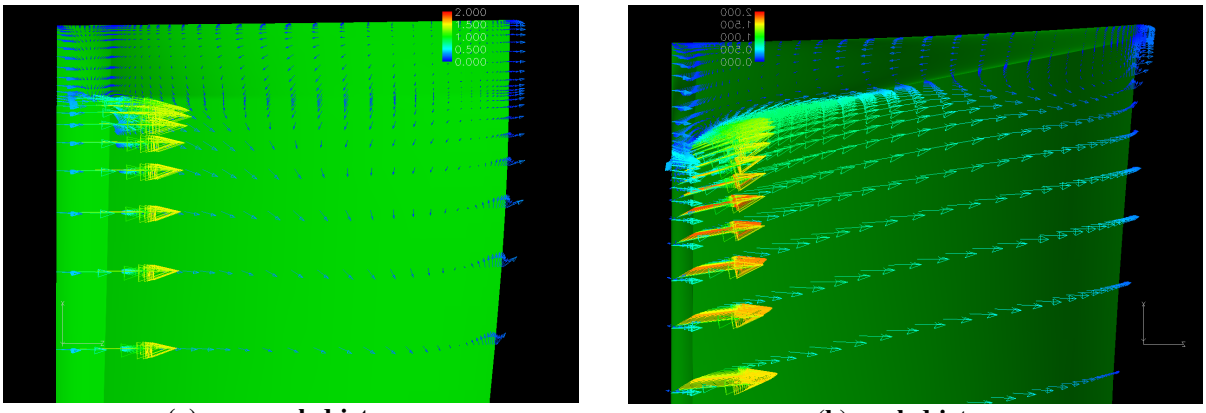

(a) non-angled jet **(b) angled jet**

Figure D11: Flow differences between the non-angled jet and the angled jet

Version comparison

The plot in Figure D12 is a plot of percent span versus the turning angle for all aforementioned versions. The blue line in Figure D12 represents the turning angles created by version 21. This model matched the cambered IGV much better than the other models between 21 and 75 percent of the span before the first stage of the TESCOM rig. Furthermore, version 21 experienced less turning loss in the tip section than any other model as a direct result of the angled jet. Unlike version 19, version 21 actually demonstrated lower turning below 25 percent of the span than the cambered IGV. As demonstrated by version 19, a sharper radius in the lower section of the IGV (the first 25 percent of the span) would allow the IGV to better match the turning of the cambered IGV.

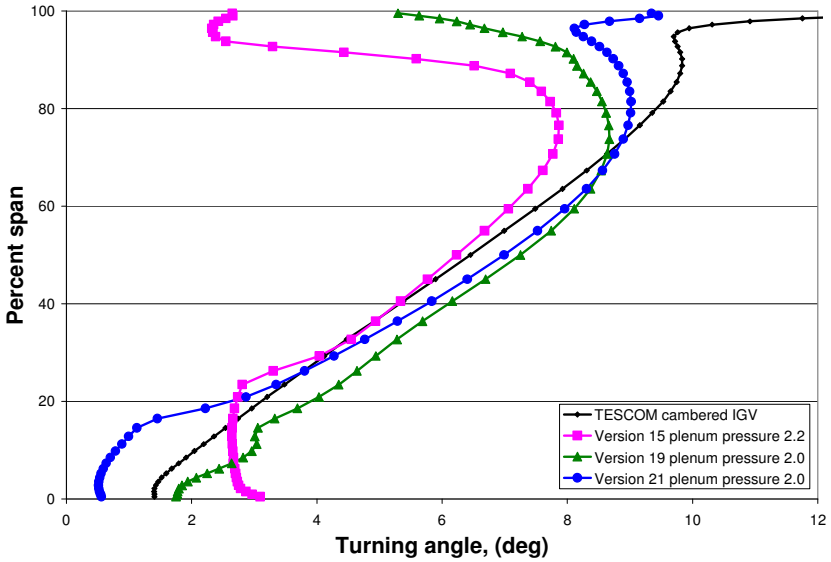

Figure D12: Turning angle comparison

One dimensional values calculated between the inlet, exit, and jet exit planes are tabulated below in Table D2 for all models discussed, including the cambered IGV.

Table D2: 1 Dimensional quantity comparison

Version	Plenum pressure ratio	Percent core flow	Corrected pressure loss	Momentum Coefficient
TESCOM	0	0	0.1369	0
Version 15	2.2	0.32%	0.1022	0.012
Version 19	2.0	0.61%	0.1565	0.021
Version 21	2.0	1.01%	0.1901	0.037

Version 21 was able to better match the turning from the Cambered IGV from a location of 25 percent of the span all the way up to the tip. However, in order to achieve nearly the same level of turning as the cambered IGV, it had to use a larger percentage of the total mass flow rate, and it had the highest pressure losses of all the models tested. Version 19 performed better than version 21 when the mass flow rate ratios and the pressure losses were compared. Version 15 actually had the lowest pressure loss of all the circulation control IGV's and it used the least percent of the total core flow, but it did not meet the turning angle requirements as well as the other circulation control IGVs. None of the IGVs discussed had lower pressure losses than the cambered IGV.

Conclusion

The ability of a three dimensional IGV to nearly match the turning ability of a cambered IGV was demonstrated in this study. The circulation control IGVs were able to achieve nearly the same distribution of turning as the cambered IGV - up to 75 percent of the span. Even though the results show that the circulation control IGVs incur higher pressure losses than a cambered IGV, the results of this study show promise that a circulation control IGV may be able to replace a mechanical IGV.